INTRACELLULAR DEGRADATION

OF LOW-DENSITY LIPOPROTEIN PROBED

WITH TWO-COLOR FLUORESCENCE MICROSCOPY

A Thesis
Presented to
The Academic Faculty

by

William Henry Humphries IV

In Partial Fulfillment
Of the Requirements for the Degree
Doctor of Philosophy in the
School of Chemistry

Georgia Institute of Technology

December, 2011

INTRACELLULAR DEGRADATION

OF LOW-DENSITY LIPOPROTEIN PROBED

WITH TWO-COLOR FLUORESCENCE MICROSCOPY

Approved by:

Dr. Christine K. Payne, Advisor
School of Chemistry and Biochemistry
Georgia Institute of Technology

Dr. Bridgette A. Barry
School of Chemistry and Biochemistry
Georgia Institute of Technology

Dr. Jennifer E. Curtis
School of Physics
Georgia Institute of Technology

Dr. Robert M. Dickson
School of Chemistry and Biochemistry
Georgia Institute of Technology

Dr. Joseph W. Perry
School of Chemistry and Biochemistry
Georgia Institute of Technology

Date Approved: October 27, 2011

“Sometimes a scream is better than a thesis.”
-Manfred Eigen

To anyone who makes me laugh

ACKNOWLEDGMENTS

If you know me, you should know that, unless this is your first, this won't be the most formal acknowledgments section you have ever read. With that as a backdrop, I would like to thank a number of people.

First and foremost, I must thank my parents. Without their sacrifices, love, guidance and financial support, I would never have had a chance to become the person I am today. They gave me every opportunity to excel, which is important because we all know I didn't excel on my first try. They set high expectations and I will continue to try to meet them.

Secondly, I would like to thank my wife, Jessica. Through all the trials presented by graduate school, she was the one that I always leaned on. Her words of confidence, ability to plan around my ever-changing schedule and ability to force me to take a break has kept me sane throughout the last five years. I couldn't imagine having a better family life.

Of course, I would be amiss if I did not thank the people who assisted me scientifically in this endeavor. My advisor, CKP, has challenged, threatened, assisted and encouraged me in just the right proportions to keep me working to the top of my abilities. I can only hope that I will be the worst Ph.D. student to come out of her group. I would also like to my colleagues in the Payne lab, Ger, Craig, Candace and Jairo. Their assistance throughout their terms in the Payne lab has been nothing less than essential to my success.

I would also like to thank Dr. Jeff Gray and Dr. Dave Kurtz, two professors from Ohio Northern University that truly opened my eyes to my capabilities. Without them, I

would have never dreamed of going to graduate school. Their never-ending support has been nothing less than extraordinary

Last and definitely least of all, my friends that I have made during my time at Georgia Tech have kept life interesting. With friends like Nick Haase, Adam Offenbacher Erik Dreaden, Evan Davey, Scott Brombosz, Kathy Woody, Anthony Baldridge, Johnny Bryant, John Bustamante, Carley Shulman, Steve Arnstein, Natalie John and Amy Jablonski, this shouldn't be surprising. I sincerely hope that I remain in communication with all of them because they are the smartest, most fun people I could ever count as friends.

In all seriousness, thank you to everyone who has helped me reach this goal in my life. I have always desired to be the best at whatever I decided to do with my life. Earning a doctorate degree is a major step along that path. I plan to continue to make those how have supported me proud.

GO STEELERS! (I had to put that somewhere…)

CONTENTS

LIST OF TABLES

LIST OF FIGURES

Chapter 4

Chapter 5

Chapter 6

LIST OF SYMBOLS AND ABBREVIATIONS

AF647	Alexa fluor 647
BSA	Bovine serum albumin
CME	Clathrin-mediate endocytosis
DiD	1,1'-dioctadecyl-3,3,3',3'-tetramethylindodicarbocyanine perchlorate
E. coli	*Escherichia coli*
ECFP	Enhanced cyan fluorescence protein
EEA1	Early endosome antigen 1
EGF	Epidermal growth factor
EGFP	Enhanced green fluorescence protein
EGFR	Epidermal growth factor receptor
EYFP	Enhanced yellow fluorescent protein
FBS	Fetal bovine serum
GTP	Guanosine triphosphate
HEPES	4-(2-Hydroxyethyl)piperazine-1-ethanesulfonic acid
LAMP1	Lysosome associated membrane protein 1
LAMP2	Lysosome associated membrane protein 2
LB	Luria-Bertani
LDL	Low-density lipoprotein
M6PR	Mannose-6 phosphate receptor
MEM	Minimum essential medium
SPT	Single particle tracking

SUMMARY

The vesicle-mediated degradation of low-density lipoprotein (LDL) is an essential cellular function due to its role in cellular biosynthesis of membranes and steroids. Using multi-color single particle tracking fluorescence microscopy, the intracellular degradation of LDL was probed in live, intact cells. Unique to these experiments is the direct observation of LDL degradation using an LDL-based probe that increases fluorescence intensity upon degradation. Specifically, individual LDL particles were labeled with multiple fluorophores resulting in a quenched fluorescent signal. The characteristics of the vesicle responsible for degradation were determined and the vesicle dynamics involved in LDL degradation were quantified. Visualization of early endosomes, late endosomes and lysosomes was accomplished by fluorescently labeling vesicles with variants of GFP. Transient colocalization of LDL with specific vesicles and the intensity of the LDL particle were measured simultaneously. These studies, which are the first to directly observe the degradation of LDL within a cell, strive to completely describe the endo-lysosomal pathway and quantify the dynamics of LDL degradation in cells.

CHAPTER 1

INTRODUCTION

1.1 Intracellular chemical reactions

Living cells mediate chemical reactions by a variety of mechanisms. The redox state of the iron bound to the heme group determines the function of hemoglobin.[1] For many common enzymes, such as pepsin, enzymatic activity is dependent on the pH of the solution.[2,3] The light-induced cis-trans isomerization of the protein rhodopsin is the initial step in eyesight.[4] Each method allows for the cell to influence a specific chemical reaction.

In vesicle-mediated chemical reactions, the cell separates the two reactants necessary for a chemical reaction in different vesicles.[5] The fusion of reactant-containing vesicles serves as the initiation of the chemical reaction. As in many chemical reactions, the extent of the reaction is highly dependent on the environment in which the reaction takes place. Identifying details of the intracellular surroundings is difficult because the environment in which chemical reactions take place is often dynamic and intracellular compartments are not readily accessible. However, understanding the environment of the vesicle in which the chemical reaction takes place is necessary to completely describe the reaction.

In this thesis, intracellular vesicle-mediated chemical reactions are probed using fluorescence microscopy. Specifically, using a dequenching labeling scheme, the enzymatic degradation of two extracellular cargo, low-density lipoprotein (LDL) and

bovine serum albumin (BSA), are characterized. The results are used to quantify the vesicle dynamics necessary for degradation reactions. The vesicle populations responsible for degradation are characterized using two complementary techniques, colocalization in fixed cells and single particle tracking in live intact cells.

1.2 Clathrin-mediated endocytosis

Both LDL and BSA are taken into the cell by endocytosis. Generically, endocytosis is the uptake of extracellular materials by the cell and is an essential process for the uptake of nutrients. This process is an important step in the communication between a cell and the extracellular environment.[6] Endocytosis is classified into four basic mechanisms based on the proteins associated with uptake: macropinocytosis, clathrin-mediated endocytosis, caveolae-mediated endocytosis, and clathrin- and caveolae-independent endocytosis.[6] Materials may be bound to the cell surface, by receptor or electrostatics, or free in the extracellular fluid. The experiments to be discussed in this thesis focus on extracellular cargos that enter the cell via the pathway mediated by the protein clathrin.

Clathrin-mediated endocytosis occurs in all mammalian cells and is often associated with the continuous uptake of extracellular cargo (Figure 1.1).[6] Clathrin lines the inside of plasma membrane invaginations to form a clathrin coated pit. This pit grows to about 120 nm in diameter and is pinched off from the plasma membrane to form a clathrin-coated vesicle.[7] Clathrin-mediated endocytosis does not necessarily require a receptor, but most cases of clathrin-mediated endocytosis are also receptor-mediated.

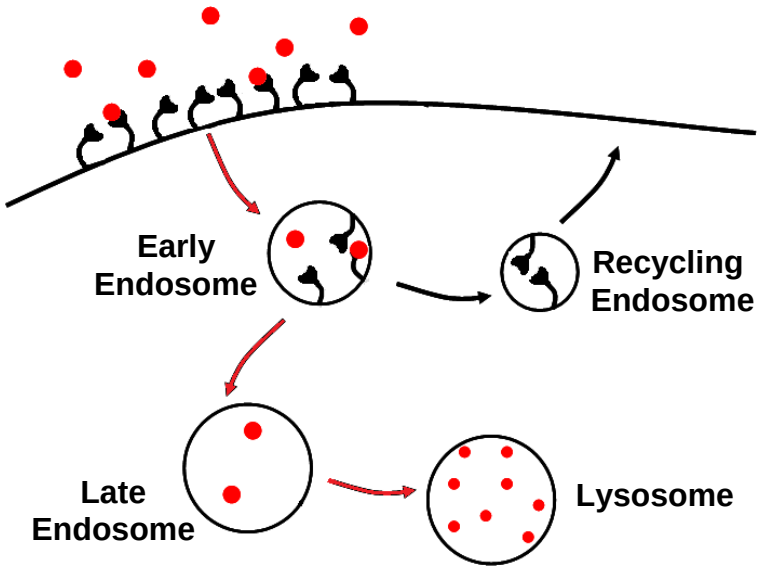

Figure 1.1 The endocytic pathway of low-density lipoprotein. LDL (red circles) binds to the LDL receptor. Once internalized, LDL bound for degradation dissociates from the receptor in the early endosome and the receptors are recycled to the cell surface. Early endosomes then mature into late endosomes. In the conventional picture of degradation, the late endosome contains the substrate and the lysosome contains the enzymes necessary for degradation. Red arrows follow the endocytic pathway of LDL and black arrow follow the receptor recycling pathway.

Clathrin proteins dissociate from the outside of the vesicle and the resulting vesicle is called an early endosome. In this endosome, the pH decreases to approximately 6. In some cases of receptor-mediated endocytosis, the acidic environment causes the dissociation of extracellular cargo from the receptor.[8]

Early endosomes are characterized by the presence of two transmembrane proteins, Rab5 and early endosome antigen 1 (EEA1).[9-11] Rab proteins are small, GTP-binding proteins that regulate membrane trafficking.[12] In early endosomes, Rab5 regulates early endosome fusion.[11,13] However, Rab5 does not function alone and must act in concert with cytosolic factors, such as EEA1. EEA1 is also found on the early endosome membrane and is necessary for vesicle fusion.[11]

Similar to Rab5 and EEA1 for early endosomes, Rab7 and Rab9 are important proteins to determining the character of late endosomes.[14] Live cell microscopy has been used to visualize the maturation of early to late endosomes,[14] which is marked by the dissociation of Rab5[15] and the recruitment of Rab7 from the trans-Golgi.[16]

Late endosomes are defined by the presence of the transmembrane proteins, Rab7 and Rab9.[16-18] Rab7 controls homotypic fusion of late endosomes and may also function in the fusion of late endosomes and lysosomes.[19] Rab9 controls late endosome fusions with cytoplasmic domains and facilitates cargo collection.[16,20] Although Rab7 and Rab9 are commonly found on the same vesicle, they have distinct biosynthetic pathways and occupy separate domains of the vesicle.[16]

Lysosomes are conventionally considered the site of degradation reactions because they contain 80% of the lysosomal enzymes available to the endocytic pathways.[21,22] Since the discovery of the lysosome in 1963 by de Duve, lysosomal biogenesis remains an active area of research.[21,23-27] Lysosomal proteins are synthesized *de novo* in the endoplasmic reticulum and separate from the Golgi apparatus to form lysosomes.[28] Lysosomes can also be formed by fusion of the primary lysosome with other membrane-bound organelles.[29]

Lysosomes are acidic vesicles (pH = 4.5 - 5.5), which is important because the lysosomal enzymes function most efficiently in an acidic environment. The low pH of the lysosome also assists degradation reactions by denaturing proteins, allowing the enzymes access to the protein. Any enzymes leaked out of the lysosome may be inactivated by the neutral pH of the cytosol.[28]

The lysosomal-associated membrane proteins, LAMP1 and LAMP2, are known to localize on both late endosomes and lysosomes.[27] They are highly glycosylated proteins responsible for protecting the vesicle membrane from unwanted degradation by the enzymes contained in the lysosome.[30] It has been proposed that LAMP proteins cover as much as 50% of enzymatically active vesicles.[31]

Medically, the endosomal-lysosomal pathway is of interest because of the relation of endocytosis to a number of diseases, termed lysosomal storage disorders. Malfunction of a single enzyme or the lysosome as a whole organelle is termed a lysosomal storage disease. Of the fifty lysosomal storage diseases known, many are characterized by high concentrations of a secondary metabolite and cause central nervous system disorders. These diseases are overall rare but as common as 1:5000 live births in certain cultural groups.[32] The experiments in this thesis provide information on the characteristics of the degradation vesicles. It is possible that the secondary effects of a misfolded or missing enzyme could be detected using the characteristics determined in this thesis.

1.3 Examples of extracellular cargo

Endosomal transport of a number of extracellular cargos was studied. Endocytosed materials are generically termed extracellular cargo. Examples of extracellular cargo include low-density lipoprotein (LDL), bovine serum albumin (BSA), epidermal growth factor (EGF), transferrin and dextran.

LDL is one of the best-studied extracellular cargo.[8,14,28,33-35] The individual LDL particle is 22 nm in diameter, enclosed by a lipid monolayer. The remained of the

approximately spherical particle is composed of a single apolipoprotein B-100 protein, cholesteryl esters, phospholipids, and cholesterols.[28,36-38] LDL is internalized after binding to the LDL receptor. The pH decrease in the early endosomes causes LDL to dissociate from the receptor. The receptor is recycled to the cell surface while LDL proceeds through the endosomal pathway.[14,34]

LDL is of specific interest because of its importance to cellular homeostasis. The cell is incapable of providing all of the molecules necessary for life. Rather, molecules are internalized from outside of the cell and must be modified before being useful to the cell. For example, LDL cannot be utilized by the cell without degradation by lysosomal enzymes. Degradation of LDL is the primary means by which cholesterol is provided for steroidogenesis.[39] Various human steroid hormones are biosynthesized from a common precursor, pregnenonlone, which is processed directly from cholesterol provided to the cell by LDL.[39]

BSA is a 585 amino acid, 66 kDa protein highly abundant in blood plasma.[40] It is commonly used in molecular biology because it non-specifically binds to proteins and lipids. As an extracellular cargo, it is internalized via receptor-mediated endocytosis.[41] Similar to LDL, BSA dissociates from its receptor in the early endosomes due to the pH change.

EGF is a 6 kDa peptide with high affinity for the epidermal growth factor receptor (EGFR).[42,43] At low concentrations (>0.2 μg/mL), EGF internalizes via clathrin-mediated endocytosis and remains bound to the EGF receptor throughout internalization and degradation.[44] At higher concentrations, internalization occurs though clathrin-independent pathways.[34,45,46]

Dextran is a hydrophilic polysaccharide that is impermeable to lipid membranes and internalized by all types of endocytosis.[47] Dextran is taken up by all vesicles, similar to the extracellular fluid, and is termed a fluid phase marker. Dextrans are biologically inert due to a physiologically uncommon 1,6 glycosilation.[48] The length of the sugar chain determines the molecular weight which can range from 3 to 500 kDa.

1.4 Physical description of quenching and dequenching

The method developed in this thesis to probe the degradation of extracellular cargo utilizes quenched fluorophores. Quenching is any process that decreases the fluorescence intensity of a system.[49] Energy may be diverted from fluorescence processes by energy transfer between a donor fluorophore and a second, accepting molecule. The requirement for energy transfer is that the donor fluorophore must be in close proximity, typically less than 10 nm, to an accepting molecule.

Dequenching is the restoration of fluorescence to a system that was previously quenched. Dequenching has been used as an analytical method to quantify the binding of biotin.[50] Also, dynamic events have been quantified in biochemical reactions in a variety of systems using dequenching. Intracellular virus disassembly was probed using a BODIPY-labeled capsid[51] and virus fusion onto live cells was imaged using a lipophilic dye.[52,53] In live mice, a quenched peptide has been utilized to image protease activity.[54]

Unique to the experiments in this thesis is the direct observation of LDL degradation using an LDL-based probe that dequenches, or increases fluorescence intensity, upon degradation. Individual LDL particles are labeled with multiple

fluorophores resulting in a quenched fluorescent signal that is clearly detectable by fluorescence microscopy. Upon the vesicle-mediated, enzymatic degradation of LDL, an increase in fluorescence intensity is observed. The ability to directly observe LDL degradation allows for the quantification of the vesicle dynamics involved in degradation reactions. In our experiments, quenching is not 100% efficient so the molecule remains weakly fluorescent and viewable with fluorescence microscopy.

1.5 Motivation and significance

Prior to our work, lysosomes were considered the principal site for the degradation of extracellular cargo because it holds the bulk of the enzymes necessary for degradation.[28] A few groups had observed degradation of extracellular cargo in the late endosome, prior to the lysosome.[22,25] For example, EGF and BSA have been shown to undergo degradation before reaching the lysosome.[55-57] Isolated and ruptured endosomes have been shown to have the enzymatic ability to degrade LDL but intracellular LDL degradation has no been observed in these vesicles.[58] However, these observations were made in isolated, ruptured vesicle. To the best of our knowledge, no previous experiments have been able to directly observe degradation in the cell.

The overall goal of this thesis is to characterize the vesicle populations responsible for the degradation of extracellular cargo. To this end, we studied the degradation of two extracellular cargos, LDL and BSA. These cargos are chosen because the internalization and trafficking of each cargo has been well characterized. Conclusions answer basic cell biology questions and are applicable to a number of emerging fields.

1.6 Thesis overview

In this thesis, the vesicle-mediated enzymatic degradation of extracellular cargo is visualized using multi-color single particle tracking fluorescence microscopy.

In Chapter 2, the materials and methods used in all subsequent chapters are discussed. This chapter also includes control experiments that confirm the specific labeling of endocytic vesicles.

In Chapter 3, LDL particles labeled with many fluorophores are used to probe for degradation reactions. Unique to these experiments is the ability to observe a chemical reaction in intact, live cells. Our results revise the conventional cell biology description of the endocytic pathway and support a model in which lysosomes act as enzyme storage vesicles that deliver enzymes to late endosomes.[5]

In Chapter 4, single particle tracking is utilized to quantify the motion of vesicle populations. In the endocytic pathway, the proteins Rab7 and LAMP1 are highly colocalized. By tracking the vesicles specific during their periods of separation, we find that Rab7-vesicles travel more quickly but less efficiently than LAMP1-vesicles.[59]

In Chapter 5, late endosomes and lysosomes are characterized on two levels. First, colocalization of endo-lysosomal proteins is used to describe endosome populations. Second, vesicles populations are characterized in terms of cargo transport. Our results suggest that receptor-mediated cargos are retained in Rab7-vesicles while fluid phase markers, such as dextran are trafficked into terminal LAMP1-vesicles at long incubation times.[60]

In Chapter 6, the use of dequenching for sensing chemical reactions in the intracellular environment is extended to extracellular cargo other than LDL. Specifically,

bovine serum albumin (BSA) is labeled and dequenching is measured *in vitro* and *in vivo*. Dequenching is then characterized in single vesicles, single cells and bulk cellular samples.[61]

1.7 References

1 Kakar, S.; Hoffman, F. G.; Storz, J. F.; Fabian, M.; Hargrove, M. S., Structure and reactivity of hexacoordinate hemoglobins. *Biophys. Chem.* **2010**, *152*, 1-14.

2 Weber, G.; Young, L. B., Fragmentation of boine serum albumin by pepsin. 1. Origin of acid expansion of albumin molecule. *J. Biol. Chem.* **1964**, *239*, 1415-1423.

3 Weber, G.; Young, L. B., Fragmentation of bovine serum albumin by pepsin. 2. Isolation, amino acid composition, and physical properties of fragments. *J. Biol. Chem.* **1964**, *239*, 1424-1432.

4 Birge, R. R., Photophysics of light transduction in rhodopsin and bacteriorhodopsin. *Annu. Rev. Biophys. Bioeng.* **1981**, *10*, 315-354.

5 Humphries, W. H.; Fay, N. C.; Payne, C. K., Intracellular degradation of low-density lipoprotein probed with two-color fluorescence microscopy. *Integr. Biol.* **2010**, *2*, 536-544.

6 Conner, S. D.; Schmid, S. L., Regulated portals of entry into the cell. *Nature* **2003**, *422*, 37-44.

7 Ramachandran, R.; Schmid, S. L., Real-time detection reveals that effectors couple dynamin's GTP-dependent conformational changes to the membrane. *EMBO J.* **2008**, *27*, 27-37.

8 Goldstein, J. L.; Brown, M. S.; Anderson, R. G. W.; Russell, D. W.; Schneider, W. J., Receptor-mediated endocytosis: concepts emerging from the LDL receptor system. *Annu. Rev. Cell Biol.* **1985**, *1*, 1-39.

9 Simonsen, A.; Lippe, R.; Christoforidis, S.; Gaullier, J. M.; Brech, A.; Callaghan, J.; Toh, B. H.; Murphy, C.; Zerial, M.; Stenmark, H., EEA1 links PI(3)K function to Rab5 regulation of endosome fusion. *Nature* **1998**, *394*, 494-498.

10 Chavrier, P.; Parton, R. G.; Hauri, H. P.; Simons, K.; Zerial, M., Localization of low-molecular-weight GTP-binding proteins to exocytic and endocytic compartments. *Cell* **1990**, *62*, 317-329.

11 Christoforidis, S.; McBride, H. M.; Burgoyne, R. D.; Zerial, M., The Rab5 effector EEA1 is a core component of endosome docking. *Nature* **1999**, *397*, 621-625.

12 Stenmark, H., Rab GTPases as coordinators of vesicle traffic. *Nat. Rev. Mol. Cell Biol.* **2009**, *10*, 513-525.

13 Gorvel, J. P.; Chavrier, P.; Zerial, M.; Gruenberg, J., Rab5 controls early endosome fusion *in vitro*. *Cell* **1991**, *64*, 915-925.

14 Rink, J.; Ghigo, E.; Kalaidzidis, Y.; Zerial, M., Rab conversion as a mechanism of progression from early to late endosomes. *Cell* **2005**, *122*, 735-749.

15 Poteryaev, D.; Datta, S.; Ackema, K.; Zerial, M.; Spang, A., Identification of the Switch in Early-to-Late Endosome Transition. *Cell* **2010**, *141*, 497-508.

16 Barbero, P.; Bittova, L.; Pfeffer, S. R., Visualization of Rab9-mediated vesicle transport from endosomes to the trans-Golgi in living cells. *J. Cell Biol.* **2002**, *156*, 511-518.

17 Zerial, M.; McBride, H., Rab proteins as membrane organizers. *Nat. Rev. Mol. Cell Biol.* **2001**, *2*, 107-117.

18 Soldati, T.; Rancano, C.; Geissler, H.; Pfeffer, S. R., Rab7 and Rab9 are recruited onto late endosomes by biochemically distinguishable processes. *J. Biol. Chem.* **1995**, *270*, 25541-25548.

19 Wang, T.; Ming, Z.; Xiaochun, W.; Hong, W., Rab7: Role of its protein interaction cascades in endo-lysosomal traffic. *Cell. Signal.* **2011**, *23*, 516-521.

20 Carroll, K. S.; Hanna, J.; Simon, I.; Krise, J.; Barbero, P.; Pfeffer, S. R., Role of Rab9 GTPase in facilitating receptor recruitment by TIP47. *Science* **2001**, *292*, 1373-1376.

21 Kornfeld, S.; Mellman, I., The biogenesis of lysosomes. *Annu. Rev. Cell Biol.* **1989**, *5*, 483-525.

22 Tjelle, T. E.; Brech, A.; Juvet, L. K.; Griffiths, G.; Berg, T., Isolation and characterization of early endosomes, late endosomes and terminal lysosomes: Their role in protein degradation. *J. Cell Sci.* **1996**, *109*, 2905-2914.

23 Saftig, P.; Klumperman, J., Lysosome biogenesis and lysosomal membrane proteins: trafficking meets function. *Nat Rev Mol Cell Biol* **2009**, *10*, 623-635.

24 Mullins, C.; Bonifacino, J. S., The molecular machinery for lysosome biogenesis. *Bioessays* **2001**, *23*, 333-343.

25 Pillay, C. S.; Elliott, E.; Dennison, C., Endolysosomal proteolysis and its regulation. *Biochem. J* **2002**, *363*, 417-429.

26 Luzio, J. P.; Pryor, P. R.; Bright, N. A., Lysosomes: fusion and function. *Nat Rev Mol Cell Biol* **2007**, *8*, 622-632.

27 Clague, M. J., Molecular aspects of the endocytic pathway. *Biochem. J* **1998**, *336*, 271-282.

28 Alberts, B.; Bray, D.; Lewis, J.; Raff, M.; Roberts, K.; Watson, J. D. *Molecular Biology of the Cell*. 3 edn, (Garland Publishing, 1994).

29 Lodish, H.; Berk, A.; Matsudaira, P.; Kaiser, C. A.; Krieger, M.; Scott, M. P.; Zipursky, S. L.; Darnell, J. *Molecular Cell Biology, 5th edn.*, (W. H. Freeman & Company, 2004).

30 Eskelinen, E. L.; Tanaka, Y.; Saftig, P., At the acidic edge: emerging functions for lysosomal membrane proteins. *Trends Cell Biol.* **2003**, *13*, 137-145.

31 Marsh, M.; Schmid, S.; Kern, H.; Harms, E.; Male, P.; Mellman, I.; Helenius, A., Rapid analytical and preparative isolation of functional endosomes by free flow electrophoresis. *J. Cell Biol.* **1987**, *104*, 875-886.

32 Vitner, E. B.; Platt, F. M.; Futerman, A. H., Common and uncommon pathogenic cascades in lysosomal storage diseases. *J. Biol. Chem.* **2010**, *285*, 20423-20427.

33 Davis, C. G.; Goldstein, J. L.; Sudhof, T. C.; Anderson, R. G. W.; Russell, D. W.; Brown, M. S., Acid-dependent ligand dissociation and recycling of LDL receptor mediated by growth-factor homology region. *Nature* **1987**, *326*, 760-765.

34 Lakadamyali, M.; Rust, M. J.; Zhuang, X., Ligands for clathrin-mediated endocytosis are differentially sorted into distinct populations of early endosomes. *Cell* **2006**, *124*, 997-1009.

35 Dunn, K. W.; McGraw, T. E.; Maxfield, F. R., Iterative fractionation of recycling receptors from lysosomally destined ligands in an early sorting endosome. *J. Cell Biol.* **1989**, *109*, 3303-3314.

36 Voet, D.; Voet, J. G. *Biochemistry*. 3 edn, (John Wiley & Sons, 2004).

37 Segrest, J. P.; Jones, M. K.; De Loof, H.; Dashti, N., Structure of apolipoprotein B-100 in low density lipoproteins. *J. Lipid Res.* **2001**, *42*, 1346-1367.

38 Hevonoja, T.; Pentikainen, M. O.; Hyvonen, M. T.; Kovanen, P. T.; Ala-Korpela, M., Structure of low density lipoprotein (LDL) particles: Basis for understanding

molecular changes in modified LDL. *Biochim. Biophys. Acta-Mol. Cell Biol. Lipids* **2000**, *1488*, 189-210.

39 Hu, J.; Zhang, Z.; Shen, W.-J.; Azhar, S., Cellular cholesterol delivery, intracellular processing and utilization for biosynthesis of steroid hormones. *Nutr. Metab.* **2010**, *7*, 47.

40 Peters Jr, T. *All about albumin: biochemistry, genetics, and medical applications*. (Academic Press, 1996).

41 Schnitzer, J. E.; Oh, P., Albondin-mediated capillary-permeability to albumin-differential role of receptors in endothelial transcytosis and endocytosis of native and modified albumins. *J. Biol. Chem.* **1994**, *269*, 6072-6082.

42 Carpenter, G.; Cohen, S., Epidermal growth factor. *J. Biol. Chem.* **1990**, *265*, 7709-7712.

43 Lax, I.; Johnson, A.; Howk, R.; Sap, J.; Bellot, F.; Winkler, M.; Ullrich, A.; Vennstrom, B.; Schlessinger, J.; Givol, D., Chicken epidermal growth-factor (EGF) receptor - cDNA cloning, expression in mouse cells, and differential binding of EGF and transforming growth factor-alpha. *Mol. Cell. Biol.* **1988**, *8*, 1970-1978.

44 Carpenter, G.; Cohen, S., Epidermal growth-factor. *Annu. Rev. Biochem.* **1979**, *48*, 193-216.

45 Jiang, X.; Sorkin, A., Epidermal growth factor receptor internalization through clathrin-coated pits requires Cbl RING finger and proline-rich domains but not receptor polyubiquitylation. *Traffic* **2003**, *4*, 529-543.

46 Sigismund, S.; Woelk, T.; Puri, C.; Maspero, E.; Tacchetti, C.; Transidico, P.; Di Fiore, P. P.; Polo, S., Clathrin-independent endocytosis of ubiquitinated cargos. *Proc. Natl. Acad. Sci. USA* **2005**, *102*, 2760-2765.

47 Hacker, U.; Albrecht, R.; Maniak, M., Fluid-phase uptake by macropinocytosis in Dictyostelium. *J. Cell Sci.* **1997**, *110*, 105-112.

48 Lohmar, R., Evidence of new linkages in dextranse. *J. Am. Chem. Soc.* **1952**, *74*, 4974-4974.

49 Lakowicz, J. R. *Principles of Fluorescence Spectroscopy*. 3 edn, (Springer Science and Bussiness Media, LLC, 2006).

50 Wu, Y.; Simons, P. C.; Lopez, G. P.; Sklar, L. A.; Buranda, T., Dynamics of fluorescence dequenching of ostrich-quenched fluorescein biotin: A multifunctional quantitative assay for biotin. *Anal. Biochem.* **2005**, *342*, 221-228.

51 Da Poian, A. T.; Gomes, A. M. O.; Coelho-Sampaio, T., Kinetics of intracellular viral disassembly and processing probed by Bodipy fluorescence dequenching. *J. Virol. Methods* **1998**, *70*, 45-58.

52 van der Schaar, H. M.; Rust, M. J.; Waarts, B.-L.; van der Ende-Metselaar, H.; Kuhn, R. J.; Wilschut, J.; Zhuang, X.; Smit, J. M., Characterization of the early events in dengue virus cell entry by biochemical assays and single-virus tracking. *J. Virol.* **2007**, *81*, 12019-12028.

53 Blumenthal, R.; Gallo, S. A.; Viard, M.; Raviv, Y.; Puri, A., Fluorescent lipid probes in the study of viral membrane fusion. *Chem. Phys. Lipids* **2002**, *116*, 39-55.

54 Blum, G.; Weimer, R. M.; Edgington, L. E.; Adams, W.; Bogyo, M., Comparative assessment of substrates and activity based probes as tools for non-invasive optical imaging of cysteine protease activity. *Plos One* **2009**, *4*, e6374.

55 Authier, F.; Posner, B. I.; Bergeron, J. J. M., Endosomal proteolysis of internalized proteins. *FEBS Lett.* **1996**, *389*, 55-60.

56 Renfrew, C. A.; Hubbard, A. L., Sequential processing of epidermal growth factor in early and late endosomes of rat liver. *J. Biol. Chem.* **1991**, *266*, 4348-4356.

57 Diment, S.; Stahl, P., Macrophage endosomes contain proteases which degrade endocytosed protein ligands. *J. Biol. Chem.* **1985**, *260*, 5311-5317.

58 Runquist, E. A.; Havel, R. J., Acid hydrolases in early and late endosome fractions from rat liver. *J. Biol. Chem.* **1991**, *266*, 22557-22563.

59 Szymanksi, C. J.; Humphries, W. H.; Payne, C. K., Single particle tracking as a method to resolve differences in highly colocalized proteins. *Analyst* **2011**, *136*, 3527-3533.

60 Humphries, W. H.; Szymanski, C. J.; Payne, C. K., Endo-lysosomal Vesicles Positive for Rab7 and LAMP1 Are Terminal Vesicles for the Transport of Dextran. *PLoS One* **2011**, *Accepted*.

61 Humphries, W. H.; Payne, C. K., The Intracellular, Vesicle-mediated Intracellular Measurement of Enzyme-mediated Degradation: Dequenching of Fluorophores as a Method to Probe Chemical Reactions in Live Cells. *Submitted to Bioconjugate Chemistry* **2011**.

CHAPTER 2

MATERIALS AND METHODS

2.1 Cell culture

BS-C-1, green African monkey kidney, cells (ATCC, Manassas, VA) were used in most cellular experiments. This cell line is chosen primarily because the intracellular trafficking dynamics exhibited are representative of other cells lines.[1] Another important feature is that these cells are highly adherent and spread out on surfaces. When adhered to a surface, BS-C-1 cells typically measures approximately 120 μm in diameter but only ~4 μm on the edges and ~8 μm at the nucleus. Because of this aspect ratio, the cytoskeleton can be approximated as two dimensional, which is ideal for imaging. HeLa, human cervical cancer, cells (ATCC) were used to confirm that the measurements made in BS-C-1 cells were not specific to BS-C-1 cells.

Both cell lines were maintained in a 37°C, 5% carbon dioxide environment in minimum essential medium (MEM, 61100, Invitrogen, Carlsbad, CA) with 10% (v/v) fetal bovine serum (FBS, 10437, Invitrogen). Cells were passaged every 3 days. For fluorescence imaging, cells were cultured in 35 mm glass-bottom cell culture dishes (P35G-1.5-14-C, MatTek, Ashland, MA).

For confocal imaging, cells were fixed with 4% v/v formaldehyde (28908, Thermo Scientific) in phosphate buffered saline (PBS, 14040, Invitrogen) for 30 minutes at room temperature. Cells were then washed and imaged in PBS. For live cell imaging, cells were imaged in phenol red-free MEM (51200, Invitrogen) buffered with 0.1 M HEPES to pH 8. The imaging medium was supplemented with 2% v/v FBS, 1% w/v glucose (49159, Sigma, St. Louis, MO), and a glucose oxidase-based oxygen scavenger.

Oxygen scavenger was prepared by adding 10 mg of glucose oxidase (G2133, Sigma) to 200 μL of ice cold PBS. After gentle mixing, 50 μL of catalase (92301956,

Roche, Basel, Switzerland), an enzyme that decomposes hydrogen peroxide, was added and the reaction mixture centrifuged at 10,000 g for 5 minutes. Excess, non-soluble catalase formed a pellet and was discarded. The supernatant was filtered though a 0.22 μm pore syringe filter. Final concentrations were 0.4 mg/mL glucose oxidase and 2 μL/mL catalase. For use, the oxygen scavenger was added at a ratio of 1 part oxygen scavenger to 100 parts imaging medium. During each experiment, cells were visually verified to be healthy.

Nuclei were stained with 27.25 μM DAPI (4',6-diamidino-2-phenylindole, D3571, Invitrogen) in full growth medium for 30 minutes prior to experiments.

2.2 Expression of fluorescently-labeled endocytic proteins

Plasmids, circular 3-7 kilo base pair (kbp) pieces of DNA, encoded for GFP-variants and the main endocytic proteins were obtained: EGFP-Rab5 (a gift from M. Zerial),[2] EYFP-Rab7 (Plasmid 20164, Addgene, Cambridge, MA),[3] ECFP-Rab7 (a gift from S. Pfeffer),[4] EYFP-Rab9 (a gift from S. Pfeffer),[4] and LAMP1-EYFP (Plasmid 1816, Addgene).[5] Each plasmid contains a sequence for antibiotic resistance and has at least two sites available to restriction enzymes.

Each plasmid was amplified using chemically-competent Escherichia coli (E. coli, C404010, Top10, Invitrogen). In brief, E. coli were incubated with a single plasmid at 42°C for 30 s to cause the disruption of the bacterial cell membrane and penetration of the plasmid into the E. coli. Cells were incubated for 1 hr at 37°C before the bacteria were plated on Luria-Bertani (LB) agar (4% w/v, 61189, Acros) plates to grow single

colonies of genetically identical bacteria. Once single colonies were formed, liquid cultures of E. coli were grown in LB broth (2.5% w/v, 61187, Acros). From these liquid cultures, DNA was purified using preparation kits (mini-prep, K0503, Fermentas; maxi-prep, 12662, Qiagen). The final concentration of plasmid was measured using UV-Vis (DU800, Beckman Coulter, Fullerton, CA) for the DNA absorbance at 280 nm. Typical concentrations of purified plasmid were approximately 1.0 mg/mL.

Once purified, plasmids were characterized to ensure that the amplification and purification were successful. This was accomplished using gel electrophoresis to ensure the correct size, transfection to ensure proper character of staining and, most importantly, colocalization experiments to ensure specificity.

Plasmids were digested using restriction enzymes specific to the DNA sequence. In all cases, 1 μg of DNA was diluted into 20 μL total volume of aqueous buffer. Typically 1 μg of restriction enzyme, where the exact enzyme differs depending on the plasmid, was added for 2 hr at 37°C to digest the plasmid DNA. Reactions were quenched by adding 20 mM EDTA (0.9 μL of 0.5 M EDTA) and placed on ice. The plasmid map for EYFP-Rab7 (Figure 2.1A) illustrates that this plasmid is 5.35 kbp and has restriction sites specific to the enzymes XhoI and KpnI. The reaction mixture was then separated by electrophoresis using a 1% agarose gel, stained with ethidium bromide and visualized under UV light (Figure 2.1B).

Cells were transfected with each plasmid to ensure that the plasmid was labeling vesicles (Figure 2.1C). Transfections were performed using FuGENE 6 (11815091001, Roche, Indianapolis, IN) transfection reagent 24 - 48 hrs after plating. Transfections with one plasmid were carried out by adding 4 μL FuGENE to 96 μL phenol-red-free MEM.

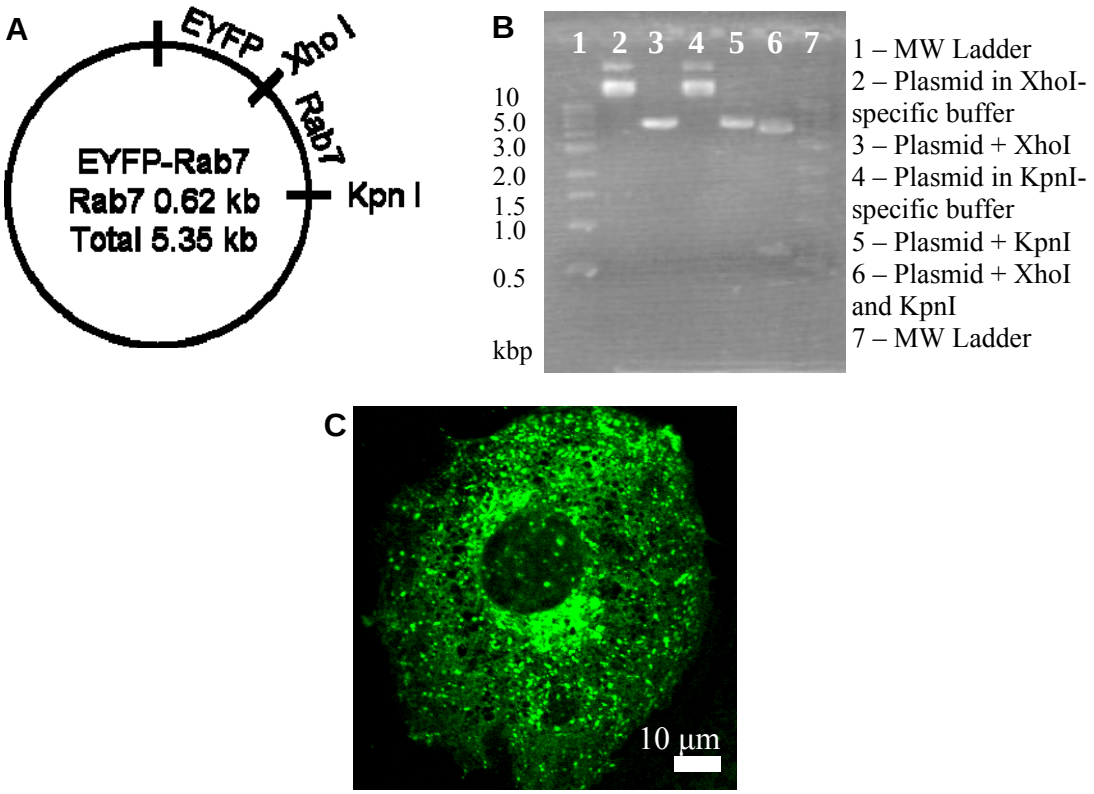

Figure 2.1 Characterization of the ECFP-Rab7 plasmid. A.) A basic plasmid map shows the enzyme restriction sites on either side of the protein of interest. B.) A 1% agarose gel that characterized the size of the plasmid. When the plasmid is digested with both XhoI and KpnI, the size of the excised DNA is appropriately 0.6 kb. C.) An image of a cell transfected with ECFP-Rab7. Further experiments are described that confirm specificity.

The mixture was tapped 8-10 times and given 5 minutes to mix. Then, 1 - 2 µg of DNA were added and given 20 minutes to interact with the transfection reagent at room temperature. This mixture was added to 1 mL of fresh MEM with 10% FBS on cells. Experiments were carried out 24 - 48 hrs after transfection.

Colocalization experiments were performed for each plasmid. In these experiments, cells were transfected with a plasmid and then the same vesicle population was fluorescently labeled using an independent technique, typically immunofluorescence. Early endosomes were labeled with Rab5 and EEA1, late endosomes were labeled with Rab7 and Rab9, and lysosomes were labeled with LAMP1 and LAMP2.

Rab5-endosomes were labeled with EGFP-Rab5 in transiently transfected cells. Immunofluorescence for EEA1 (ab15846, Abcam, Cambridge, UK) confirmed EGFP-Rab5 specificity (Figure 2.1).[6-8] For EEA1 immunofluorescence, cells were fixed with 2% formaldehyde in PBS for 40 min at room temperature and permeabilized (3% BSA, 10% FBS, 0.5% Triton-X 100 in PBS) for 15 min at room temperature. Cells were incubated for 1 hr in blocking buffer (10% FBS, 3% BSA in PBS) before the addition of each antibody. The primary antibody was added to cells at 1-5:1000 dilutions in blocking buffer and incubated for 3 – 18 hrs at 4ºC. The secondary antibody was added to cells at a

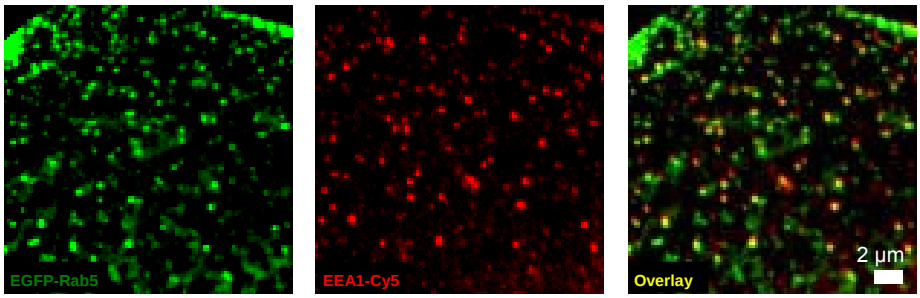

Figure 2.2 Colocalization of Rab5 with EEA1. Rab5-EGFP (green) shows ~85% colocalization with EEA1-Cy5 (red).

1:1000 dilution in blocking buffer and incubated for 30 min at room temperature. Cells were washed (0.3% BSA, 0.1% Triton-X 100 in PBS) three times between each step.

Late endosomes were transfected with EYFP-Rab7 and EYFP-Rab9 plasmids. Transfections with multiple plasmids were prepared by doubling the volume of FuGENE and using 1 - 2 µg of each plasmid. The total volume of the plasmid solution was held constant at 100 µL. The results of this experiment confirm proper labeling and are discussed in detail in Chapter 4.

LAMP1-vesicles were fluorescently labeled with LAMP1-EYFP in a stably transfected cell line. Immunofluorescence with LAMP2 (ab25631, Abcam) was used to confirm expression (Figure 2.3) using the same protocol as discussed for EEA1.

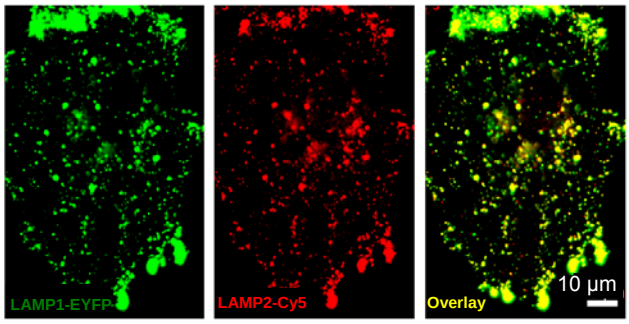

Figure 2.3 Colocalization of LAMP1 with LAMP2. LAMP1-EYFP (green) shows ~100% colocalization with LAMP2-Cy5 (red).

Lysosomes are defined as lacking the cation independent mannose 6-phosphate receptor (M6PR).[9-13] Immunofluorescence for M6PR is based on the method of J.X. Kang, et al. (Figure 2.4).[14] Cells were fixed with 4% formaldehyde for 30 min at room temperature and permeabilized (0.1% Triton-X 100 in PBS) for 5 min at room

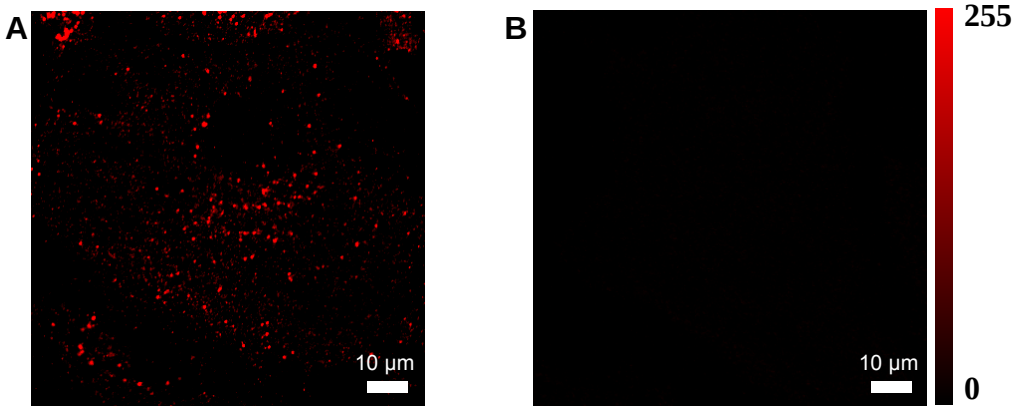

Figure 2.4 M6PR immunofluorescence. Confocal microscopy image showing the Cy5 emission from a BS-C-1 cell labeled with a primary antibody for M6PR and a Cy5-labeled secondary antibody. B) The Cy5 emission of a BS-C-1 cell, under the same fixation, permeabilization, blocking, and imaging conditions in the absence of the primary M6PR antibody.

temperature. The primary antibody, mouse M6PR (MA1-066, Fisher Scientific), was added to cells at a 1:400 dilution in blocking buffer (10% FBS, 3% BSA in PBS) and incubated for 1 hr at room temperature. The secondary antibody, Cy5 rabbit anti-mouse (AP160S, Chemicon, Temecula, CA) was added to cells at a 1:1000 dilution in blocking buffer and incubated for 30 min at room temperature. Cells were incubated in blocking buffer for 1 hr prior to the addition of each antibody and washed in PBS three times between each step.

2.3 Fluorescent-labeling of extracellular cargo

Human low-density lipoprotein (LDL, BT-903, Biomedical Technologies, Stoughton, MA) was labeled with 1,1'-dioctadecyl-3,3,3',3'-tetramethylindodicarbocyanine perchlorate (DiD, D-307, Invitrogen) at a concentration of 1.8 mM for a ratio of 200 DiD:LDL. LDL (50 μL of 5 mg/mL) and DiD (3.8 μL of 25 mM) were mixed by pipet every 10 min for 1 hr. Excess dye was removed by a Nap5 size exclusion column (17-0853-02, GE Healthcare, Buckinghamshire, UK). The ratio of DiD molecules per LDL particle was measured using a UV-Vis spectrophotometer. A spectrofluorophotometer (RF-5301PC, Shimadzu, Japan) was used to measure changes in fluorescence emission. LDL-DiD was excited at 600 nm with emission measured at 667 nm. The calculation of number of dyes per LDL and the calculation of dequenching is discussed further in Chapter 3.

For cellular imaging experiments, cells were incubated with 10 μg/mL of LDL-DiD for 10 min at 37°C. Immediately before imaging experiments cells were washed

with phenol-red free MEM buffered with 0.1 M HEPES. For single particle tracking experiments the imaging medium was supplemented with 2% FBS, 1% glucose, and oxygen scavenger (0.2 mg/mL glucose oxidase and 1 μL/mL catalase).

Bovine serum albumin (BSA, BP1600, Fisher Bioreagents) was labeled with AlexaFluor647 (AF647, A20006, Invitrogen) according to the manufacturer's instructions. To obtain different labeling ratios, 136 μM BSA was incubated with 91 mM, 68 mM or 0.91 mM AF647 for 1 hr resulting in 2.48, 0.93 or 0.07 AF647 per BSA, respectively. A labeling ratio of 2.70 AF647 per BSA was obtained by allowing 136 μM BSA to incubate with 91 mM AF647 for 16 hours. In all cases, the reaction was stopped with 1.5 M hydroxylamine and free AF647 was separated from BSA using a NAP5 size exclusion column (17–0853-02, GE Healthcare, Buckinghamshire, UK). Final concentrations of BSA and AF647 were measured with a UV-Vis spectrophotometer (DU800, Beckman Coulter, Fullerton, CA, USA). The extinction coefficient of BSA was measured to be 37,000 M^{-1} cm^{-1}. Cells were incubated with 83 μg/mL of BSA-AF647 for 1 hr or 18 hr at 37°C in complete cell culture medium and then fixed with 4% formaldehyde for 30 minutes at room temperature.

Other extracellular cargos were purchased pre-labeled: Dextran-AF647 (D22914, Invitrogen, 10,000 MW, fixable) and EGF-AF647 (E35351, Invitrogen). Dextran incubation conditions were with 0.25 mg/mL dextran at 37°C in MEM supplemented with 10% FBS for the specified duration. EGF-AF647 was incubated at a concentration of 0.2 μg/mL under the same conditions.

2.4 Disruption of intracellular trafficking and inhibition of enzymes

Wortmannin (W1628, Sigma, St Louis, MO) was used to inhibit phosphatidylinositol-3-OH kinase (PI(3)K),[15-17] a signaling molecule responsible for early endosome fusion, resulting in the disruption of LDL-DiD transport to the late endosomes.[7,18] Cells were incubated in MEM supplemented with 240 nM wortmannin for 30 min prior to addition of LDL-DiD and replenished after each washing step. The efficiency of the wortmannin treatment was examined by colocalization of LDL-DiD with EYFP-Rab7, which is described in Chapter 3.

Nocodazole (60 μM, 487928, Calbiochem, San Diego, CA, USA) was used to interfere with the polymerization of microtubules.[19] This drug binds to β-tubulin monomers and prevents the formation of new microtubules. Nocodazole was added to cells 30 min prior to experiments and remained present throughout the course of the experiment. This treatment will be discussed in Chapter 5.

Pepstatin A methyl ester (pepstatin, 516485, EMD Chemicals), a cell permeable derivative of pepstatin, was used to inhibit two important enzymes, cathepsin D and pepsin. Cathepsin D is known to be important to the degradation of LDL and pepsin is responsible for the degradation of BSA.[20,21] Before treatment with pepstatin, cells were incubated in serum-deficient medium (MEM with 0.2% FBS) for 18 hr before incubation with 10 μM pepstatin. Cells were pre-treated with pepstatin for 2 hrs and it remained present throughout the course of each experiment. This treatment will be utilized in Chapter 6.

2.5 Fluorescence microscopy

Microscopy provides high spatial and temporal resolution which allows for identification and tracking of subcellular components. Since the isolation and characterization of the green fluorescence protein (GFP),[22-24] fluorescence microscopy has been a powerful tool for visualizing intracellular processes. Combining the molecular biology afforded by GFP and fluorescence microscopy, a high level of specificity though the direct labeling of molecules or proteins in live, intact cells can be achieved. Development of a full palette of spectrally-separated fluorescent proteins has allowed for the extension of fluorescence microscopy to multiple colors.[25] The advantage of this technique is that it allows for observation of multiple fluorophores interacting in real time.

2.5.1 Live cell imaging

In the Payne Lab, an inverted multi-color microscope (IX71, Olympus, Center Valley, PA), shown in Figure 2.5, capable of imaging two colors simultaneously or three colors quasi-simultaneously has been constructed. Multi-color fluorescence microscopy has been used previously by other groups to study the internalization and trafficking of extracellular cargo.[3,26-28]

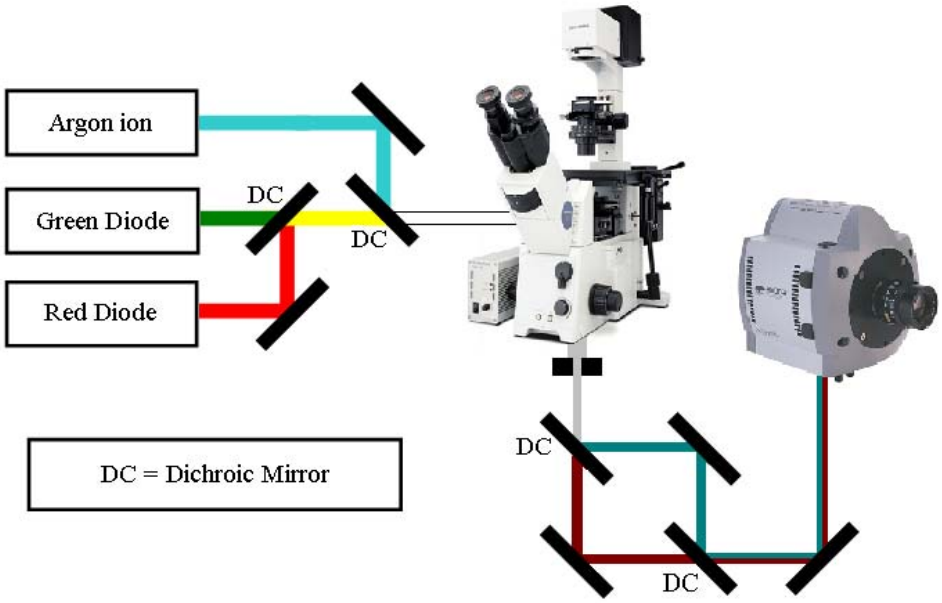

Figure 2.5 Multi-color fluorescence microscope. Three lasers simultaneously excite three distinct fluorophores. Dichroic mirrors (DC) are used to separate the signals of the fluorophores. Images are recorded on an EMCCD camera.

All microscopes have three basic elements: excitation, illumination of a sample, and detection. The excitation for the microscope was supplied by three lasers, a tunable argon ion laser (35-LAP-431-208, Melles Griot, Carlsbad, CA), a green diode (Green532, Crystalaser, Reno, NV), and a red diode (635-25C, Coherent, Santa Clara, CA). Excitation beams were overlapped using dichroic mirrors (Z488RSC and Z532BCM, Chroma, Rockingham, VT) and focused on the back focal plane of the microscope objective allowing for simultaneous excitation of multiple fluorophores. Using a dichroic mirror inside the microscope (Z458/532/633RPC, Z488/532/633RPC, Z514/633RPC, Chroma), all excitation beams were reflected through the objective onto a fluorescently-labeled sample. The fluorescence from the sample was then collected back through the objective, passed through the same dichroic mirror and directed out of the side port of the microscope. In a two-color configuration, a dichroic mirror was inserted into the emission

pathway to split the emission into two paths, one short and one long wavelength path. A second dichroic mirror was then used to record images side by side on a single CCD camera (iXon 888, Andor, Belfast, Northern Ireland).

When extended to a three-color setup, emission filters (ECFP – Brightline 483/32 (Semrock, Rochester, NY), EGFP – HQ550/50 (Chroma), EYFP – HQ580/50 (Chroma), DiD – HQ680/60 (Chroma)) were mounted in a rotating filter wheel and placed in the short wavelength path. Images were recorded sequentially. The relatively fast switching time of the filter wheel (200-400 ms) in comparison to the motion of the vesicles (<1 μm/s) means that sequential imaging is approximately equivalent to simultaneous imaging. In this time between images, a vesicle could move 400 nm or 3 pixels, approximately the same size as vesicles.

Images taken with the multi-color microscope consist of two separate channels per image. To overlap the images into a single two-color image, they must be divided, rotated, scaled, cropped and merged. The parameters necessary to execute these functions were obtained via calibration with 200 nm fluorescent beads. FluoSphere beads (F8811 and F8809, Invitrogen) are extremely bright and have a broad emission spectra. When excited with either 458, 488 or 514 nm light from the argon ion laser, the beads were visible in all channels. Microscope slides were made with a 1 to 10,000 dilution of the beads and imaged to obtain calibration parameters. Once imaged, two beads were picked to obtain scaling and rotation information. After the calibration image was adjusted based on these parameters, one more bead was selected to obtain proper cropping parameters. The resulting overlapped bead image served as a calibration and provides the parameters necessary to overlap subsequent image sets.

Multi-color live cell experiments are performed using the microscope in Figure 2.5. A plate of cells are prepared and placed on the stage. The microscope is focused on the sample through the eyepieces and the image is verified on the camera. Exposure times between 100-300 ms are used for all images. The interval between images for all experiments is 2 seconds.

In each image set, one cell is imaged for 10 to 30 minutes. Each single particle tracking experiment is comprised of 3-15 cells with 1-5 particles. Control experiments to optimize buffer conditions and stage temperature assist in ensuring that cells are healthy throughout the duration of the experiment.

There are two main ways that these experiments fail. The first is where cells de-adhere from the cell plate. This typically happens when the cells are not as confluent as desired. These cells are not analyzed or included in any further experiment. The second type of failed experiment is when there are no particles that fit the defined characteristics for dequenching. This can be due to focus drift, insufficient uptake of cargo, poor labeling of cargo or photobleaching.

2.5.2 Confocal microscopy

The main benefit of using confocal microscopy over widefield microscopy is increased z-resolution. However, because the excitation and emission are focused through a pinhole, the image is made of single pixel measurements. This drastically decreases the time resolution of the technique. In this thesis, confocal microscopy was used for colocalization experiments on fixed cells.

Two confocal microscopes were used. Confocal microscopy images displayed in Chapter 3 were taken with an LSM 510 confocal microscope (Carl Zeiss Inc., Jena, Germany) using a 1.40 N.A., 63x, oil immersion objective. EYFP and EGFP were excited with the 488 nm line of an argon ion laser. For EYFP, a 530 - 600 nm band pass filter was used and for EGFP, a 505 - 530 nm band pass filter was used. DiD, Cy5 and AF647 were excited with the 633 nm line of a helium-neon laser and emission was filtered through a 650 nm long pass filter.

All other confocal microscopy images were collected with a FluoView 1000 laser scanning confocal microscope (Olympus) using a 1.42 N.A., 60x, oil immersion objective. ECFP was excited with a 405 nm diode laser, EYFP was excited with the 515 nm line of an argon ion laser and AF647, DiD, and Cy5 were excited by a 635 nm diode laser. For ECFP, a 480–495 nm band pass filter was used to filter emission, for EYFP, a 535–565 nm band pass filter, and for AF647, DiD, and Cy5, a 655-755 nm band pass filter was used. For all images, the pinhole was set to obtain a 1 μm thick optical slice.

2.6 Data analysis

2.6.1 Image processing

For all intensity measurements, raw images were analyzed. Images for presentation were processed equally within each data set using a number of common techniques.

To eliminate cross-channel signal, intensity levels for image analysis were determined by imaging cells labeled with single fluorophores and measuring the light

leaking through incorrect filters. Brightness and contrast were adjusted equally within each data set.

For display images, background was subtracted from images using a built-in ImageJ function. This function performs a top-hat transform on the image using a paraboloid structuring element, called the rolling ball. The rolling ball is the main adjustable parameter of the function and is to be set to a value larger than the radius of the largest feature in the image. Typical rolling balls used for cellular images were 10-50 pixels, depending feature sizes represented in the image.

2.6.2 Colocalization in static images

For the automated colocalization measurements made in Chapter 4, the nuclear and perinuclear region were cropped from images, background was subtracted to allow measurement of the cytoplasm. This was done to eliminate aggregated vesicles and to focus on the vesicles of interest in the cytosol. The aggregated vesicles may or may not have different characteristics than the single cytosolic vesicles characterized in this thesis.

Colocalization was quantified with the ImageJ plugin, JACoP (Just Another Colocalization Plugin; http://rsb.info.nih.gov/ij/plugins/track/jacop.html).[29] Three coefficient measurements were made using JaCOP: Peasons, overlap and Manders'.

The most simple method for measuring colocalization is by plotting the intensity of each pixel of one color against a second color. This creates a scatter plot where a line can be fit. The Pearsons coefficient measures the "spread of this distribution with respect to the fitted line".[29] Output values range from -1, complete

$$r_p = \frac{\sum\left(\left(R_i - R_{avg}\right)\left(G_i - G_{avg}\right)\right)}{\sqrt{\sum\left(R_i - R_{avg}\right)^2 \sum\left(G_i - G_{avg}\right)^2}} \qquad \text{Equation 1}$$

exclusion, to 0, no correlation, to +1, complete correlation. Pearson's coefficient is calculated by Equation 1, where R_i and G_i are the intensities in the red and green channels of pixel i, respectively, and R_{avg} and G_{avg} are the average intensities in the red and green channels.

The overlap coefficient is similar to the Pearson's coefficient but does not take into account the line of best fit . This is manifested by the lack of the average values

$$M_1 = \frac{\sum R_{i,coloc}}{\sum R_i} \quad \text{and} \quad M_2 = \frac{\sum G_{i,coloc}}{\sum G_i} \qquad \text{Equation 2}$$

in the mathematical expression (Equation 2). Because the average is not subtracted, the lowest output value is 0 for complete exclusion and remains 1 for complete correlation. The deletion of the average also makes the overlap coefficient insensive to differences in signal intensities between the channels. This is important for images were the channels are not equally bright.

A main limitation of the Pearson's and overlap coefficients is their inability to measure scenarios were there are many features in one channel and very few features in another. The Manders' coefficient overcomes this by splitting the overlap coefficient into two separate coefficients to determine the degree of colocalization. Output values range from 0, complete exclusion, to +1, complete correlation. Equation 3 is used to determine Manders' coefficient values, where $R_{i,coloc} = R_i$ where

$$R = \frac{\sum R_i \cdot G_i}{\sqrt{\sum R_i^2 \cdot \sum G_i^2}}$$ Equation 3

$G_i > 0$ and $R_{i,coloc} = 0$ where $G_i = 0$ for M_1 and where $G_{i,coloc} = G_i$ where $R_i > 0$ and $G_{i,coloc} = 0$ where $R_i = 0$ for M_2.

In the end, these measurements are hampered by imperfections in overlap, different intensity of two fluorophores and high background. To avoid these imperfections and to ensure that experiments done on different days will provide similar values, we manually measure colocalization. Vesicles were randomly selected by overlaying a 100 μm^2 square grid onto the cell image. Vesicles closest to the center of each square were analyzed. Manual colocalization was assisted by the ImageJ plugin "Image5D" (http://rsb.info.nih.gov/ij/plugins/image5d.html), which allows for the viewing of indiviudal channels.

2.6.3 Colocalization in live cell image sequences

In live cell images, colocalization is defined as one fluorophore having identical motion as a second fluorophore. An important questions is, how long does one have to observe colocalization to differentiate correlated movement from coincident diffusion?

The first constraint is that the there must be at least three consecutive time points where the fluorophores appear colocalized. There is a distinct possiblity of two sequential images where fluorophores appear overlapped, but are not. In all of the live cell image sequences in this thesis, the time between images is 2 s. This requires that the shortest allowable time to qualify as colocalization is 4 s.

Second, using the diffusion of endosomes, the area that a vesicle can possibly sample in 4 s is calculated. Using the Stokes-Einstein equations and approximating the viscosity of the cytosol as six times that of water and the vesicle as having a radius of 125 nm, we calculate the diffusion coefficient of an endocytic vesicle to be $5.56 * 10^{-13}$ m^2/s. This corresponds to a 2.1 μm radius area where the vesicle can possibly be found after 4 s of diffusion.

Using MATLAB, a simulation of two diffusing particles making a random walk with a gaussian distribution of step sizes demonstrates that two diffusing vesicles separate after 4 s. In this simulation, two vesicles start at exactly the same spot. After 4 seconds of independent diffusion, the distance between the two vesicles is measured. For 100 sets of 100 measurements, in 2.7 ± 1.6% the final distance is less than 250 nm, roughly the difraction limit of visible light (Figure 2.6A). This represents an upper bound for miscounted cases as most vesicles will not start at *exactly* the same place and not all will undergo solely diffusional motion.

Increasing the 4 s minimum requirement further decreases false-positive events where non-fully fusing vesicles from being counted. In Chapter 5, the minimum interaction time is raised to 10 seconds. To quantify the increased selectivity, the same simulation was run to measure vesicle separation after 10 s. After 100 sets of 100 measurements, 1.3 ± 1.2% particles were still found in the same diffraction limited area (Figure 2.6B), a 2-fold improvement over the same measurement after 4 seconds.

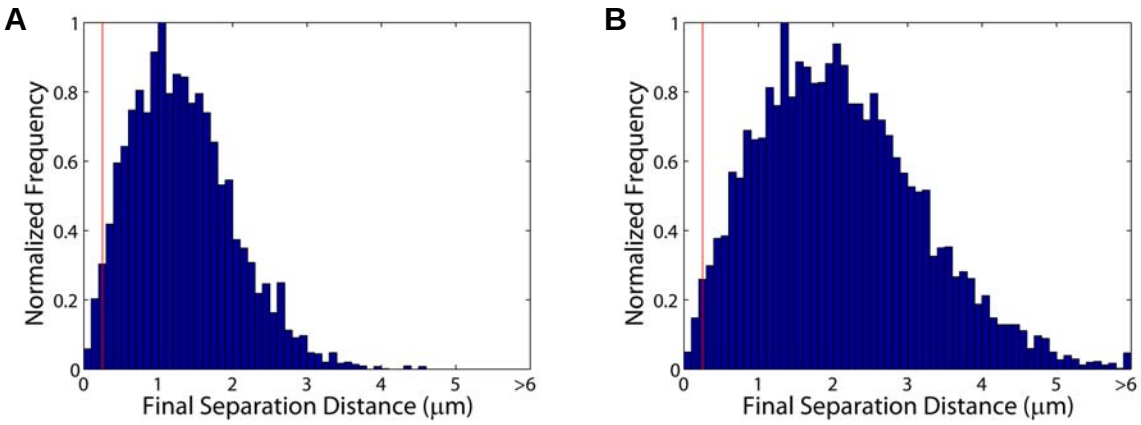

Figure 2.6 Simulation of vesicle diffusion in live cells. A) The separation distance of two vesicles after diffusing for 4 seconds. The red line indicates the diffraction limit. Vesicles below this distance appear colocalized. B) The same measurement after diffusing for 10 s. When the minimum interaction distance is lengthened from 4 s to 10 s, the possibility of an incorrect measurement is 2 times less likely.

2.6.4 Single particle tracking

ImageJ (http://rsb.info.nih.gov/ij/) was used to track and quantify colocalization. Particle tracking was performed with the ImageJ plugin, "Manual Tracking" (http://rsb.info.nih.gov/ij/plugins/track/track.html). Using this plug in, a vesicle of interest was clicked on in each image of an image sequence. The plugin then finds the pixel with the highest intensity in a user-defined region and records its position and intensity. In all experiments a 5 x 5 pixel area, representative of the largest vesicles tracked, is used.

2.6.5 Significance testing

Significance testing was performed using p-values. A p-value is the probability that two measured distributions are from the same statistical set. The p-values reported in Chapters 4 and 5 are obtained using a two-tailed Welch's t-test. The Welch's t-test is similar to the more common student t-test but does not assume that the variance of the two distributions are the same.[30]

2.7 References

1 Hopps, H. E.; Tjio, J. H.; Bernheim, B. C.; Smadel, J. E.; Nisalak, A., Biologic characteristics of a continuous kidney cell line derived from african green monkey. *J. Immunol.* **1963**, *91*, 416-424.

2 Sonnichsen, B.; De Renzis, S.; Nielsen, E.; Rietdorf, J.; Zerial, M., Distinct membrane domains on endosomes in the recycling pathway visualized by multicolor imaging of Rab4, Rab5, and Rab11. *J. Cell Biol.* **2000**, *149*, 901-914.

3 Lakadamyali, M.; Rust, M. J.; Zhuang, X., Ligands for clathrin-mediated endocytosis are differentially sorted into distinct populations of early endosomes. *Cell* **2006**, *124*, 997-1009.

4 Barbero, P.; Bittova, L.; Pfeffer, S. R., Visualization of Rab9-mediated vesicle transport from endosomes to the trans-Golgi in living cells. *J. Cell Biol.* **2002**, *156*, 511-518.

5 Sherer, N. M.; Lehmann, M. J.; Jimenez-Soto, L. F.; Ingmundson, A.; Horner, S. M.; Cicchetti, G.; Allen, P. G.; Pypaert, M.; Cunningham, J. M.; Mothes, W., Visualization of retroviral replication in living cells reveals budding into multivesicular bodies. *Traffic* **2003**, *4*, 785-801.

6 Chavrier, P.; Parton, R. G.; Hauri, H. P.; Simons, K.; Zerial, M., Localization of low-molecular-weight GTP-binding proteins to exocytic and endocytic compartments. *Cell* **1990**, *62*, 317-329.

7 Simonsen, A.; Lippe, R.; Christoforidis, S.; Gaullier, J. M.; Brech, A.; Callaghan, J.; Toh, B. H.; Murphy, C.; Zerial, M.; Stenmark, H., EEA1 links PI(3)K function to Rab5 regulation of endosome fusion. *Nature* **1998**, *394*, 494-498.

8 Christoforidis, S.; McBride, H. M.; Burgoyne, R. D.; Zerial, M., The Rab5 effector EEA1 is a core component of endosome docking. *Nature* **1999**, *397*, 621-625.

9 Geuze, H. J.; Slot, J. W.; Strous, J. A. M.; Hasilik, A.; Vonfigura, K., Possible pathways for lysosomal-enzyme delivery. *J. Cell Biol.* **1985**, *101*, 2253-2262.

10 Geuze, H. J.; Stoorvogel, W.; Strous, G. J.; Slot, J. W.; Bleekemolen, J. E.; Mellman, I., Sorting of mannose 6-phosphate receptors and lysosomal membrane-proteins in endocytic vesicles. *J. Cell Biol.* **1988**, *107*, 2491-2501.

11 Griffiths, G.; Hoflack, B.; Simons, K.; Mellman, I.; Kornfeld, S., The mannose 6-phosphate receptor and the biogenesis of lysosomes. *Cell* **1988**, *52*, 329-341.

12 Sahagian, G. G.; Neufeld, E. F., Biosynthesis and turnover of the mannose 6-phosphate receptor in cultured chinese-hamster ovary cells. *J. Biol. Chem.* **1983**, *258*, 7121-7128.

13 Brown, W. J.; Goodhouse, J.; Farquhar, M. G., Mannose-6-phosphate receptors for lysosomal-enzymes cycle between the golgi-complex and endosomes. *J. Cell Biol.* **1986**, *103*, 1235-1247.

14 Kang, J. X.; Bell, J.; Leaf, A.; Beard, R. L.; Chandraratna, R. A. S., Retinoic acid alters the intracellular trafficking of the mannose-6-phosphate/insulin-like growth factor II receptor and lysosomal enzymes. *Proc. Natl. Acad. Sci. U. S. A.* **1998**, *95*, 13687-13691.

15 Li, G.; D'Souza-Schorey, C.; Barbieri, M. A.; Roberts, R. L.; Klippel, A.; Williams, L. T.; Stahl, P. D., Evidence for phosphatidylinositol 3-kinase as a regulator of endocytosis via activation of Rab5. *Proc. Natl. Acad. Sci. USA* **1995**, *92*, 10207-10211.

16 Martys, J. L.; Wjasow, C.; Gangi, D. M.; Kielian, M. C.; McGraw, T. E.; Backer, J. M., Wortmannin-sensitive trafficking pathways in Chinese hamster ovary cells: Differential effects on endocytosis and lysosomal sorting. *J. Biol. Chem.* **1996**, *271*, 10953-10962.

17 Shpetner, H.; Joly, M.; Hartley, D.; Corvera, S., Potential sites of PI-3 kinase function in the endocytic pathway revealed by the PI-3 kinase inhibitor, wortmannin. *J. Cell Biol.* **1996**, *132*, 595-605.

18 Gruenberg, J.; Stenmark, H., The biogenesis of multivesicular endosomes. *Nat Rev Mol Cell Biol* **2004**, *5*, 317-323.

19 Payne, C. K.; Jones, S. A.; Chen, C.; Zhuang, X. W., Internalization and trafficking of cell surface proteoglycans and proteoglycan-binding ligands. *Traffic* **2007**, *8*, 389-401.

20 Weber, G.; Young, L. B., Fragmentation of boine serum albumin by pepsin. 1. Origin of acid expansion of albumin molecule. *J. Biol. Chem.* **1964**, *239*, 1415-1423.

21 Weber, G.; Young, L. B., Fragmentation of bovine serum albumin by pepsin. 2. Isolation, amino acid composition, and physical properties of fragments. *J. Biol. Chem.* **1964**, *239*, 1424-1432.

22 Shimomura, O., Structure of the chromophore of aequorea green fluorescent protein. *FEBS Lett.* **1979**, *104*, 220-222.

23 Chalfie, M.; Tu, Y.; Euskirchen, G.; Ward, W. W.; Prasher, D. C., Green Fluorescent Protein as a Marker for Gene Expression. *Science* **1994**, *263*, 802-805.

24 Tsien, R. Y., The green fluorescent protein. *Annu. Rev. Biochem* **1998**, *67*, 509-544.

25 Giepmans, B. N. G.; Adams, S. R.; Ellisman, M. H.; Tsien, R. Y., Review - The fluorescent toolbox for assessing protein location and function. *Science* **2006**, *312*, 217-224.

26 Brandenburg, B.; Zhuang, X. W., Virus trafficking - learning from single-virus tracking. *Nature Reviews Microbiology* **2007**, *5*, 197-208.

27 Lakadamyali, M.; Rust, M. J.; Babcock, H. P.; Zhuang, X. W., Visualizing infection of individual influenza viruses. *Proc. Natl. Acad. Sci. U. S. A.* **2003**, *100*, 9280-9285.

28 Rust, M. J.; Lakadamyali, M.; Zhang, F.; Zhuang, X. W., Assembly of endocytic machinery around individual influenza viruses during viral entry. *Nat. Struct. Mol. Biol.* **2004**, *11*, 567-573.

29 Bolte, S.; Cordelieres, F. P., A guided tour into subcellular colocalization analysis in light microscopy. *J. Microsc.-Oxford* **2006**, *224*, 213-232.

30 Welch, B. L., The generalization of `student's' problem when several different population variances are involved. *Biometrika* **1947**, *34*, 28-35.

CHAPTER 3

INTRACELLULAR DEGRADATION OF LOW-DENSITY LIPOPROTEIN PROBED WITH TWO-COLOR FLUORESCENCE MICRSCOPY

3.1 Summary

The intracellular, vesicle-mediated degradation of extracellular cargo is an essential cellular function. Using two-color single particle tracking fluorescence microscopy, we have probed the intracellular degradation of low-density lipoprotein (LDL) in living cells. Unique to these experiments are individual LDL particles heavily labeled with multiple fluorophores resulting in a quenched fluorescent signal. The degradation of the LDL particle then results in an increase in fluorescence. Endocytic vesicles were fluorescently labeled with variants of GFP. We imaged their transient colocalization of LDL with endocytic vesicles while simultaneously measuring the intensity of the LDL particle as an indicator of degradation. These studies, which are the first to directly observe the degradation of LDL within a living cell, demonstrate that late endosomes are active sites of degradation for LDL. Measurement of the time from colocalization with lysosome-associated membrane protein 1 (LAMP1) vesicles to degradation suggests that LAMP1-vesicles initiate the degradative event**.** Observing degradation as it occurs in living cells makes it possible to describe the complete endocytic pathway of LDL from internalization to degradation. More generally, this research provides a model for the intracellular degradation of extracellular cargo and a method for its study in living cells.

3.2 Introduction

Cells require the intracellular degradation of extracellular cargo to utilize nutrients and down-regulate receptors.[2] LDL is perhaps the best-studied example of extracellular

cargo.[2-7] Intracellular hydrolysis of LDL provides the necessary cholesterol for the formation of new membranes. Extensive studies of LDL have made it a benchmark for endocytic transport.[1,8-10] In brief, LDL binds to the LDL receptor, is internalized through a clathrin-mediated pathway, and is then transported to early endosomes. A decrease in the pH of the early endosomes causes LDL to dissociate from the receptor. The receptor is recycled to the cell surface while LDL proceeds through the endosomal pathway with the maturation of early endosomes to form late endosomes.[8,10]

LDL cannot be utilized by the cell without enzyme-mediated degradation. The intracellular degradation of extracellular cargo encompasses multiple chemical reactions mediated by lysosomal enzymes. To fully understand the degradative process it is necessary to observe the degradative event and associated transport as it occurs within a living cell. A key step in this process is the interaction of lysosomal enzymes with the endocytosed LDL. In a classic model of lysosomal degradation, a LDL-containing late endosome transports LDL to an enzyme-containing lysosome. Lysosomal enzymes degrade LDL and the degraded components are able to diffuse out of the lysosome for processing by the cell. A more detailed examination of the degradation pathway demonstrates that lysosomal enzymes are not restricted to the lysosomes, but are also present and active in early and late endosomes,[11-15] presenting a more complex picture of lysosomal degradation. Multiple types of extracellular cargo, including EGF and BSA, have been shown to undergo at least partial degradation before reaching the lysosomes.[11,13,16] LDL exposed to isolated and ruptured early and late endosomes is degraded, although prelysosomal degradation of LDL was not observed *in vivo*.[14]

The goal of our research is to measure the degradation of LDL directly, without the need to isolate endosomes or cargo. By imaging specific populations of vesicles and the degradative event simultaneously, we are able to not only determine which endosomal or lysosomal vesicle is responsible for degradation, but what specific interactions lead to degradation. These questions must be probed on an organelle-specific level, to distinguish late endosomes and lysosomes, and with sufficient time resolution to monitor the continual transport of LDL and endocytic vesicles within the cell. Fluorescence microscopy, combined with single particle tracking analysis, provides a method to follow the motion of individual vesicles and LDL particles within living cells.[17-19] Used in a two-color configuration, single particle tracking allows us to capture transient interactions that would not be detected in fixed cells. Organelle-specificity can be accomplished using GFP variants to label specific populations of endocytic vesicles, such as early and late endosomes.

Unique to our experiments is the ability to correlate interactions of vesicles with the enzyme-mediated degradation of LDL, all within live cells. This is accomplished with the use of a labeling scheme that takes advantage of the photophysical properties of a lipophilic fluorophore. By labeling the LDL particle with multiple fluorophores, the fluorescent signal from the LDL particle is quenched resulting in weak emission from the LDL particle. As the LDL particle degrades and the fluorophores are no longer in close proximity, the fluorescence increases. Dequenching has been used previously to monitor changes in particle integrity, perhaps most commonly in virology.[20] We apply the same photophysical principles to monitor an intracellular enzymatic degradation. Our labeling scheme provides an extra dimension to fluorescence imaging. In addition to identifying

interactions between endocytic vesicles and LDL, we simultaneously measure reactivity as an increase in intensity of the LDL particle is indicative of hydrolytic degradation. Using this labeling scheme it is possible to associate vesicle interactions with productive degradation.

Using this approach, we show that the degradation of LDL occurs in an endosome that is positive for the standard late endosomal proteins Rab7 and cation-independent mannose-6-phosphate receptor (M6PR). We also demonstrate that transport to the late endosome is essential for degradation, with minimal degradation observed in early endosomes or in wortmannin-treated cells. We measure the time from colocalization to degradation and find that it is highly correlated with the lysosomal protein, LAMP1, supporting a model in which lysosomes act as enzyme storage vesicles.[21-23] In the case of LDL, observing degradation as it occurs in living cells makes it possible to describe the complete endocytic pathway of LDL from internalization to degradation. More generally, characterizing the intracellular degradation of LDL provides a model for the intracellular degradation of extracellular cargo.

3.3 Results

3.3.1 Fluorescent labeling of LDL to observe intracellular degradation

LDL particles were labeled with multiple copies of the lipophilic dye, DiD. The standard labeling scheme for the LDL used in the experiments described below was ~200 DiD molecules for each LDL particle. As the LDL-DiD particle undergoes enzyme-

mediated degradation and the DiD molecules are no longer in close proximity, we expect to observe a concomitant increase in fluorescence, described as dequenching.

The number of fluorescent DiD molecules per LDL particle are calculated from the absorption spectrum of the labeled LDL after excess dye is removed using size exclusion chromatography. The absorption of pure LDL or pure DiD of known concentrations is measured to calculate the extinction coefficient of the dye in PBS, the solvent used for the DiD-labeled LDL. LDL absorbs at 280 nm and DiD absorbs at 650 nm. In the absorption ranges used, the signal from LDL at 650 nm or DiD at 280 nm is negligible.

The determination of the extinction coefficient is achieved by plotting the absorption at a specific wavelength as a function of concentration. The slope of the best fit line is the extinction coefficient multiplied by the known path length. Using this method, we measure the extinction coefficient of LDL in PBS as 860,000 M^{-1} cm^{-1} and the extinction coefficient of DiD in PBS is determined to be 6,100 M^{-1} cm^{-1}. The data used to calculate the extinction coefficients is shown in Figure 3.1. Using these values

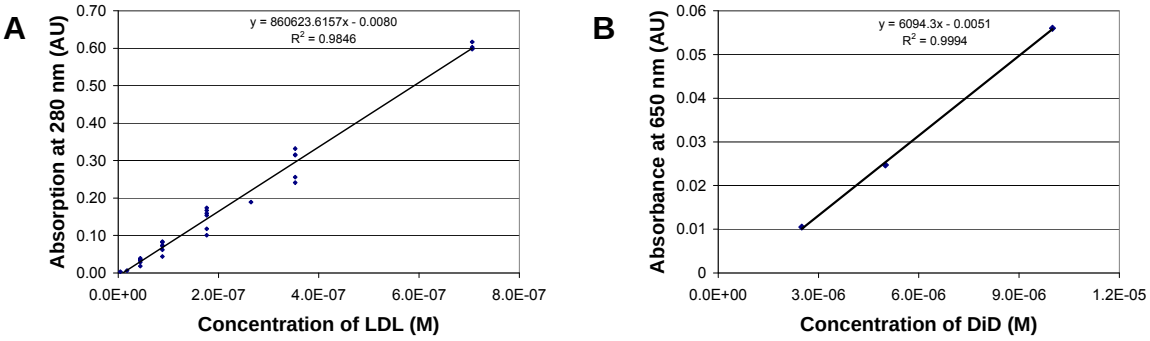

Figure 3.1 Measuring extinction coefficients of LDL and DiD. (A) A plot of concentration and absorption of LDL. This slop of this plot is equal to the extinction coefficient of LDL, which is measured to be 860,000 M^{-1} cm^{-1}. (B) A similar plot for DiD. The extinction coefficient of DiD is determined to be 6,100 M^{-1} cm^{-1}.

and Beer's Law, the concentration of LDL and DiD can be independently calculated. The ratio of DiD molecules to LDL molecules is then reported.

3.3.2 Dequenching of LDL-DiD requires enzymatic activity

Characterization of the fluorescently labeled LDL, referred to as LDL-DiD, was first carried out *in vitro*, in the absence of cells, using a fluorimeter to measure changes in fluorescence emission (Figure 3.2). Dequenching was measured as a ratio of fluorescence emission before and after incubation with trypsin (2 hrs, 37°C), a degradative enzyme, or, as a control, at room temperature in the absence of enzyme. Incubation with trypsin at 37°C resulted in a factor of 2.3 increase in fluorescence. No change in signal would be a value of 1. In comparison, identically labeled LDL-DiD incubated at room temperature or 37°C for 2 hrs in the absence of trypsin showed minimal increase in fluorescence intensity. Similarly, incubation at pH 5.5, the pH of the late endosome,[2] and 37°C resulted in little change in intensity. Emission measurements were normalized by the absorption of LDL-DiD before and after incubation, although there was relatively little change in absorption (Figure 3.2B).

Trypsin, while sufficient to show the change in fluorescence intensity due to degradation of the protein component of LDL, is not a biologically relevant enzyme. Cathepsin B is a known protease for apolipoprotein B-100, the protein component of LDL, in the endocytic pathways.[24] Because of this, degradation of the DiD-labeled LDL with cathepsin B (0.66 mg/mL) was examined. Surprisingly, cathepsin B does not cause dequenching by itself (Figure 3.3). This lack of dequenching upon degradation with cathepsin B is most likely due to the inability of cathepsin to repeatedly cut the protein,

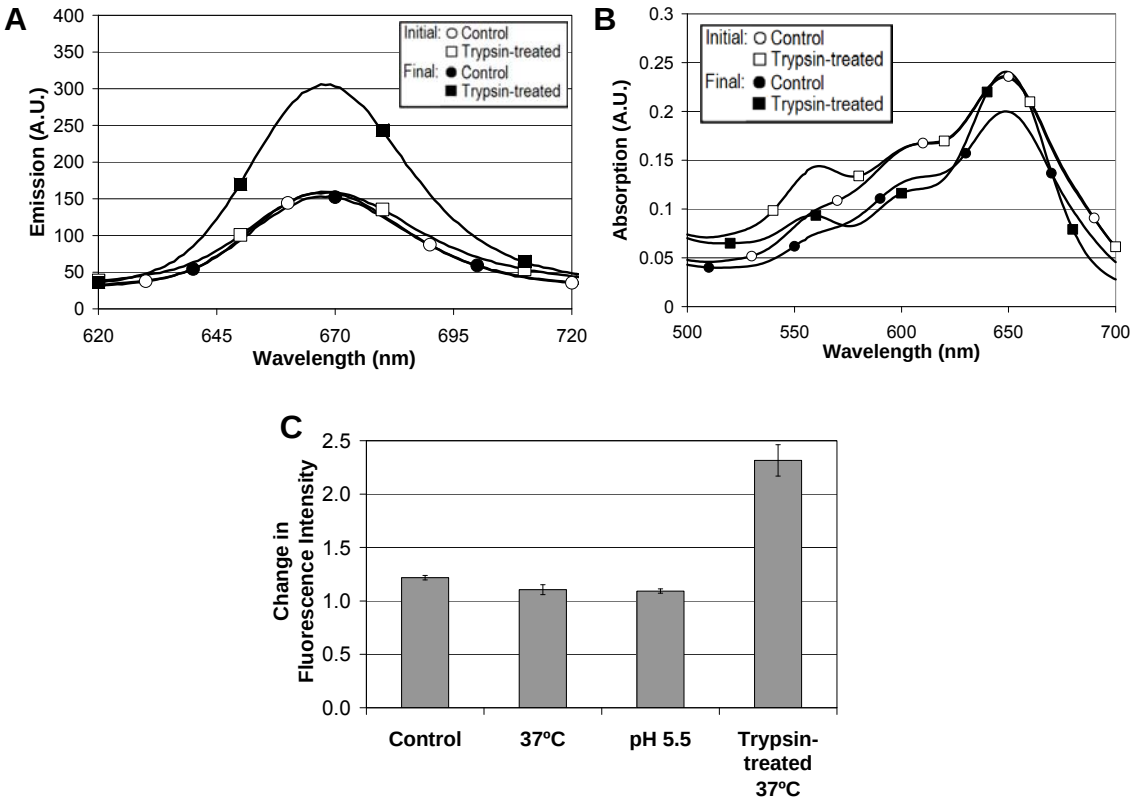

Figure 3.2 *In vitro* dequenching of LDL. (A) Emission spectra of LDL-DiD in solution following excitation at 600 nm. Final spectra were measured after a 2 hr incubation at either room temperature (control) or in the presence of trypsin at 37ºC. Absorption spectra showed little change after incubation and are included in the Electronic Supplemental Information Figure S1. (B) The absorption of LDL-DiD shows little change after a 2 hr incubation with trypsin at 37°C. The control is a 2 hr incubation at room temperature in the absence of trypsin. (C) Trypsin-treated LDL-DiD particles increased emission by a factor of 2.3 compared to a control sample incubated at room temperature. In the absence of trypsin, LDL-DiD showed only a slight increase in emission. A value of 1.0 indicates no change. The pH 5.5 incubation mimics the pH of the late endosome. Error bars represent the standard deviation of 3 experiments.

like trypsin. It is possible that multiple proteases can cause dequenching of LDL-DiD. However, further experiments are required to fully elucidate the combination of biologically relevant proteases are necessary to cause the dequenching of LDL-DiD.

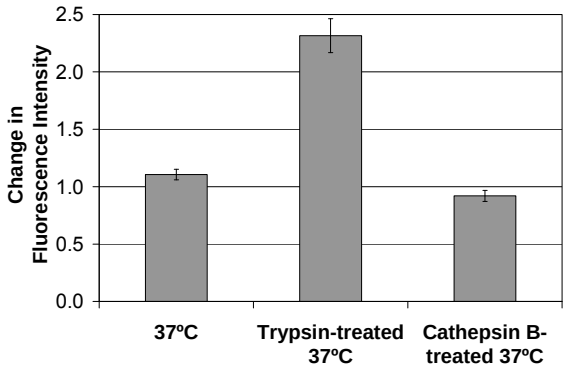

Figure 3.3 Comparison of dequenching due to trypsin and cathepsin B. Trypsin causes a 2.3 change in fluorescence intensity. However, cathepsin B-treatment does not cause a change in fluorescence intensity. This may be due to the number of cleavage sites available to the enzyme. This is expected because cathepsin B is a much more selective enzyme than trypsin.

3.3.3 Trypsin degrades LDL-DiD

To confirm that the increased fluorescence of LDL-DiD was a result of LDL degradation, we used gel electrophoresis to measure the degradation of the LDL apolipoprotein B-100. LDL-DiD was incubated in the presence of trypsin (2 hrs, 37°C) and then loaded onto a polyacrylamide gel (4-20% gradient). Cathepsin B (0.66 mg/mL), a known protease for apolipoprotein B-100,[24] was used as a comparison to trypsin. As expected from the dequenching results, trypsin leads to the appearance of multiple protein fragments, indicative of degradation (Figure 3.4A). Incubation with cathepsin B also leads to degradation. LDL incubated for 2 hrs in the absence of trypsin or cathepsin B does not show degradation. Additionally, labeling with DiD does not inhibit or alter degradation as LDL and LDL-DiD show similar staining patterns under all conditions.

Each enzyme, trypsin and cathepsin B, have characteristic bands. The molecular weight of trypsin is 23 kDa and the molecular weight of mature cathepsin B is 26 kDa.

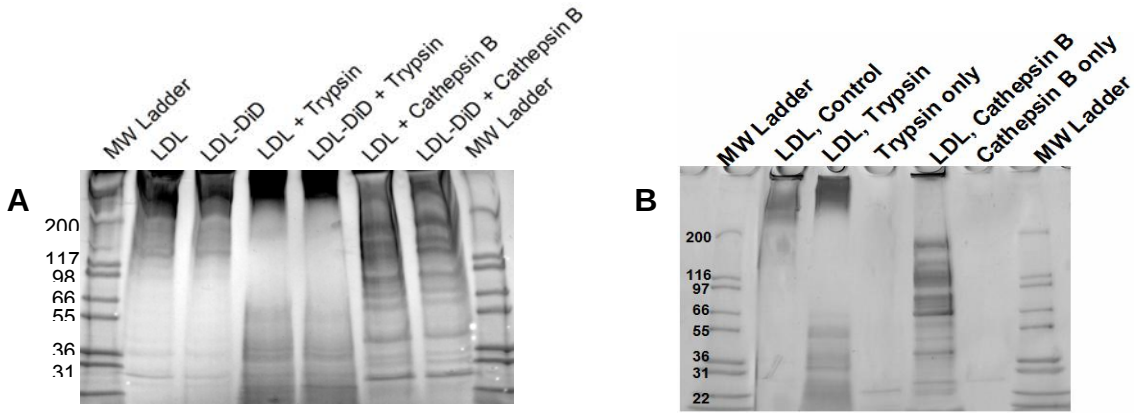

Figure 3.4 Trypsin degrades LDL-DiD. (A) Gel electrophoresis (4-20% gradient, polyacrylamide, SimplyBlue SafeStain) shows that treatment of LDL with trypsin or cathepsin B results in the appearance of multiple protein fragments in comparison to untreated LDL. DiD labeling of LDL (~200 DiD:LDL) does not inhibit degradation with trypsin or cathepsin B. (B) Further studies show the reproducibility of the degradation and also the bands due to the enzymes used.

Bands in the SDS-PAGE gel can be assigned to these enzymes by control experiments (Figure 3.4B)

Another piece of information that is found in Figure 3 is that trypsin-treated causes LDL to appear larger. This can be confirmed by DLS and verified by the literature.[24] Trypsin-treatment degrades the protein component of LDL leaving a liposome-like particle capable of fusing with other degraded LDL particles. For Figure

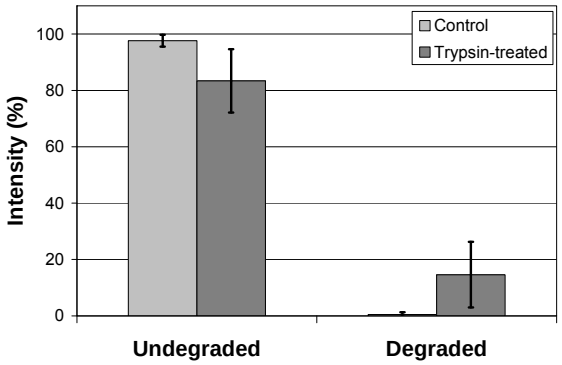

Figure 3.5 LDL becomes fusogenic upon trypsin-treatment. Dynemic light scattering measurements quantify the percent of larger liposome-like particles. Samples are prepared as in Figure 3.2 and then diluted to 1 mL for measurement.

3.5, unlabeled LDL solutions degraded similar to those measured in Figure 3.2. After degradation, the samples were diluted to 1 mL and measured using a Malvern NanoZS. The results show that approximately 15% of the LDL fuses into larger particles.

3.3.4 Endocytosis of LDL is not disrupted by DiD

The endocytic pathway of LDL is well-characterized; LDL binds to the LDL receptor on the cell surface, is internalized via clathrin-mediated endocytosis, and is transported by early endosomes which mature into late endosomes.[2-4] It is important to ensure that the high degree of DiD labeling does not affect endocytosis of LDL-DiD. Endocytosis was tested using less heavily labeled LDL-DiD, with ~50 DiD molecules per LDL particle, as a control. To ensure internalization and transport were not disrupted by DiD labeling, colocalization with LAMP1, indicative of delivery to a terminal vesicle, was measured with confocal microscopy at a series of time points following incubation with LDL-DiD (Figure 3.6A and 3.6B). Over a time period of 1 hr, both LDL labeling schemes resulted in the same level of transport to LAMP1-vesicles with close to 100% colocalization at 1 hr (Figure 3.6E). No difference in internalization or transport was observed as a function of the degree of labeling.

3.3.5 Two-color single particle tracking of Rab7-endosomes and LDL-DiD

Single particle tracking allows us to follow the motion of fluorescently-labeled cargo or organelles, in real time, in live cells. In a two-color configuration, interactions between two different fluorophores can also be observed. This is especially important for transient interactions which cannot be detected in static fluorescence microscopy. Using

the increase in LDL-DiD signal as a measure of degradation, two-color single particle tracking was used to correlate degradation of LDL with localization in a specific population of endosomes.

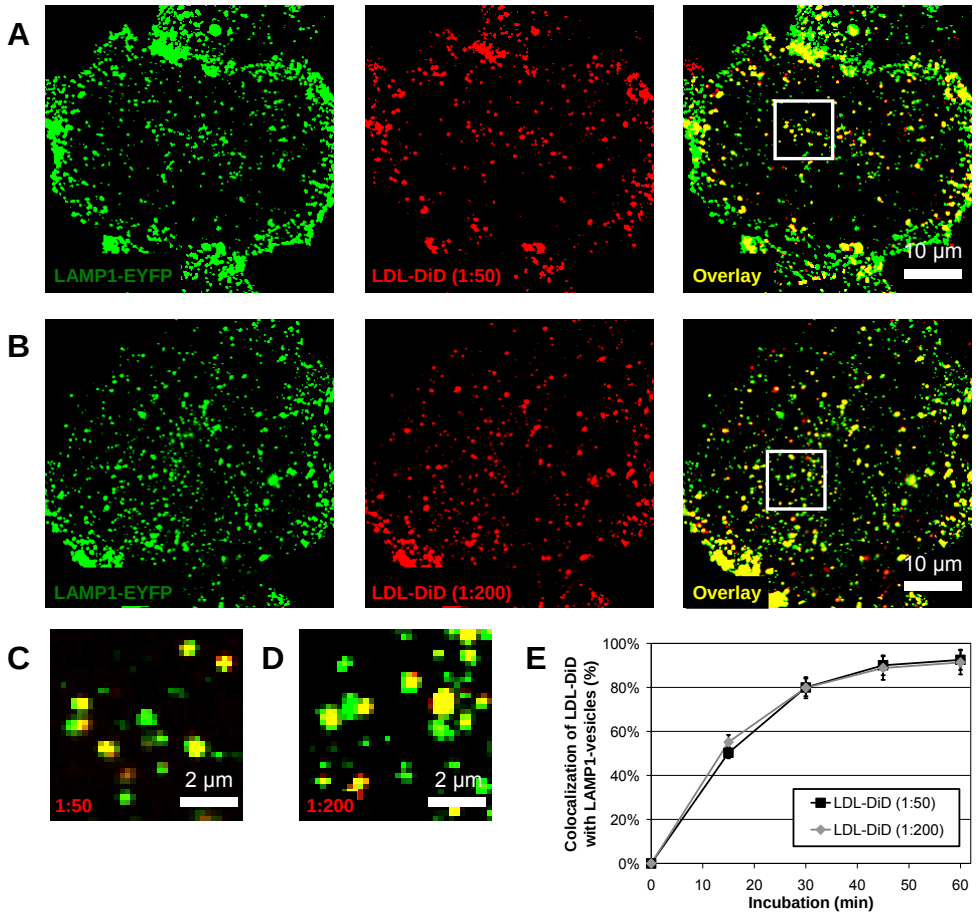

Figure 3.6 Cellular internalization of LDL is not disrupted by DiD**.** (A) Confocal microscopy image of LDL labeled with 50 DiD molecules (red), a previously described labeling scheme,[1] and LAMP1-EYFP (green), following a 1 hr incubation. LAMP1 serves as a marker of a terminal vesicle in the endocytic pathway. (B) Confocal microscopy image of LDL labeled with 200 DiD molecules (red) and LAMP1-EYFP (green) following a 1 hr incubation. A ratio of 200 DiD:LDL was used in dequenching experiments. (C) Expanded region (shown in white box) of (A). (D) Expanded region (shown in white box) of (B). (E) Colocalization of LDL-DiD with LAMP1-EYFP, measured at increasing times following the addition of LDL-DiD, shows that the labeling density does not affect the intracellular transport of LDL-DiD. Colocalization was scored manually and error bars show the standard deviation for >150 LDL-DiD particles per cell in 4-5 cells.

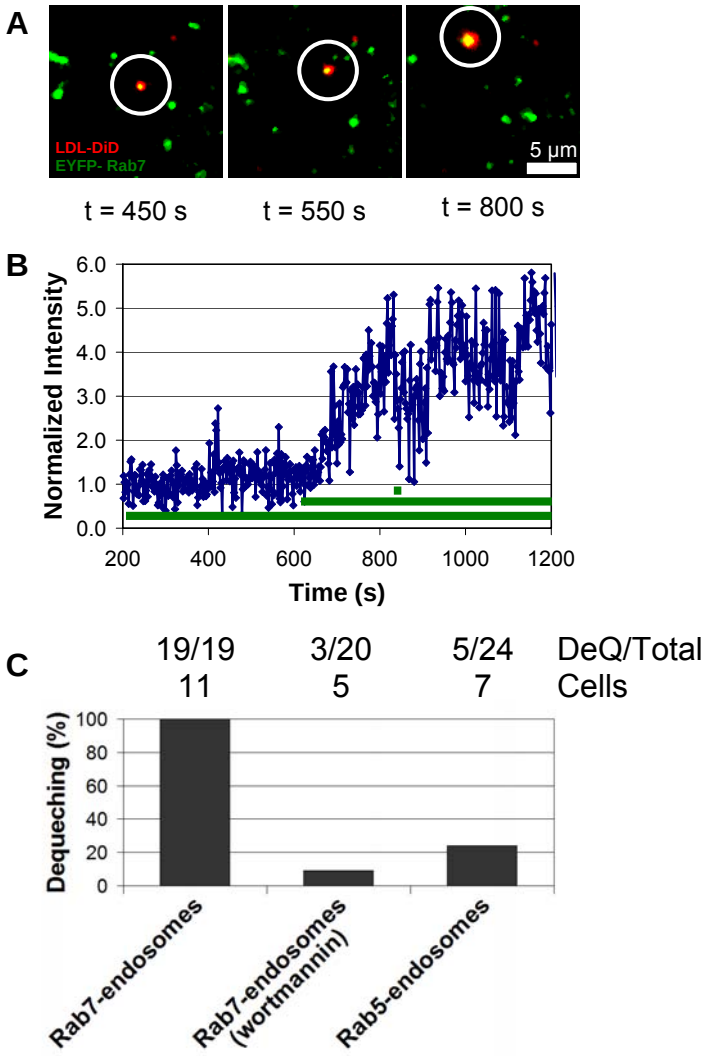

Figure 3.7 Two-color single particle tracking of LDL-DiD and EYFP-Rab7. (A) Snapshots illustrating the dequenching of LDL-DiD (red) following interactions with an EYFP-Rab7 labeled endosome (green). Images are recorded at a rate of 0.5 Hz. (B) Intensity of the LDL-DiD particle as a function of time. The horizontal bars under the intensity trace indicate periods during which LDL-DiD was colocalized with a Rab7-endosome. (C) All dequenching events were observed during colocalization with a Rab7-endosome. The use of wortmannin to inhibit transport to the late endosomes significantly reduced the number of dequenching events observed. The observation of dequenching in ECFP-Rab5 labeled early endosomes was similarly rare. All dequenching percentages are normalized against untreated Rab7-endosomes.

Data are collected as movies from which the motion of Rab7-endosomes (green) and LDL-DiD (red) are tracked simultaneously (Figure 3.7A). The intensity of the LDL-DiD particle is recorded during tracking measurements (Figure 3.7B). LDL-DiD is considered dequenched if the intensity of the particle increases by a factor of 2 within a period of 100 s. The horizontal bars under the intensity trace indicate times during which the LDL-DiD particle was colocalized with a Rab7-endosome. To be considered colocalized, the respective fluorescent signals had to overlap and move through the cell together for a minimum of 4 s. The behavior displayed in this plot is representative of all the LDL-DiD particles that dequenched. Colocalization with Rab7-endosomes occurred soon after internalization of LDL-DiD, often before tracking began. Typically a second, or even third, Rab7-endosome fused with the initial Rab7-endosome containing the LDL-DiD particle. Dequenching occurred while the LDL-DiD particle was colocalized with Rab7-endosomes. Dequenching of LDL-DiD particles in Rab7-endosomes was observed for 19 LDL-DiD particles in 11 cells. Dequenching was not observed in the absence of colocalization with Rab7-endosomes.

3.3.6 Wortmannin treatment blocks the dequenching of LDL-DiD

To confirm that colocalization with Rab7-endosomes is necessary for dequenching, we used wortmannin, a PI(3)K inhibitor, to block endocytic transport of LDL to late endosomes.[25-29] The use of wortmannin (240 nM) to block transport to the Rab7-endosomes was measured with confocal microscopy following a 1 hr incubation with LDL-DiD (Figure 3.8). A 60% decrease in colocalization with Rab7 was observed following wortmannin treatment, in good agreement with previous results.[1] In

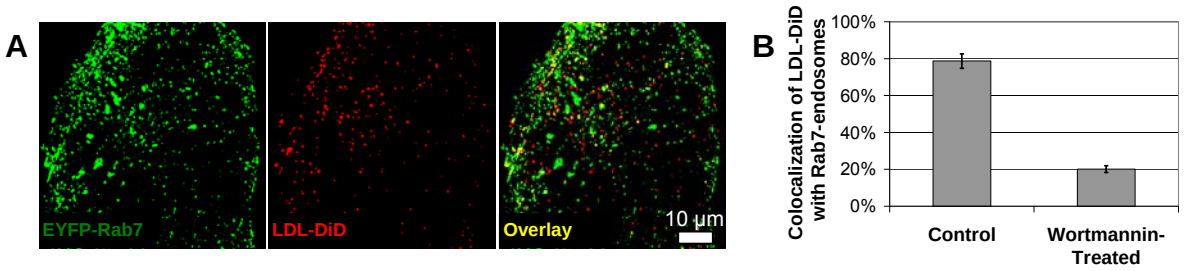

Figure 3.8 Wortmannin inhibits transport of LDL to the late endosomes. (A) Confocal microscopy image of a cell treated with wortmannin (240 nM) and incubated with LDL-DiD (red) for 1 hr. (B) Decreased colocalization of LDL-DiD with EYFP-Rab7 (green) shows that transport to Rab7-endosomes is inhibited by wortmannin. Error bars represent the standard deviation of 120 LDL-DiD particles/cell in 3 cells.

wortmannin-treated cells, with the transport to the late endosomes inhibited, dequenching of LDL-DiD was rarely observed (Figure 3.7C). Only three, of twenty particles tracked, underwent dequenching in wortmannin-treated cells. These experiments also serve as a control to insure that the increase in LDL fluorescence, interpreted as dequenching resulting from degradation, is not due to a decrease in the number of photoactive fluorophores following photobleaching or a shift in microscope focus.

3.3.7 Colocalization with Rab5-endosomes does not lead to dequenching

As a second control, we tested whether entry into an early endosome could lead to dequenching, either due to lysosomal enzyme activity in the early endosomes[14] or as an artifact through the transfer of DiD to the endosomal membrane. While the wortmannin experiments address these questions by blocking transport of LDL-DiD to the late endosomes, we also tested this in a drug-free assay. We labeled the early endosomes with EGFP-Rab5, an early endosomal protein,[29,30] which was confirmed with EEA1 colocalization.[29-31] Two-color imaging experiments show very little dequenching during the interaction of LDL-DiD with Rab5-endosomes (Figure 3.7C), further demonstrating that the interaction with Rab7-endosomes is necessary and specific for dequenching.

3.3.8 Two-color single particle tracking of LAMP1-vesicles and LDL-DiD

The observed degradation of LDL-DiD in a Rab7-endosome raises the question of the role of the lysosome, the canonical degradative vesicle, in this process. Despite the name, the lysosome-associated membrane protein 1 (LAMP1) is associated with late endosomes as well as lysosomes.[21,32] For this reason, we refer to the LAMP1-associated organelle generically as a vesicle. In the BS-C-1 cells used in these experiments, we measure >80% colocalization of ECFP-Rab7 and LAMP1-EYFP (Figure 3.9A). Two-color live cell images demonstrate that these two populations of vesicles, while highly colocalized, are distinct and dynamic (Figure 3.9B). Tracking these vesicles over time shows that Rab7 and LAMP1 are typically colocalized, but undergo short periods of separation before pairing with new vesicles (Figure 3.9C). A histogram of times during

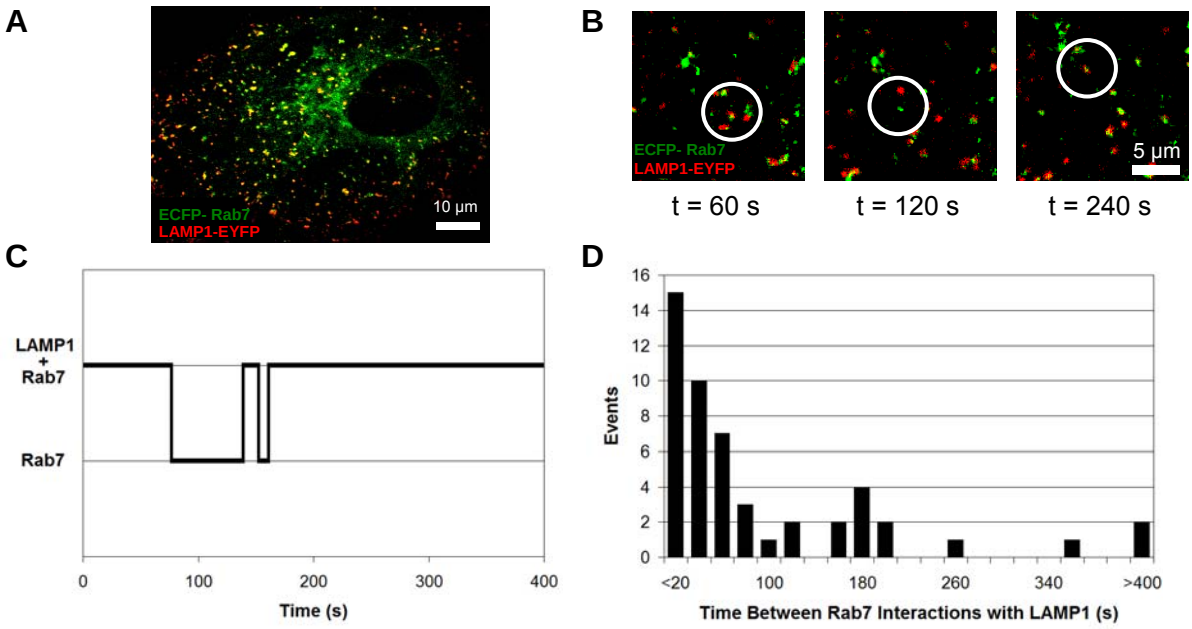

Figure 3.9 Interaction of Rab7-endosomes and LAMP1-vesicles. (A) Colocalization of ECFP-Rab7 (green) and LAMP1-EYFP (red). (B) Snapshots illustrating two-color single particle tracking of ECFP-Rab7 (green) and LAMP1-EYFP (red) show a Rab7- and LAMP1-positive vesicle that separates before the Rab7-endosome interacts with a different LAMP1-vesicle. (C) Measurement of colocalization as a function of time. (D) A histogram of time periods during with Rab7 and LAMP1 are not colocalized.

with Rab7 and LAMP1 are separated shows that most periods of separation are <100s (Figure 3.9D). On average, 10% of Rab7-endosomes and LAMP1-vesicles are found in the cell as distinct, non-colocalized, vesicles.

The short periods during which LAMP1-vesicles were not associated with Rab7-endosomes encouraged us to examine the role of LAMP1-vesicles in LDL degradation. Using the same two-color tracking scheme as described for EYFP-Rab7 and LDL-DiD,

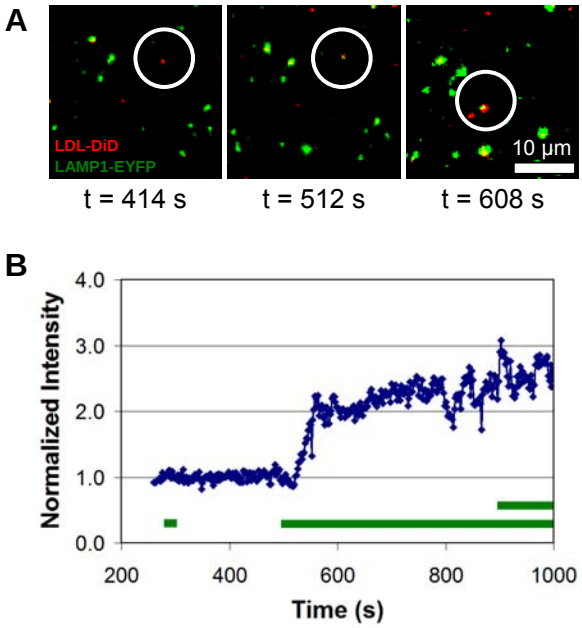

Figure 3.10 Two-color single particle tracking of LDL-DiD and LAMP1-EYFP. (A) Snapshots illustrating the dequenching of LDL-DiD (red) following interactions with a LAMP1-EYFP labeled vesicle (green). Images are recorded at a rate of 0.5 Hz. (B) Intensity of the LDL-DiD particle as a function of time. The horizontal bars under the intensity trace indicate periods during which LDL-DiD was colocalized with a LAMP1-vesicle.

LAMP1-EYFP and LDL-DiD were imaged simultaneously (Figure 3.10A). Intensity traces were collected for 22 dequenching events in 12 cells (Figure 3.10B). Unlike the dequenching events observed following Rab7 colocalization, LAMP1 colocalization was followed immediately by dequenching.

3.3.9 Time from colocalization to dequenching

For both the Rab7 and LAMP1 data, the time from colocalization to dequenching can be measured to test for possible correlations. The time from the colocalization of LDL-DiD with a Rab7-endosome to the dequenching of LDL-DiD varies, but occurs

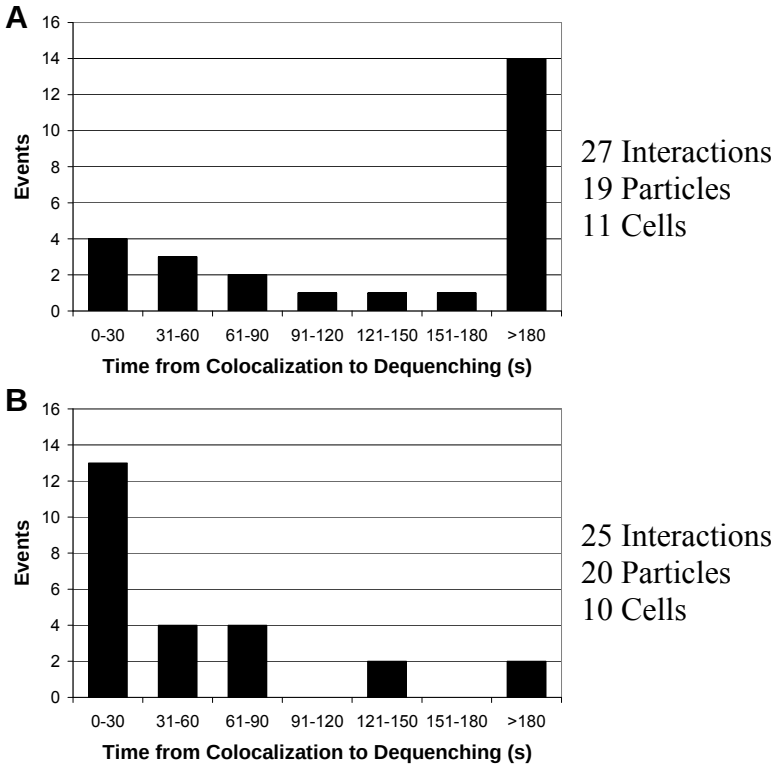

Figure 3.11 Time from interaction of Rab7-endosomes and LAMP1-vesicles with LDL-DiD to dequenching of LDL-DiD. (A) Rab7-endosomes. A histogram of times measured from colocalization with Rab7-endosomes to dequenching shows that dequenching typically occurs after long (>180 s) of colocalization. (B) LAMP1-vesicles. A histogram of times measured from colocalization with LAMP1-vesicles to dequenching shows that dequenching typically occurs within 30 s of colocalization.

after at least 180 s for >50% of dequenching events. (Figure 3.11A). This is a conservative measure as many LDL-DiD particles are already localized in Rab7-endosomes at the start of imaging. In comparison, colocalization with LAMP1-vesicles is followed shortly by dequenching (Figure 3.11B). The majority of dequenching events occur within 30 s of colocalization with a LAMP1-vesicle.

3.4 Discussion

The goal of this research is to use a quantitative approach to relate endosomal and lysosomal dynamics to the degradation of endocytic cargo. We chose LDL, a classic endocytic marker, as the extracellular cargo to probe for degradation. While the endocytic pathway of LDL is well-studied, the final degradative step had not been characterized in live cells previously. Using a highly labeled LDL particle, we were able to correlate an increase in fluorescence intensity with the degradation of the LDL particle. Using two-color fluorescence microscopy, we measured colocalization of LDL-DiD with Rab7-endosomes and LAMP1-vesicles while simultaneously measuring the degradation of LDL. Our approach is dynamic, observing transient interactions in live cells; quantitative, measuring the time from colocalization to degradation; and specific, using GFP-protein markers of endosome populations.

This research provides the first direct observation, in intact live cells, of enzyme-mediated degradation occurring in the late endosome (Figure 3.7). These observations build on previous *in vitro* assays which showed that lysosomal enzymes are both present and active in the early and late endosomes and that degradation of EGF, BSA, and LDL could occur before entry into a lysosome,[11-14,16] in contrast with the classic model of lysosomal degradation. Most similarly, previous work has described the degradation of LDL after exposure to isolated and ruptured early and late endosomes.[14] Despite the observation of degradation *in vitro*, LDL degradation was not observed *in vivo*. To some extent, single cell imaging experiments provide a link between *in vitro* experiments with isolated endosomes and *in vivo* experiments measuring LDL degradation in rat livers. *In vitro*, degradation was observed following incubation with isolated and ruptured early

and late endosomes held at a pH of 4.3 to 5. In comparison, we do not observe degradation within the early endosomes. In intact cells, it is likely that the pH of the early endosomes is higher than 5, thereby inhibiting enzyme activity.[2] It is more difficult to make comparisons to *in vivo* experiments, although it is possible that the short incubations times (7.5 min and 15 min) used for *in vivo* experiments were insufficient for internalization and transport following intravenous injection of radio-labeled LDL.

While Rab7 is a well-established marker for late endosomes,[8,32-36] the description of LAMP1-vesicles is more difficult. LAMP1 associates with both late endosomes and lysosomes.[21,32] The BS-C-1 cells used in these experiments show a high degree of colocalization between Rab7 and LAMP1 (Figure 3.9A) with degradation occurring within vesicles that are positive for both proteins. These observations raise the broader question of the differences between late endosomes and lysosomes. M6PR is the distinguishing feature of late endosomes, with lysosomes defined as M6PR-negative.[21,32] Experiments concerning M6PR will be discussed in detail in Chapter 5.

Previous work has described a distinct set of vesicles resulting from the fusion of late endosomes and lysosomes has been isolated and identified as hybrid organelles.[37,38] These vesicles are M6PR positive and contain lysosomal enzymes. Our results are consistent with the existence of this form of hybrid organelle which has late endosomal character, shown by the presence of Rab7, with sufficient enzyme activity for the degradation of LDL. Most similar to our work are previous results demonstrating degradation of an isotopically labeled ovalbumin complex in Rab7-endosomes.[23] Using subcellular fractionation it was found that degradation of the ovalbumin complex occurred in Rab7-endosomes rather than lysosomes, which were defined as a lysosomal

enzyme-rich population of vesicles. While late endosomes contained only 20% of lysosomal enzyme activity, they were responsible for the degradation of 80% of the endocytic cargo.

More subtle mechanistic details provided by single particle tracking highlight the differences between Rab7-endosomes and LAMP1-vesicles in the degradation of LDL. Despite the high level of colocalization between Rab7 and LAMP1, two-color single particle tracking measurements show that these proteins are associated with distinct, highly dynamic vesicles. Most interesting are the differences observed between Rab7 and LAMP1 in the degradation of LDL. Entry of LDL into a LAMP1-vesicle leads to the rapid degradation of the LDL particle. In comparison, no correlation is observed between entry into a Rab7-endosome and degradation of LDL. This behavior suggests that LAMP1 defines a more reactive, enzyme rich, vesicle that triggers the degradation of LDL. Taken together, these results support a previously proposed model in which lysosomes function as enzyme storage vesicles that deliver enzymes to late endosomes or hybrid organelles for degradation.[21-23]

3.5 Conclusions

To understand the final step in the endocytic pathway of LDL, we observe the degradation of LDL, and associated transport, as it occurs inside a living cell. To detect degradation, we use an LDL particle heavily labeled with the fluorophore DiD. Control experiments are carried out to demonstrate that degradation of the LDL particle corresponds to an increase in fluorescence. Late endosomes are specifically labeled with

EYFP-Rab7 to directly monitor the interaction of these vesicles with the LDL cargo. Using two-color fluorescence microscopy, we measure the transient colocalization of LDL-DiD with fluorescently-labeled late endosomes while simultaneously measuring the degradation of LDL. This imaging approach provides direct evidence that the degradation of LDL occurs in the late endosome. No degradation was observed in the early endosomes. Measuring the time to degradation following interaction with vesicles suggests that LAMP1-vesicles may serve as enzyme storage vesicles that deliver enzymes to late endosomes, forming a hybrid organelle, in which degradation occurs. In the case of LDL, understanding the degradation of LDL completes the description of this important endocytic pathway. More generally, characterizing the intracellular degradation of LDL provides a model for endosomal-lysosomal degradation. The use of single particle tracking fluorescence microscopy combined with dequenching demonstrates a new method to address questions of cellular transport and protein degradation in intact cells.

3.6 References

1 Payne, C. K.; Jones, S. A.; Chen, C.; Zhuang, X. W., Internalization and trafficking of cell surface proteoglycans and proteoglycan-binding ligands. *Traffic* **2007**, *8*, 389-401.

2 Alberts, B.; Bray, D.; Lewis, J.; Raff, M.; Roberts, K.; Watson, J. D. *Molecular Biology of the Cell*. 3 edn, (Garland Publishing, 1994).

3 Goldstein, J. L.; Brown, M. S.; Anderson, R. G. W.; Russell, D. W.; Schneider, W. J., Receptor-mediated endocytosis: concepts emerging from the LDL receptor system. *Annu. Rev. Cell Biol.* **1985**, *1*, 1-39.

4 Davis, C. G.; Goldstein, J. L.; Sudhof, T. C.; Anderson, R. G. W.; Russell, D. W.; Brown, M. S., Acid-dependent ligand dissociation and recycling of LDL receptor mediated by growth-factor homology region. *Nature* **1987**, *326*, 760-765.

5 Voet, D.; Voet, J. G. *Biochemistry*. 3 edn, (John Wiley & Sons, 2004).

6 Segrest, J. P.; Jones, M. K.; De Loof, H.; Dashti, N., Structure of apolipoprotein B-100 in low density lipoproteins. *J. Lipid Res.* **2001**, *42*, 1346-1367.

7 Hevonoja, T.; Pentikainen, M. O.; Hyvonen, M. T.; Kovanen, P. T.; Ala-Korpela, M., Structure of low density lipoprotein (LDL) particles: Basis for understanding molecular changes in modified LDL. *Biochim. Biophys. Acta-Mol. Cell Biol. Lipids* **2000**, *1488*, 189-210.

8 Lakadamyali, M.; Rust, M. J.; Zhuang, X., Ligands for clathrin-mediated endocytosis are differentially sorted into distinct populations of early endosomes. *Cell* **2006**, *124*, 997-1009.

9 Dunn, K. W.; McGraw, T. E.; Maxfield, F. R., Iterative fractionation of recycling receptors from lysosomally destined ligands in an early sorting endosome. *J. Cell Biol.* **1989**, *109*, 3303-3314.

10 Rink, J.; Ghigo, E.; Kalaidzidis, Y.; Zerial, M., Rab conversion as a mechanism of progression from early to late endosomes. *Cell* **2005**, *122*, 735-749.

11 Authier, F.; Posner, B. I.; Bergeron, J. J. M., Endosomal proteolysis of internalized proteins. *FEBS Lett.* **1996**, *389*, 55-60.

12 Bowser, R.; Murphy, R. F., Kinetics of hydrolysis of endocytosed substrates by mammalian cultured cells-Early introduction of lysosomal enzymes into the endocytic pathway. *J. Cell. Physiol.* **1990**, *143*, 110-117.

13 Renfrew, C. A.; Hubbard, A. L., Sequential processing of epidermal growth factor in early and late endosomes of rat liver. *J. Biol. Chem.* **1991**, *266*, 4348-4356.

14 Runquist, E. A.; Havel, R. J., Acid hydrolases in early and late endosome fractions from rat liver. *J. Biol. Chem.* **1991**, *266*, 22557-22563.

15 Roederer, M.; Bowser, R.; Murphy, R. F., Kinetics and temperature dependence of exposure of endocytosed material to proteolytic enzymes and low pH: Evidence for a maturation model for the formation of lysosomes. *J. Cell. Physiol.* **1987**, *131*, 200-209.

16 Diment, S.; Stahl, P., Macrophage endosomes contain proteases which degrade endocytosed protein ligands. *J. Biol. Chem.* **1985**, *260*, 5311-5317.

17 Brandenburg, B.; Zhuang, X. W., Virus trafficking - learning from single-virus tracking. *Nature Reviews Microbiology* **2007**, *5*, 197-208.

18 Damm, E. M.; Pelkmans, L., Systems biology of virus entry in mammalian cells. *Cell. Microbiol.* **2006**, *8*, 1219-1227.

19 Payne, C. K., Imaging gene delivery with fluorescence microscopy. *Nanomedicine* **2007**, *2*, 847-860.

20 Loyter, A.; Citovsky, V.; Blumenthal, R., The use of fluorescence dequenching measurements to follow viral membrane fusion events. *Methods Biochem. Anal.* **1988**, *33*, 129-164.

21 Pillay, C. S.; Elliott, E.; Dennison, C., Endolysosomal proteolysis and its regulation. *Biochem. J* **2002**, *363*, 417-429.

22 Luzio, J. P.; Pryor, P. R.; Bright, N. A., Lysosomes: fusion and function. *Nat Rev Mol Cell Biol* **2007**, *8*, 622-632.

23 Tjelle, T. E.; Brech, A.; Juvet, L. K.; Griffiths, G.; Berg, T., Isolation and characterization of early endosomes, late endosomes and terminal lysosomes: Their role in protein degradation. *J. Cell Sci.* **1996**, *109*, 2905-2914.

24 Linke, M.; Gordon, R. E.; Brillard, M.; Lecaille, F.; Lalmanach, G.; Bromme, D., Degradation of apolipoprotein B-100 by lysosomal cysteine cathepsins. *Biol. Chem.* **2006**, *387*, 1295-1303.

25 Li, G.; D'Souza-Schorey, C.; Barbieri, M. A.; Roberts, R. L.; Klippel, A.; Williams, L. T.; Stahl, P. D., Evidence for phosphatidylinositol 3-kinase as a regulator of endocytosis via activation of Rab5. *Proc. Natl. Acad. Sci. USA* **1995**, *92*, 10207-10211.

26 Martys, J. L.; Wjasow, C.; Gangi, D. M.; Kielian, M. C.; McGraw, T. E.; Backer, J. M., Wortmannin-sensitive trafficking pathways in Chinese hamster ovary cells: Differential effects on endocytosis and lysosomal sorting. *J. Biol. Chem.* **1996**, *271*, 10953-10962.

27 Petiot, A.; Faure, J.; Stenmark, H.; Gruenberg, J., PI3P signaling regulates receptor sorting but not transport in the endosomal pathway. *J. Cell Biol.* **2003**, *162*, 971-979.

28 Gruenberg, J.; Stenmark, H., The biogenesis of multivesicular endosomes. *Nat Rev Mol Cell Biol* **2004**, *5*, 317-323.

29 Simonsen, A.; Lippe, R.; Christoforidis, S.; Gaullier, J. M.; Brech, A.; Callaghan, J.; Toh, B. H.; Murphy, C.; Zerial, M.; Stenmark, H., EEA1 links PI(3)K function to Rab5 regulation of endosome fusion. *Nature* **1998**, *394*, 494-498.

30 Chavrier, P.; Parton, R. G.; Hauri, H. P.; Simons, K.; Zerial, M., Localization of low-molecular-weight GTP-binding proteins to exocytic and endocytic compartments. *Cell* **1990**, *62*, 317-329.

31 Christoforidis, S.; McBride, H. M.; Burgoyne, R. D.; Zerial, M., The Rab5 effector EEA1 is a core component of endosome docking. *Nature* **1999**, *397*, 621-625.

32 Clague, M. J., Molecular aspects of the endocytic pathway. *Biochem. J* **1998**, *336*, 271-282.

33 Feng, Y.; Press, B.; Wandinger-Ness, A., Rab 7: An important regulator of late endocytic membrane traffic. *J. Cell Biol.* **1995**, *131*, 1435-1452.

34 Soldati, T.; Rancano, C.; Geissler, H.; Pfeffer, S. R., Rab7 and Rab9 are recruited onto late endosomes by biochemically distinguishable processes. *J. Biol. Chem.* **1995**, *270*, 25541-25548.

35 Vitelli, R.; Santillo, M.; Lattero, D.; Chiariello, M.; Bifulco, M.; Bruni, C. B.; Bucci, C., Role of the small GTPase RAB7 in the late endocytic pathway. *J. Biol. Chem.* **1997**, *272*, 4391-4397.

36 Barbero, P.; Bittova, L.; Pfeffer, S. R., Visualization of Rab9-mediated vesicle transport from endosomes to the trans-Golgi in living cells. *J. Cell Biol.* **2002**, *156*, 511-518.

37 Mullock, B. M.; Bright, N. A.; Fearon, G. W.; Gray, S. R.; Luzio, J. P., Fusion of lysosomes with late endosomes produces a hybrid organelle of intermediate density and is NSF dependent. *J. Cell Biol.* **1998**, *140*, 591-601.

38 Bright, N. A.; Reaves, B. J.; Mullock, B. M.; Luzio, J. P., Dense core lysosomes can fuse with late endosomes and are re-formed from the resultant hybrid organelles. *J. Cell Sci.* **1997**, *110*, 2027-2040.

CHAPTER 4

SINGLE PARTICLE TRACKING

AS A METHOD TO RESOLVE DIFFERENCES

IN HIGHLY COLOCALIZED PROTEINS

4.1 Summary

Single particle tracking fluorescence microscopy was used to study two late endosomal proteins, Rab7 and LAMP1, that appear to be highly colocalized in static fluorescence microscopy images. Imaging these proteins simultaneously reveals that Rab7 and LAMP1 undergo periods of separation within the cell. Single particle tracking carried out during these periods of separation shows that Rab7-vesicles have greater velocities, but undergo less efficient transport, than LAMP1-vesicles. This research demonstrates the use of single particle tracking as a tool to resolve functional differences in highly colocalized proteins in intact live cells.

4.2 Introduction

Single particle tracking (SPT) fluorescence microscopy provides the ability to quantify the inherently dynamic environment of living cells.[1-5] This technique uses a combination of fluorescence microscopy, to record a time series of images, and computational algorithms, to record the position of the particles as a function of time. For cellular applications, the fluorescently-labeled particle of interest may be a biomolecule, such as a protein, an organelle, or a nanoparticle. In a one color configuration, SPT provides trajectories, particle positions as a function of time, from which information related to mobility can be extracted. In a multicolor configuration, SPT provides information on the mobility of each spectrally-distinct particle as well as the interactions between particles. SPT has been used extensively to address biophysical questions related to cellular dynamics including motor protein motion,[6-8]

gene delivery,[9-12] and virus trafficking.[13-16] We demonstrate the use of SPT as an analytical method to distinguish and differentiate between highly colocalized proteins in live cells. Specifically, we compare the intracellular dynamics of Rab7- and LAMP1-vesicles.

Rab7 and LAMP1 are membrane proteins associated with late endosomes, a key organelle for intracellular transport.[17-22] They are highly colocalized in static fluorescence microscopy images although they are distinct proteins. Rab7 is essential in the maturation of early to late endosomes.[23-25] LAMP1, although an acronym for lysosome-associated membrane protein 1, is closely associated with both late endosomes and lysosomes.[21,22] The high level of glycosylation of LAMP1 provides stability in the low-pH, enzyme-rich environment of the late endosomes and lysosomes.[26] Previous research has shown that Rab7-vesicles and LAMP1-vesicles interact differently with internalized low-density lipoprotein.[27] Entry into a LAMP1-vesicle results in the rapid degradation of low-density lipoprotein while degradation in Rab7-vesicles occurs over a range of timescales. This difference in interaction with low-density lipoprotein suggests that the high colocalization in static images, while real, masks the existence of two distinct populations of vesicles.

Understanding intracellular vesicles requires knowledge of their mobility within the cell. SPT fluorescence microscopy provides an ideal method to address questions of intracellular mobility. Variants of green fluorescent protein (GFP) can be used as genetically encoded fluorescent probes.[28,29] The wide variety of GFPs means that multiple proteins, labeled with spectrally-distinct variants of GFP, can be imaged simultaneously. To quantify intracellular mobility, live cell fluorescence microscopy

was combined with SPT for a comparison of Rab7 and LAMP1. We used two-color SPT fluorescence microscopy to image the dynamics of both Rab7 and LAMP1 simultaneously. Tracking the motion of both proteins enables us to focus on the brief periods when they are not colocalized and to use their motion during these periods for characterization. We used velocity and efficiency as parameters for characterization of the entire trajectory of Rab7- and LAMP1-vesicles. For the purposes of this thesis, efficiency was defined as the distance the vesicle travels relative to the absolute distance to its fusion site. Most interestingly, our results show that Rab7-vesicles are slightly faster, but are less efficient, sampling more of the cell before fusing with another vesicle.

This research demonstrates that SPT can be used to differentiate between highly colocalized proteins in intact live cells. In the same way that proteins can be separated biochemically based on size or charge, we propose that intracellular motion is a parameter that can be used to distinguish unique protein populations. While the tracked protein cannot be characterized at the same level as an isolated protein, SPT does have the advantage of providing relevant functional information such as the mobility of transport vesicles. The utility of this method is demonstrated by resolving differences in mobility between Rab7 and LAMP1. These mobility studies demonstrate that Rab7 and LAMP1 are associated with different populations of vesicles and point towards future studies aimed at understanding the differences between these vesicles in relation to endocytic transport.

4.3 Results

4.3.1 Colocalization of fluorescent proteins

The correlation or overlap of two or more distinct fluorescent species is described as their colocalization. While conceptually straightforward, the quantification of colocalization depends on multiple factors including intensity, shape, background, and microscope configuration. To handle this range of parameters,

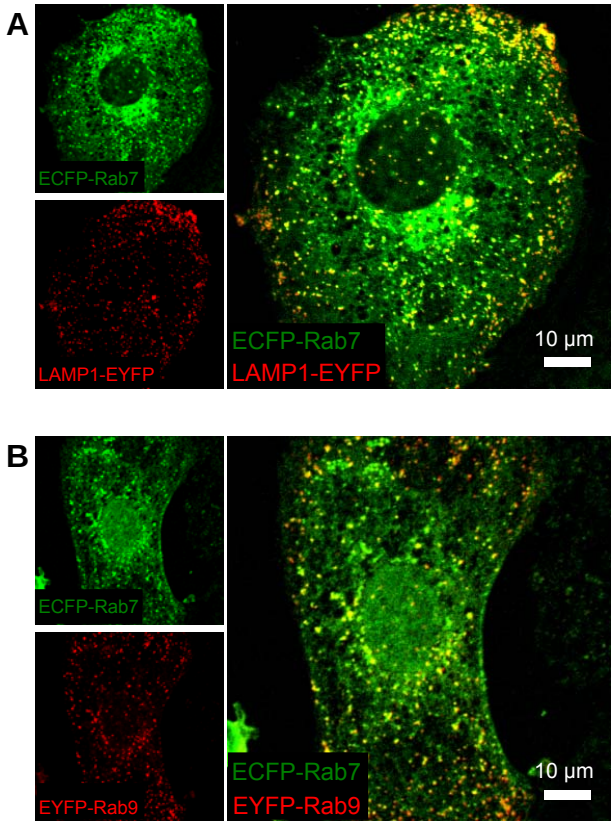

Figure 4.1. Colocalization of the endosomal proteins Rab7, Rab9 and LAMP1. The endosomal proteins Rab7, Rab9, and LAMP1 appear highly colocalized in static confocal microscopy images. A) Colocalization of ECFP-Rab7 (green) and LAMP1-EYFP (red). B) Colocalization of ECFP-Rab7 (green) and EYFP-Rab9 (red). Colocalized proteins appear yellow in the overlaid images. Cells were fixed in 4% formaldehyde for 30 minutes then rinsed and imaged in PBS.

different measures of colocalization have been developed for different applications and environments. The most common measurements of colocalization include Pearson's coefficient, overlap coefficient (k1 and k2), Manders' coefficient, and manual methods.[30-34] We first apply these measures of colocalization to two sets of proteins; Rab7 with LAMP1 and Rab7 with Rab9, each labeled with a variant of GFP. Rab7, Rab9, and LAMP1 are membrane proteins associated with late endosomes.[17-22] Their association with vesicles that have a diameter near, or below, the diffraction limit of visible light means fluorescence images of these proteins should appear punctate. This is confirmed with confocal images of ECFP-Rab7, LAMP1-EYFP, and EYFP-Rab9 (Figure 4.1). ECFP and EYFP are spectrally-separable fluorophores that can be imaged without cross-talk between channels (Figure 4.2).

For each measurement of colocalization (Table 4.1), 5-10 cells were imaged using confocal microscopy. Representative images are shown in Figure 4.1. Pearson's coefficient quantifies the linear correlation between two data sets with a range from +1, complete colocalization, to -1, complete exclusion of signal.[31] When applied to confocal images of cells expressing fluorescently-labeled Rab7, Rab9, and LAMP1, Pearson's coefficient showed a high degree of correlation for both protein pairs; 0.73 for Rab7 and LAMP1 and 0.74 for Rab7 and Rab9. Pearson's coefficient is strongly influenced by fluorescence intensity and background, making it poorly suited for noisy environments.[33] The measurement of the overlap coefficient is similar to Pearson's coefficient, but does not use the average value of the data set in the calculation of the correlation making it less influenced by background.[30] It can also be implemented using a user-defined threshold which further reduces the importance of

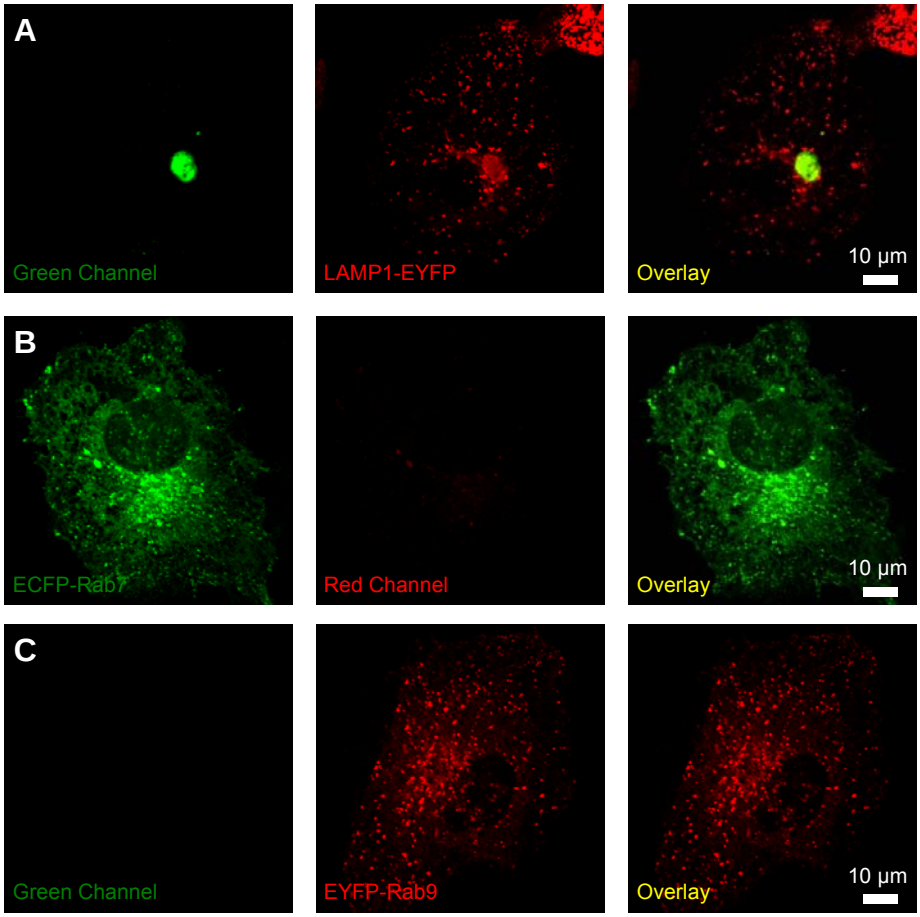

Figure 4.2 Images of cross-talk in opposing channels. The use of ECFP and EYFP, in combination with the appropriate microscope parameters, does not lead to cross-talk with the opposing channel. This was confirmed using BS-C-1 cells transfected with a single fluorescent protein. A) LAMP1-EYFP B) ECFP-Rab7 C) EYFP-Rab9

background signal. The overlap coefficient can range from 0 to 1 and does not distinguish between individual channels. As with Pearson's coefficient, the overlap coefficient reflected high colocalization between Rab7-LAMP1 (0.84) and Rab7-Rab9 (0.88).

	Single Value Coefficients			
	Rab7 and LAMP1 Vesicles		*Rab7 and Rab9 Vesicles*	
Pearson's Coefficient	0.73 ± 0.05		0.74 ± 0.05	
Overlap Coefficient	0.84 ± 0.04		0.88 ± 0.04	
	Measurements by Vesicle Protein			
	Rab7 with LAMP1	*LAMP1 with Rab7*	*Rab7 with Rab9*	*Rab9 with Rab7*
Manual Count	0.88 ± 0.06	0.81 ± 0.13	0.86 ± 0.07	0.80 ± 0.12
Manders' Coefficients	0.77 ± 0.09	0.62 ± 0.12	0.66 ± 0.10	0.63 ± 0.07

Table 4.1 Quantification of colocalization. Rab7-LAMP1 colocalization and Rab7-Rab9 colocalization were measured using standard algorithms. Colocalization and standard deviation was measured for 10 cells for Pearson's, overlap, and Manders' coefficients and 5 cells for the manual count.

A limitation of both the Pearson's and overlap coefficients is that they do not discriminate between two different channels making it difficult to determine if every Rab7-vesicle is also positive for LAMP1, or the converse. The most direct measure of colocalization for two channels is a manual approach in which individual vesicles, or a randomly selected subset of vesicles, are scored for colocalization with the opposite channel. This provides the percentage of colocalized vesicles. For the manual count provided in Table 1, a random selection of vesicles was chosen by overlaying the cell image with a grid consisting of 100 μm^2 squares. The vesicles in the center of each square were then tallied. The manual count of colocalization was in good agreement with the previous values with 88% of Rab7-vesicles also positive for LAMP1 and 81% of LAMP1-vesicles positive for Rab7. The measurement of Rab7 and Rab9 colocalization produced similarly high values with 86% of Rab7-vesicles positive for

Rab9 and 80% of Rab9-vesicles positive for Rab7. While the grid was used to reduce selection bias, this approach will result in an over-sampling of sparse regions and an under-sampling in regions with many vesicles. This manual approach does benefit from insensitivity to background and intensity variations. Manders' coefficient is an automated method used to quantify colocalization in two channels using a correlation value based on pixel intensities in each channel.[30,31] It can range from 0, for non-overlapping images, to 1 for complete overlap. A user-defined threshold was applied to these images to reduce the contribution from background. Similarly high levels of colocalization were measured using Manders' coefficient; 0.77 for Rab7 with LAMP1 and 0.62 LAMP1 with Rab7. Rab7 had a 0.66 correlation with Rab9 while Rab9 had a 0.63 correlation with Rab7.

Overall, these values reflect a high level of colocalization of Rab7 with LAMP1 and Rab7 with Rab9 as observed in static confocal fluorescence microscopy images (Figure 4.1). This high level of colocalization of Rab7 with LAMP1 and Rab9 is not unique to the BS-C-1 cells used in these experiments, but was also observed in HeLa cells (Figure 4.3). Based on the above results, it would be reasonable to assume that Rab7, Rab9, and LAMP1 are associated with a single population of vesicles. We propose that live cell imaging, in which the time component provides an additional parameter to differentiate these two protein pairs, can be used to test this assumption. We first determine if these proteins are fully colocalized when undergoing transport in live cells. We then use SPT to characterize differences in the intracellular motion.

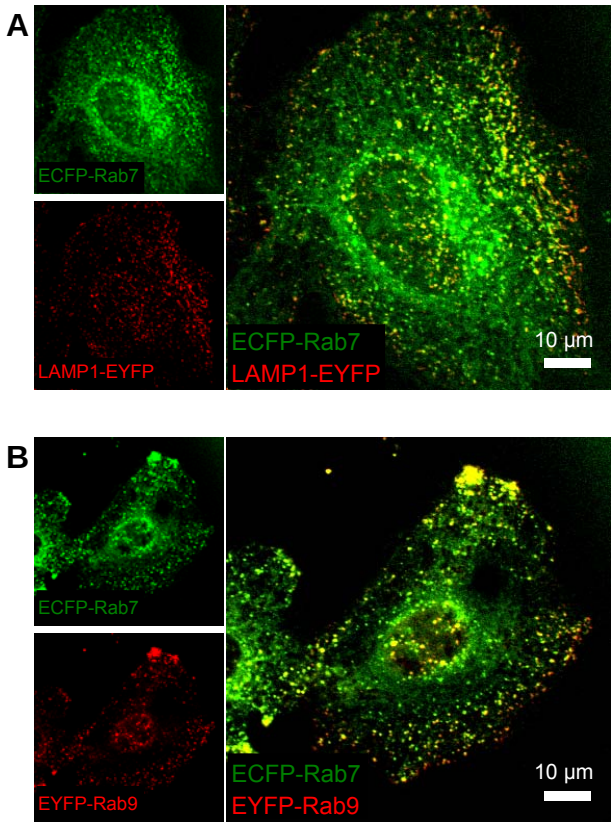

Figure 4.3 The colocalization of Rab7-LAMP1 and Rab7-Rab9 in HeLa cells. A) Colocalization of ECFP-Rab7 (green) and LAMP1-EYFP (red). B) Colocalization of ECFP-Rab7 (green) and EYFP-Rab9 (red). Colocalized proteins appear yellow in the overlaid images. Cells were fixed in 4% formaldehyde for 30 minutes then rinsed and imaged in PBS.

4.3.2 Intracellular dynamics of Rab7- and LAMP1-vesicles

Rab7- and LAMP1-vesicles have been shown to interact differently with endocytic cargo,[27] suggesting that they are associated with distinct populations of vesicles despite the high level of colocalization observed in static images. Rab7 and Rab9 are used as a point of comparison. These proteins are known markers of late endosomes and were shown previously to reside on separate domains of the same vesicle.[19,20] In both cases, images were collected using a fluorescence microscope designed for SPT, described in Materials and Methods, and analyzed with ImageJ and

MATLAB. The first step was to determine if Rab7-LAMP1 and Rab7-Rab9 differed, as expected based on previous results, in the probability of observing periods of non-colocalization. For live cell imaging, proteins were considered colocalized if they moved through the cell together for a minimum of 10 s. To start, 50 vesicles positive for both Rab7 and LAMP1, referred to as hybrid vesicles, and 50 vesicles positive for both Rab7 and Rab9 were randomly selected from 6 cells and tracked for a period of 200 s. Of the Rab7-LAMP1 hybrid vesicles, 36% were observed to undergo periods of non-colocalization. In comparison, only 10% of Rab7-Rab9 vesicles underwent periods of separation, likely due to the distinct pathways by which Rab7 and Rab9 are recruited to the same population of vesicles.[19] The greater likelihood of separation for Rab7-LAMP1 vesicles encouraged us to probe the periods during which the two proteins were not colocalized (Figure 4.4). Typical behavior related to periods of separation for Rab7-vesicles was as follows; a Rab7-vesicle separated from a hybrid vesicle and underwent active transport through the cell before fusing with a pre-existing hybrid vesicle or, less frequently, fusing with a LAMP1-vesicle to form a hybrid vesicle. An analysis of 50 trajectories showed that this period of separation ranged from 8 s to 858 s with the majority of Rab7-vesicles non-colocalized for less than 76 s (Figure 4.4C). LAMP1-vesicles displayed similar behavior with the majority of separation times less than 44 s in duration (Figure 4.4F).

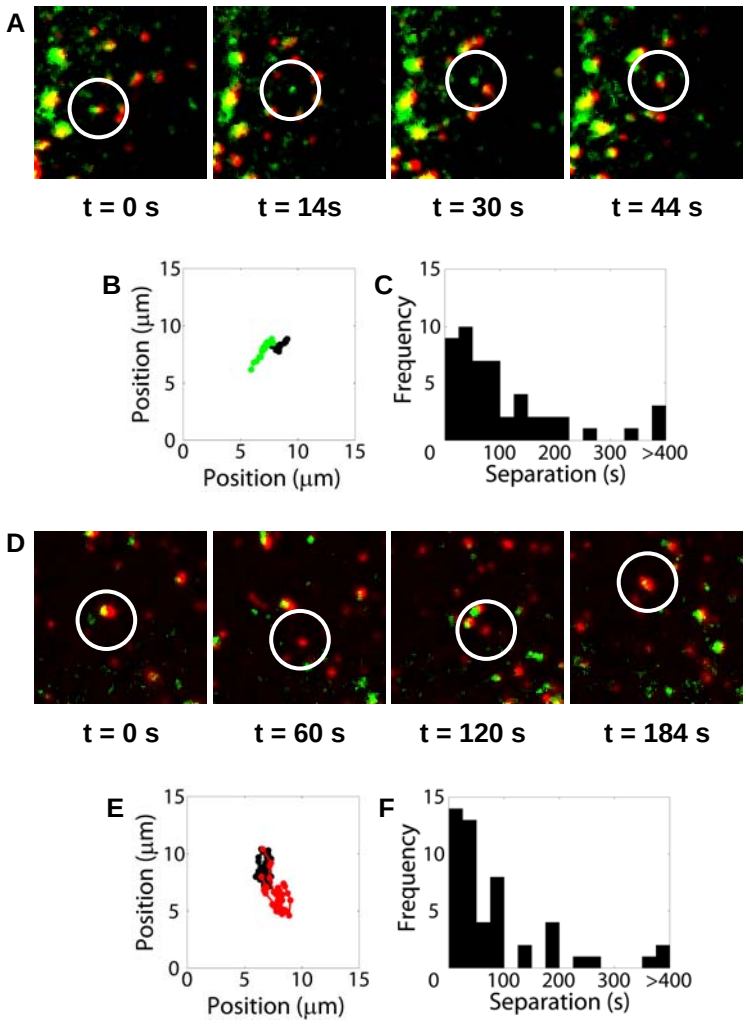

Figure 4.4 Live cell imaging of Rab7- and LAMP1-vesicles. Live cell imaging demonstrates that Rab7 and LAMP1 undergo periods of separation. Rab7 and Rab9 remain colocalized. A. Snapshots of Rab7-vesicles (green) and LAMP1-vesicles (red) during a period in which Rab7 is not colocalized with LAMP1. B. Trajectories of both the Rab7-vesicle (green) and the Rab7-LAMP1 hybrid (black) with which the Rab7-vesicle fuses. C. A histogram of time periods during which Rab7 is not colocalized with LAMP1 (n=50 Rab7-vesicles). D. Snapshots of Rab7-vesicles (green) and LAMP1-vesicles (red) during a period in which LAMP1 is not colocalized with Rab7. E. Trajectories of both the LAMP1-vesicle (red) and the Rab7-LAMP1 hybrid (black) with which the LAMP1-vesicle fuses. F. A histogram of time periods during which LAMP1 is not colocalized with Rab7 (n=50 LAMP1-vesicles). nction. n=50 vesicles for each histogram.

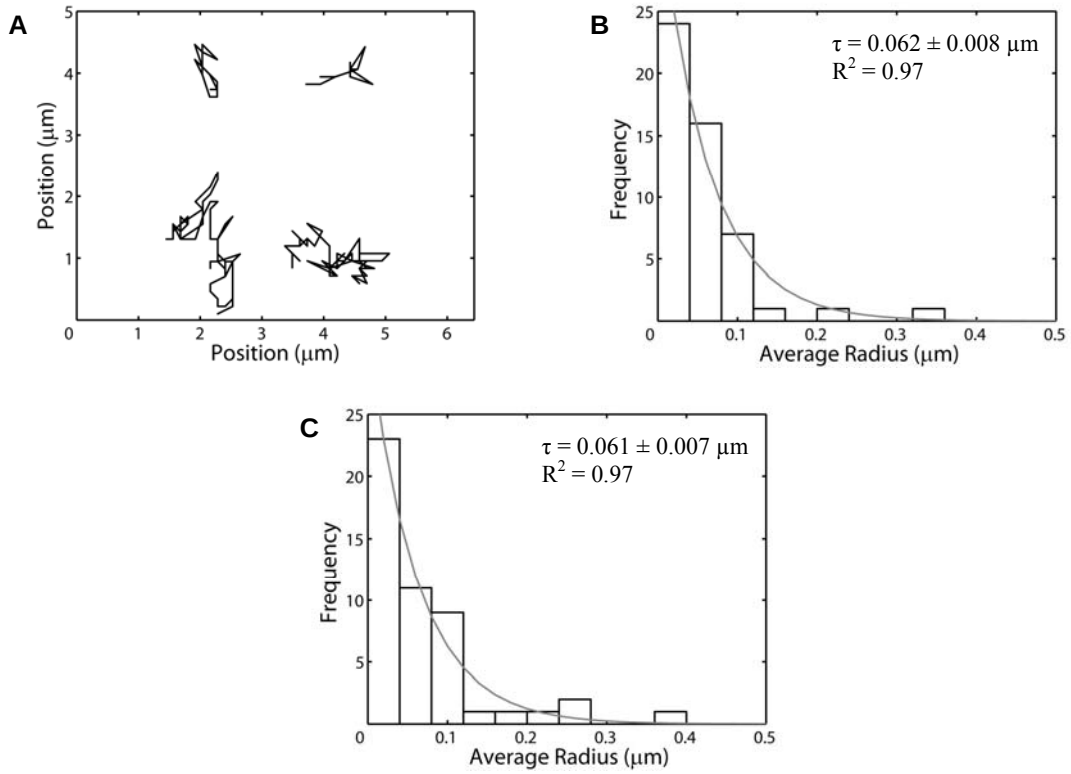

Figure 4.5 Rab7-LAMP1 hybrid vesicles are relatively stationary. A. Representative trajectories of four Rab7-LAMP1 hybrid vesicles. B. Average radial distance from the centroid of the trajectory for 50 hybrid vesicles that undergo fusion with Rab7- or LAMP1-vesicles. C. The limited mobility of hybrid vesicles is not specific to those that undergo fusion with Rab7- or LAMP1-vesicles. An identical distribution of average radii was also observed for randomly selected Rab7-LAMP1 hybrid vesicles. In comparison, Rab7- and LAMP1-vesicles have a much greater mobility with $\tau = 0.24 \pm 0.06$ μm and $\tau = 0.6 \pm 0.2$ μm, respectively (Figure 4.6). As a means of comparison, the lines are fits to a single exponential function. The errors associated with the fit are determined using monte-carlo simulations.

4.3.3 Differences in mobility of Rab7- and LAMP1-vesicles

This analysis of vesicle dynamics indicates that Rab7- and LAMP1-vesicles are distinct populations of vesicles. We next sought to use SPT to determine if there are differences in the mobility of these populations of vesicles. For subsequent analysis, we used the portion of the trajectory during which Rab7 and LAMP1 were not colocalized with the other protein. Separation of the two proteins was used as a

starting point and fusion with a hybrid vesicle was used as an end point. Hybrid vesicles were observed to be relatively stationary (Figure 4.4B and E), which was confirmed by measuring the average radius of travel. The radius of travel was defined as the distance from the geometric center of the trajectory to each point on the trajectory, divided by the square root of the period of separation. The radial distance traversed by the 50 hybrid vesicles associated with Figure 3.4 were measured, four representative hybrid trajectories are shown (Figure 4.5A). A histogram of the average radii of the 50 vesicles was fit to a single exponential function with $\tau = 0.062 \pm 0.008$ μm (Figure 4.5B). In comparison, a similar analysis was carried out for 50 Rab7- and LAMP1-vesicles (Figure 4.6) resulting in $\tau = 0.24 \pm 0.06$ μm for Rab7-vesicles and $\tau = 0.5 \pm 0.1$ μm for LAMP1-vesicles. The greater decay constant indicates a much greater level of mobility for Rab7- and LAMP1-vesicles than for the hybrid vesicles. This limited mobility was not unique to the hybrid vesicles associated with fusion events, but was also observed in a population of 50 randomly selected hybrid vesicles with their average radius fit to single exponential with $\tau = 0.061 \pm$

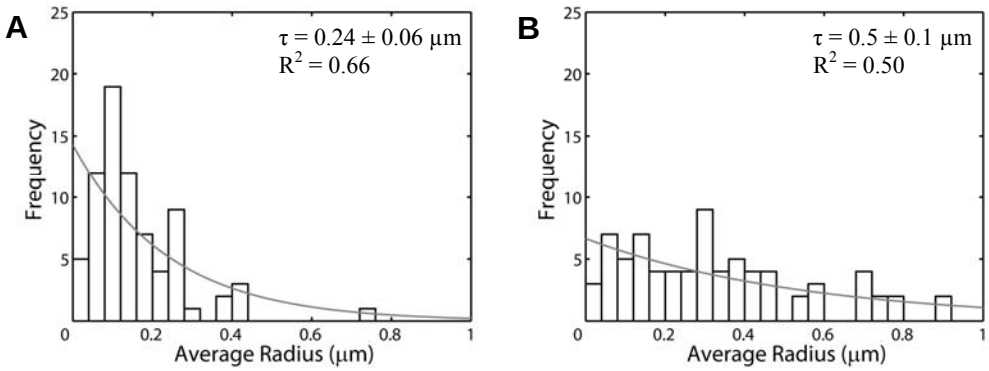

Figure 4.6 Radial distance traveled by Rab7- and LAMP1-vesicles. The radial distance traveled by Rab7- and LAMP1-vesicles is greater than that of Rab7-LAMP1 hybrid vesicles (Fig. 3). A) Average radial distance from the centroid of the trajectory for 50 Rab7-vesicles. B) Average radial distance from the centroid of the trajectory for

0.007 μm (Figure 4.5C). Overall, this analysis demonstrates that the hybrid vesicles can be treated as stationary relative to the much more mobile Rab7- and LAMP1-vesicles.

Using fusion with a hybrid vesicle as an endpoint, we measured vesicle motion prior to fusion as an assay to determine the difference, if any, between Rab7- and LAMP1-vesicles. We focused on two parameters; velocity and efficiency. Histograms of instantaneous velocities for Rab7- and LAMP1- vesicles showed that Rab7-vesicles moved through the cell with a significantly greater velocity, based on a p-value for single

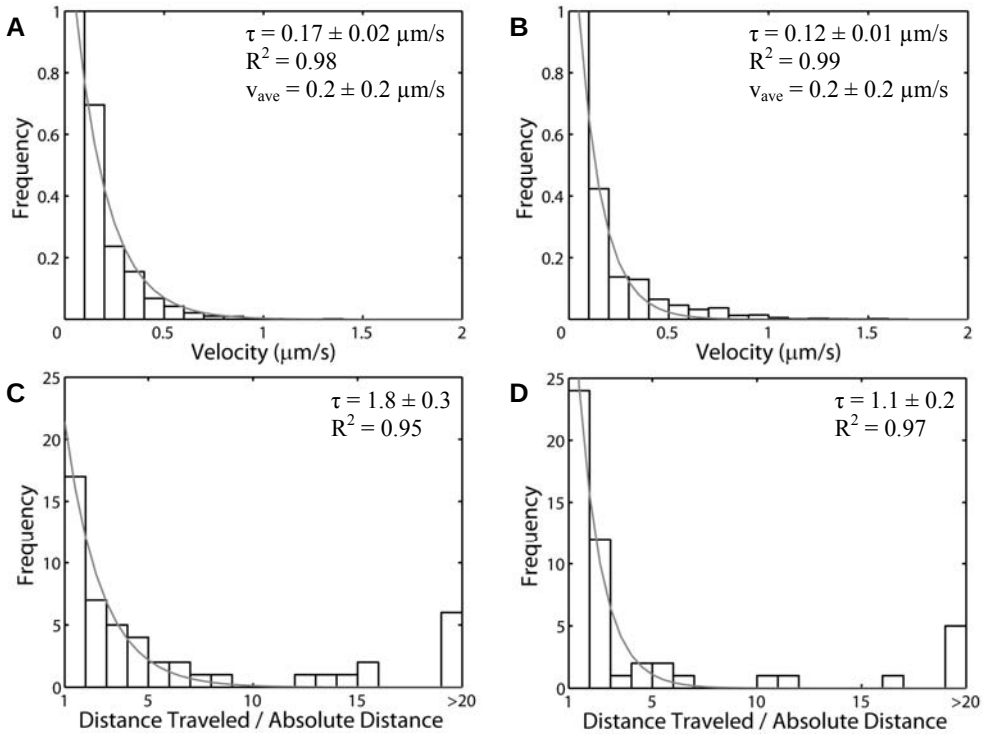

Figure 4.7 Velocity and efficiency of Rab7- and LAMP1-vesicles. Rab7- and LAMP1-vesicles have different velocities and efficiencies within the cell. (A) A histogram of the velocities of Rab7-vesicles. (B) A histogram of the velocities of LAMP1-vesicles. (C) Efficiency of Rab7-vesicles. (D) Efficiency of LAMP1-vesicles. Efficiency is defined as the ratio of the distance the vesicle travels prior to fusion relative to the absolute distance to the fusion site. Perfect efficiency

exponential fits to the distribution of velocities ($p = 0.0016$, Figure 3.7A and B). Rab7-vesicle motion was associated with $\tau = 0.17 \pm 0.02$ μm/s while LAMP1-vesicles had $\tau = 0.12 \pm 0.01$ μm/s. It is important to note that this difference is obscured when only the average velocity is considered as both Rab7- and LAMP1-vesicles have $v_{ave} = 0.2 \pm 0.2$ μm/s. Efficiency was evaluated by measuring the distance each vesicle traveled before reaching its endpoint relative to the absolute distance between the vesicle and its endpoint (Figure 4.7C and D). By this measure, a perfectly efficient vesicle would move directly to the endpoint, with a value of 1. Larger values reflect lower efficiency. The average initial separation distance between the vesicle of interest and the endpoint, defined as the absolute distance, was slightly shorter for Rab7-vesicles, 4.5 ± 4.6 μm compared to 6.4 ± 4.8 μm for LAMP1-vesicles. The average distanced traveled was 18.2 ± 21.3 μm for Rab7-vesicles and 17.0 ± 17.3 μm for LAMP1-vesicles. Histograms of the 50 trajectories recorded for each vesicle population were fit with single exponential functions with decays of $\tau = 1.8 \pm 0.3$ for Rab7-vesicles and $\tau = 1.1 \pm 0.2$ for LAMP1-vesicles (Figure 4.7C and D). These differences are significant, with a p-value below 0.001. This indicates that the LAMP1-vesicles are more efficient than Rab7-vesicles, despite the greater velocity of the Rab7-vesicles. This measure of efficiency groups the underlying physical differences into a single value. For example, this measure does not distinguish between differences in motor proteins or fraction of time spent undergoing active transport. However, it is a useful parameter for future SPT experiments that will determine the underlying differences in transport that lead to the greater efficiency of LAMP1-vesicles.

4.4 Conclusions

Essential cellular functions including transport of extracellular cargo, antigen presentation, and degradation of organelles are dependent on the mobility of intracellular vesicles.[35] A challenge in the study of intracellular vesicles, or any cellular system, is resolving subtle differences between proteins that are localized at nearly the same position in the cell. In this situation, diffraction-limited fluorescence microscopy cannot be used to distinguish differences in proteins based on location alone. We have demonstrated that SPT fluorescence microscopy can be used to resolve differences in highly colocalized proteins. By observing the intracellular transport of the highly colocalized proteins, labeled with distinct fluorophores, simultaneously, we can determine the extent of colocalization. We can then use differences in mobility to distinguish the proteins. We find that Rab7 and LAMP1, while highly colocalized in static fluorescence microscopy images, undergo periods of separation that can be observed using live cell imaging. SPT was used to characterize the motion of independent Rab7- and LAMP1-vesicles. Using this approach, we show that Rab7-vesicles have a greater intracellular velocity, but transport less efficiently. In addition to providing a proof-of-concept for the use of SPT fluorescence microscopy in distinguishing highly colocalized proteins, this research also suggests that Rab7 and LAMP are associated with distinct populations of vesicles. Future research will address the biological differences in these vesicles and their roles in intracellular transport.

4.5 References

1 Levi, V.; Gratton, E., Exploring dynamics in living cells by tracking single particles. *Cell Biochem. Biophys.* **2007**, *48*, 1-15.

2 Joo, C.; Balci, H.; Ishitsuka, Y.; Buranachai, C.; Ha, T., Advances in single-molecule fluorescence methods for molecular biology. *Annu. Rev. Biochem.* **2008**, *77*, 51-76.

3 Meijering, E.; Dzyubachyk, O.; Smal, I.; van Cappellen, W. A., Tracking in cell and developmental biology. *Semin. Cell Dev. Biol.* **2009**, *20*, 894-902.

4 Brandenburg, B.; Zhuang, X. W., Virus trafficking - learning from single-virus tracking. *Nat. Rev. Microbiol.* **2007**, *5*, 197-208.

5 Payne, C. K., Imaging gene delivery with fluorescence microscopy. *Nanomedicine* **2007**, *2*, 847-860.

6 Kural, C. *et al.*, Kinesin and dynein move a peroxisome in vivo: A tug-of-war or coordinated movement? *Science* **2005**, *308*, 1469-1472.

7 Kural, C. *et al.*, Tracking melanosomes inside a cell to study molecular motors and their interaction. *Proc. Natl. Acad. Sci. USA* **2007**, *104*, 5378-5382.

8 Nan, X. L.; Sims, P. A.; Chen, P.; Xie, X. S., Observation of individual microtubule motor steps in living cells with endocytosed quantum dots. *J. Phys. Chem. B* **2005**, *109*, 24220-24224.

9 Hess, G. T.; Humphries, W. H.; Fay, N. C.; Payne, C. K., Cellular binding, motion, and internalization of synthetic gene delivery polymers. *BBA-Mol. Cell Res.* **2007**, *1773*, 1583-1588.

10 Payne, C. K.; Jones, S. A.; Chen, C.; Zhuang, X. W., Internalization and trafficking of cell surface proteoglycans and proteoglycan-binding ligands. *Traffic* **2007**, *8*, 389-401.

11 Suh, J.; Dawson, M.; Hanes, J., Real-time multiple-particle tracking: applications to drug and gene delivery. *Adv. Drug Del. Rev.* **2005**, *57*, 63-78.

12 Bausinger, R. *et al.*, The transport of nanosized gene carriers unraveled by live-cell imaging. *Angew. Chem.* **2006**, *45*, 1568-1572.

13 Seisenberger, G. *et al.*, Real-time single-molecule imaging of the infection pathway of an adeno-associated virus. *Science* **2001**, *294*, 1929-1932.

14 Lakadamyali, M.; Rust, M. J.; Babcock, H. P.; Zhuang, X. W., Visualizing infection of individual influenza viruses. *Proc. Natl. Acad. Sci. USA* **2003**, *100*, 9280-9285.

15 Arhel, N. *et al.*, Quantitative four-dimensional tracking of cytoplasmic and nuclear HIV-1 complexes. *Nat. Methods* **2006**, *3*, 817-824.

16 Brandenburg, B. *et al.*, Imaging poliovirus entry in live cells. *PLoS Biol.* **2007**, *5*, 1543-1555.

17 Feng, Y.; Press, B.; Wandinger-Ness, A., Rab 7: An important regulator of late endocytic membrane traffic. *J. Cell Biol.* **1995**, *131*, 1435-1452.

18 Vitelli, R. *et al.*, Role of the small GTPase RAB7 in the late endocytic pathway. *J. Biol. Chem.* **1997**, *272*, 4391-4397.

19 Soldati, T.; Rancano, C.; Geissler, H.; Pfeffer, S. R., Rab7 and Rab9 are recruited onto late endosomes by biochemically distinguishable processes. *J. Biol. Chem.* **1995**, *270*, 25541-25548.

20 Barbero, P.; Bittova, L.; Pfeffer, S. R., Visualization of Rab9-mediated vesicle transport from endosomes to the trans-Golgi in living cells. *J. Cell Biol.* **2002**, *156*, 511-518.

21 Pillay, C. S.; Elliott, E.; Dennison, C., Endolysosomal proteolysis and its regulation. *Biochem. J.* **2002**, *363*, 417-429.

22 Clague, M. J., Molecular aspects of the endocytic pathway. *Biochem. J.* **1998**, *336*, 271-282.

23 Rink, J.; Ghigo, E.; Kalaidzidis, Y.; Zerial, M., Rab conversion as a mechanism of progression from early to late endosomes. *Cell* **2005**, *122*, 735-749.

24 Lakadamyali, M.; Rust, M. J.; Zhuang, X., Ligands for clathrin-mediated endocytosis are differentially sorted into distinct populations of early endosomes. *Cell* **2006**, *124*, 997-1009.

25 Poteryaev, D.; Datta, S.; Ackema, K.; Zerial, M.; Spang, A., Identification of the switch in early-to-late endosome transition. *Cell* **2010**, *141*, 497-508.

26 Eskelinen, E. L.; Tanaka, Y.; Saftig, P., At the acidic edge: emerging functions for lysosomal membrane proteins. *Trends Cell Biol.* **2003**, *13*, 137-145.

27 Humphries, W. H.; Fay, N. C.; Payne, C. K., Intracellular degradation of low-density lipoprotein probed with two-color fluorescence microscopy. *Integr. Biol.* **2010**, *2*, 536-544.

28 Giepmans, B. N. G.; Adams, S. R.; Ellisman, M. H.; Tsien, R. Y., Review - The fluorescent toolbox for assessing protein location and function. *Science* **2006**, *312*, 217-224.

29 Zhang, J.; Campbell, R. E.; Ting, A. Y.; Tsien, R. Y., Creating new fluorescent probes for cell biology. *Nat. Rev. Mol. Cell Biol.* **2002**, *3*, 906-918.

30 Manders, E. M. M.; Verbeek, F. J.; Aten, J. A., Measurement of colocalization of objects in dual-color confocal images. *J. Microsc.-Oxford* **1993**, *169*, 375-382.

31 Manders, E. M. M.; Stap, J.; Brakenhoff, G. J.; Vandriel, R.; Aten, J. A., Dynamics of 3-dimentional replication patterns during the S-phase, analyzed by double labeling of DNA and confocal microscopy. *J. Cell Sci.* **1992**, *103*, 857-862.

32 Agnati, L. F. *et al.*, New methods to evaluate colocalization of fluorophores in immunocytochemical preparations as exemplified by a study on A(2A) and D-2 receptors in Chinese hamster ovary cells. *J. Histochem. Cytochem.* **2005**, *53*, 941-953.

33 Bolte, S.; Cordelieres, F. P., A guided tour into subcellular colocalization analysis in light microscopy. *J. Microsc.-Oxford* **2006**, *224*, 213-232.

34 Zinchuk, V.; Zinchuk, O.; Okada, T., Quantitative colocalization analysis of multicolor confocal immunofluorescence microscopy images: Pushing pixels to explore biological phenomena. *Acta Histochem. Cytochem.* **2007**, *40*, 101-111.

35 Alberts, B. *et al. Molecular Biology of the Cell*. 3 edn, (Garland Publishing, 1994).

CHAPTER 5
INTRACELLULAR DYNAMICS OF HYBRID LATE ENDOSOME-LYSOSOME ORGANELLES RESOLVED WITH FLUORESCENCE MICROSCOPY

5.1 Summary

This research characterizes the organelles that compose the endo-lysosomal pathway on two levels. First, by colocalization with three endo-lysosomal proteins: Rab7, LAMP1, and cation-independent mannose 6-phosphate receptor. Second, by the transport of fluid phase and endocytic cargo through this pathway. We find that the major organelle in the endo-lysosomal pathway, both in terms of population and cargo transport, is a hybrid vesicle positive for endosomal and lysosomal proteins. Our research characterizes this vesicle and two populations of non-hybrid vesicles defined by Rab7 and LAMP1 proteins. The movement of dextran from Rab7-, LAMP1-, and hybrid vesicles at early times to LAMP1- and hybrid vesicles at late times shows that LAMP1- and hybrid vesicles are terminal vesicles in the endo-lysosomal pathway. Unlike dextran, endocytic cargo such as LDL and BSA does not move from Rab7-vesicles to LAMP1- and hybrid vesicles, but instead maintains an equal distribution in Rab7- and LAMP1-vesicles.

5.2 Introduction

The endo-lysosomal pathway is of fundamental importance in cell biology, responsible for the degradation of both extracellular cargo and intracellular housekeeping.[1-4] Understanding the endo-lysosomal pathway has taken on increasing importance with the advent of gene delivery and nanobiotechnology, fields in which delivery of DNA or nanoparticles to the lysosome is either targeted for triggered release or avoided to prevent degradation.[5,6] The central questions associated with the endo-

lysosomal pathway are best illustrated by the intracellular degradation of extracellular cargo. The intracellular degradation of extracellular cargo, including cell surface receptors, is essential for the maintenance of cellular health.[7] The degradation of extracellular cargo, such as low-density lipoprotein, is necessary for the cell to utilize lipids that cannot be produced intracellularly.[8,9] The internalization and degradation of cell surface receptors is the mechanism by which the cell down-regulates receptors and controls the internalization of cargo.[10] The conventional picture of lysosomal degradation describes internalization from the plasma membrane followed by transport from early to late endosomes leading to delivery of cargo to the lysosome; an acidic, enzyme-rich, membrane-bound organelle.[7,10,11] In recent years a more complex picture of lysosomal degradation has emerged that demonstrates degradation can occur up-stream of the lysosome and that key lysosomal proteins are not necessary for the degradation of extracellular cargo.[12-17]

An important feature of the endo-lysosomal pathway is the existence of an organelle that is a hybrid of the late endosome and lysosome, defined as positive for both late endosomal proteins and lysosomal membrane proteins or enzymes. This hybrid organelle has been observed directly using electron microscopy,[18-21] fluorescence microscopy,[22] and density gradient ultracentrifugation of cell-free endosomes and lysosomes.[23] The function of the hybrid organelle, essentially the lysosomal enzyme-mediated degradation of cargo within a late endosome, has also been observed for low-density lipoprotein (LDL) and ovalbumin.[14,17,24] Within our own lab we have observed the degradation of LDL, considered a lysosomal function, in an organelle that is positive for the late endosomal protein, Rab7.[14] Further experiments using two-color live cell

imaging of cells expressing endo-lysosomal proteins labeled with spectrally-distinguishable fluorophores revealed three distinct populations of vesicles; hybrids, positive for both Rab7 and LAMP1, Rab7-vesicles, and LAMP1-vesicles.[22] Single particle tracking was used to confirm, in intact live cells, that these three populations of vesicles were distinct with different mobilities. The existence of the hybrid organelle, as well as distinct non-hybrid vesicles, leads to the question of the definition of late endosomes and lysosomes, especially in relation to the hybrid organelle.

Defining the relationship between late endosomes and lysosomes requires understanding both their individual properties, measured by determining colocalization with known protein markers, and their function, the transport and degradation of cargo. As these questions are fundamentally dynamic, it is necessary to probe these questions with a method that captures the dynamics. For that reason, we have probed the endo-lysosomal pathway using multicolor single particle tracking fluorescence microscopy in combination with variants of GFP to provide a genetic marker of endosomal and lysosomal proteins of interest. The research described below defines Rab7-vesicles, LAMP1-vesicles, and hybrid organelles in relation to cation- independent mannose 6-phosphate receptor (M6PR), the single protein that distinguishes endosomes from lysosomes,[18,19,25-27] and the transport of cargo between these vesicles. Three classic extracellular cargos; dextran, LDL, and BSA, were labeled with fluorophores and colocalization with each population of vesicle was measured using confocal fluorescence microscopy of fixed cells. We find that Rab7-vesicles and hybrid organelle populations include both endosomes and lysosomes. LAMP1-vesicles are predominantly lysosomes, based on an absence of M6PR. All three populations are highly dynamic, undergoing

repeated fusion events. The transport of dextran, a fluid phase marker,[28-31] further reveals that LAMP1-vesicles are true terminal vesicles with dextran transport from Rab7-vesicles to LAMP1-vesicles over time. In comparison, receptor-mediated endocytosis leads to retention of cargo in Rab7-vesicles, suggesting upstream targeting.

5.3 Results

5.3.1 Characterization of the endo-lysosomal pathway

The existence of three distinct populations of vesicles; hybrids, with proteins characteristic of late endosomes and lysosomes, Rab7-, and LAMP1-vesicles raises the question of how to define these vesicles in relation to the endo-lysosomal pathway. Essentially, are they endosomes or lysosomes? We focused on three characteristic endo-lysosomal proteins, Rab7, LAMP1, and M6PR, to classify these populations of vesicles. Rab7 is a GTPase most commonly associated with late endosomes,[24,32-36]. Although nomenclature would suggest that lysosomal-associated membrane protein 1 (LAMP1) is lysosomal, it may also associate with late endosomes.[4] Similarly, conventionally lysosomal enzymes are also found in late endosomes, making these enzymes insufficient as markers to delineate late endosomes and lysosomes.[15,16,21,23] To the best of our knowledge, M6PR, which is rapidly recycled from the lysosome,[18,19,25-27] provides the best protein marker to separate endosomes from lysosomes. Lysosomes are defined as M6PR-negative. Late endosomes can be M6PR-positive, although not all late endosomes are M6PR-positive.[34,37-39] Our first step was to characterize hybrid, Rab7-, and LAMP1-

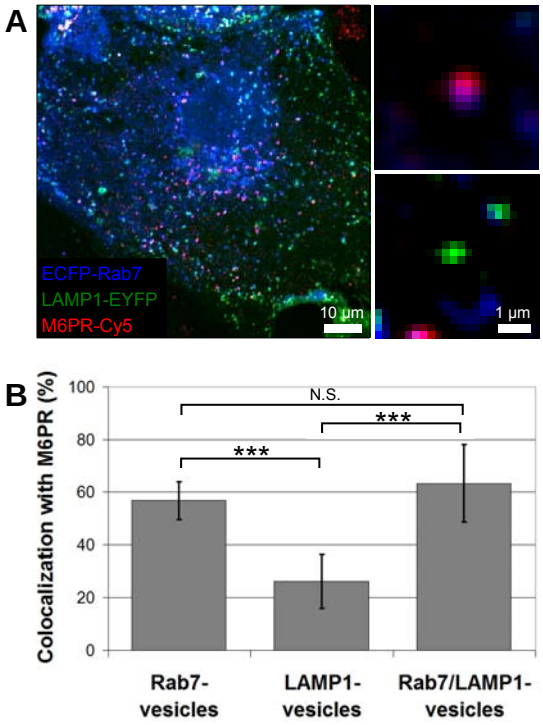

Figure 5.1 Colocalization of M6PR with Rab7-, LAMP1-, and hybrid vesicles. (A) Confocal microscopy image of ECFP-Rab7 (blue), LAMP1-EFYP (green), and an antibody against M6PR labeled with a Cy5-labeled secondary antibody (red) in BS-C-1 cells. Smaller images show a M6PR-positive (red) Rab7-vesicle (blue, top) and a M6PR-negative LAMP1-vesicle (green, bottom). (B) In BS-C-1 cells, a large fraction of Rab7- and hybrid vesicles are positive for M6PR; 57±7% and 63±15%, respectively. A much smaller fraction of LAMP1-vesicles are positive for M6PR, 23±10%. Error bars show standard deviations. The graph shows the analysis of 10-20 of each type of vesicle per cell in 10 cells from 4 distinct experiments. The graph shows the analysis of 10-15 of each type of vesicle per cell in 5 cells. P-values <0.001 are indicated by ***, <0.01 by **. N.S. indicates p-values > 0.05.

vesicles in terms of the presence or absence of M6PR and determine the interactions between the three populations of vesicles.

5.3.2 Colocalization of hybrid, Rab7-, and LAMP1-vesicles with M6PR

Confocal fluorescence microscopy was used to measure colocalization of Rab7-vesicles, LAMP1-vesicles, and Rab7-LAMP1 hybrid vesicles, with M6PR (Figure 5.1).

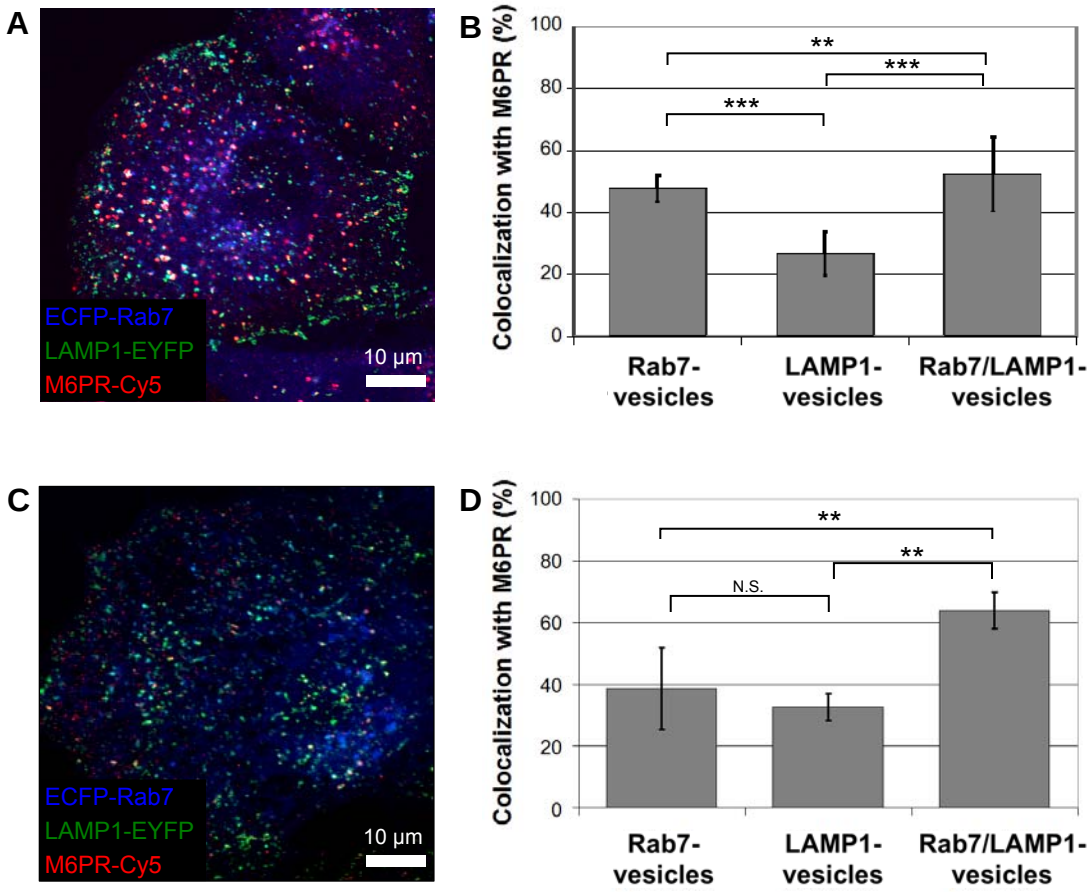

Figure 5.2. Colocalization of M6PR with Rab7-, LAMP1-, and Rab7/LAMP1-vesicles in BS-C-1 cells stably expressing ECFP-Rab7 and in HeLa cells. (A) Confocal microscopy image of ECFP-Rab7 (blue) from a BS-C-1 cell line stably expressing ECFP-Rab7, the transient expression of LAMP1-EYFP (green), and an antibody against M6PR (MA1-066, Fisher Scientific) labeled with a Cy5 secondary antibody (red, AP160S, Chemicon). (B) A significant fraction of Rab7-, LAMP1-, and Rab7/LAMP1-vesicles are positive for M6PR; 48 ± 4%, 27 ± 7 %, and 52 ± 12%, respectively. Error bars show standard deviations. The graph shows the analysis of 10 of each type of vesicle per cell in 9 cells. Similar results were obtained for BS-C-1 cells transiently expressing ECFP-Rab7, Figure 3. (C) Confocal microscopy image of ECFP-Rab7 (blue), LAMP1-EYFP (green), and an antibody against M6PR labeled with a Cy5 secondary antibody (red). (D) As with the BS-C-1 cells, a significant fraction of Rab7-, LAMP1-, and Rab7/LAMP1-vesicles are positive for M6PR; 39 ± 13%, 33 ±4 %, and 64 ± 6%, respectively. Error bars show standard deviations. The graph shows the analysis of 10-15 of each type of vesicle per cell in 5 cells. P-values < 0.001 are indicated by ***, < 0.01 by **. N.S. indicates p-values > 0.05.

Rab7 and LAMP1 were labeled directly by the expression of variants of spectrally distinct fluorescent proteins; Rab7 with ECFP (blue) and LAMP1 with EYFP (green).

Hybrid organelles were positive for both fluorescent proteins and appear turquoise in the images. M6PR was labeled with a primary antibody against M6PR and a Cy5-conjugated secondary antibody (red). Colocalization was scored manually for 10 cells, examining 10-20 of each vesicle type per cell. Sixty-three percent of Rab7-LAMP1 hybrid vesicles were positive for M6PR. Of the non-hybrid vesicles, 57% of Rab7-vesicles were M6PR-positive as compared to 26% of LAMP1-vesicles. The partial colocalization of M6PR with hybrid and Rab7-vesicles is not unique to the BS-C-1 monkey kidney cells. A similar distribution was also observed in HeLa human carcinoma cells (Figure 5.2).

5.3.3 Majority of endo-lysosomal vesicles are hybrid vesicles

Confocal fluorescence microscopy, with the same Rab7 and LAMP1 labeling and fixation parameters as described above, was used to quantify the populations of each type of vesicle in individual cells (Figure 5.3A and B). The number of hybrid, Rab7- and LAMP1-vesicles was determined manually by analyzing 10 random 100 μm^2 regions of the cell to determine the number of each type of vesicle. Values for the 10 regions were averaged and then scaled based on the total area of the cell. An analysis of 10 cells shows that 351-1288 hybrid vesicles are present in each cell and that Rab7- and LAMP1-vesicles each represent ~15% of the total endo-lysosomal vesicle population. The small fraction of Rab7- and LAMP1-vesicles was not unique to BS-C-1 cells, but was also observed in HeLa cells (Figure 5.1 and Figure 5.2).

The relatively small number of Rab7- and LAMP1-vesicles relative to hybrids raises two technical concerns. The first is that vesicles considered non-hybrids are only artifacts due to the labeling scheme used. To insure that these minority populations of

A

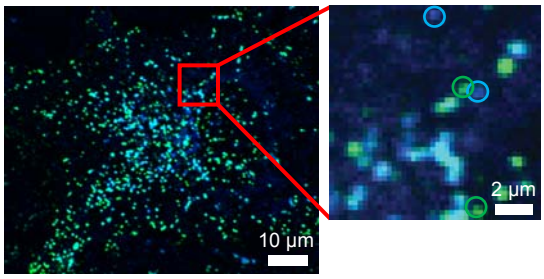

B

Hybrid Vesicles/Cell	351 - 1288
Percentage of Rab7-Vesicles	12.7 ± 3.5
Percentage of LAMP1-Vesicles	14.4 ± 6.3

C

Hybrid Vesicles/Cell (Nocodazole)	251 - 925
Percentage of Rab7-Vesicles	26.2 ± 5.6
Percentage of LAMP1-Vesicles	13.7 ± 6.5

Figure 5.3 The majority of endo-lysosomal vesicles are hybrid vesicles. (A) The majority of endo-lysosomal vesicles are positive for both Rab7 (blue) and LAMP1 (green), shown in a representative confocal microscopy image. The inset shows an enlarged region of the cell. Rab7-, and LAMP1-vesicles are circled. (B) Rab7-vesicles and LAMP1-vesicles are minority populations of vesicles. The analysis of vesicle populations was carried out for 10 cells in 2 distinct experiments. (C) Disruption of microtubules with nocodazole increased the percentage of Rab7-vesicles to 26% as compared to 13% in untreated cells, $p<0.001$. This analysis was carried out on 10 cells in 3 distinct experiments.

Rab7- and LAMP1-vesicles were not artifacts, the same imaging methods were applied to cells with a different labeling scheme. Rab7 was fluorescently labeled with EYFP, the cells were fixed and permeabilized and LAMP1-vesicles were imaged with a primary scheme. The second concern is that the large number of hybrids is due to cross-talk between emission channels; ECFP signal from Rab7 leaking through to the EYFP channel of LAMP1. For this reason, image analysis was carried out using carefully calibrated imaging parameters, obtained from single protein expressing cells, to prevent cross-talk between channels.

5.3.4 Rab7- and LAMP1-vesicles are highly dynamic

To understand the formation and dynamics of these vesicles, their interactions were probed using two-color live cell imaging. As with previous experiments, Rab7 was labeled with ECFP (blue) and LAMP1 was labeled with EYFP (green) and cells were

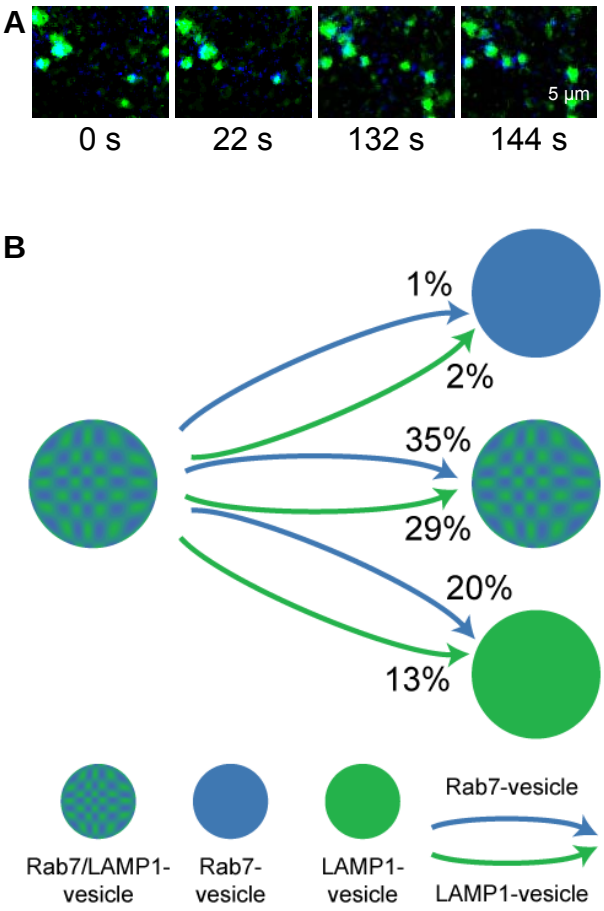

Figure 5.4 Single particle tracking fluorescence microscopy was used to follow the trajectories of Rab7- and LAMP1-vesicles. The trajectories of 50 Rab7-vesicles and 50 LAMP1-vesicles in 7 different cells were analyzed. (A) Snapshots of a trajectory obtained from two color live cell imaging experiments. These images show a LAMP1-vesicle (open arrow) split from a Rab7/LAMP1-vesicle, traffic through the cell, and then merge with a Rab7/LAMP1-vesicle (closed arrow). The corresponding movie is included in Supporting Information. (B) The majority (89%) of trajectories began with a Rab7- (blue) or LAMP1-vesicle (green) splitting from a Rab7/LAMP1-vesicle (blue-green, patterned). The percentage of each type of event is shown. For example, 1% of Rab7-vesicles that split from a Rab7/LAMP1-vesicle then merged with another Rab7-vesicle.

imaged using a custom-built multi-color microscope for live cell imaging and single particle tracking analysis. Images were recorded at a rate of 0.5 Hz for a period of 30 minutes with cells held at 37°C. Data, in the form of movies, were analyzed to detect non-hybrid vesicles and determine their interactions with other vesicles. Vesicles were considered hybrids if the blue and green signals overlapped and moved together within the cell for a minimum of 10 s. An examination of 50 Rab7-vesicles and 50 LAMP1-vesicles in 7 cells shows that the 100% of Rab7-vesicles and 78% of LAMP1-vesicles are initially part of a hybrid vesicle. The Rab7- or LAMP1-vesicle appears to pinch off, traffic through the cell, and then fuse with another vesicle. The majority of Rab7- and LAMP1-vesicles that are tracked from an initial hybrid vesicle move through the cell and then merge with another hybrid vesicle, 62% and 67%, respectively (Figure 5.2D). A smaller fraction of Rab7- and LAMP1-vesicles that split from a hybrid merge with a LAMP1-vesicle, 36% and 28%, respectively. Fusion with a Rab7-vesicle is rarely observed. The importance of microtubules in these dynamics was tested by treating cells with 60 μM nocodazole to depolymerize microtubules (Figure 5.3C) [40]. Qualitatively, the hybrid vesicles in these cells appeared to be larger and sparser. In comparison to untreated cells, which had a range of 351-1288 hybrid vesicles in each cell, the number of hybrid vesicles in the nocodazole-treated cells is in the lower range with 251-925 hybrids in each cell. An analysis of 10 cells showed that the percentage of Rab7-vesicles increased significantly ($p<0.001$), to 26% of the total endo-lysosomal vesicle population. The percentage of LAMP1-vesicles remained constant at 14%.

A visual inspection of the movies, recorded at 0.5 Hz, revealed fusion of vesicles rather than maturation or protein recruitment (Figure 5.6A). The intensity trace of a

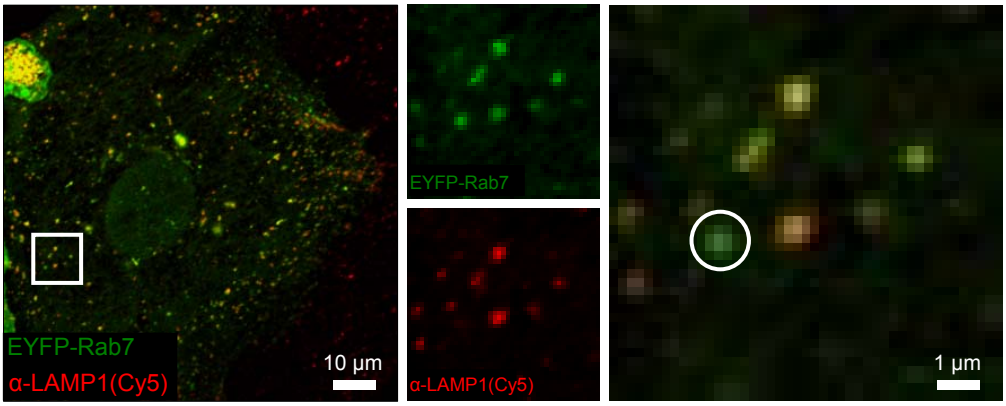

Figure 5.5 Colocalization of EYFP-Rab7 and LAMP1-Cy5. Similar levels of Rab7- and LAMP1-vesicle colocalization are observed with an alternate labeling scheme. A confocal microscopy image of BS-C-1 cells in which Rab7 is labeled with EYFP and LAMP1 is labeled with a primary antibody against LAMP1 (ab25631, Abcam, Cambridge, MA) and a Cy5-labeled secondary antibody (AP160S, Chemicon, Temecula, CA). The inset, split into its two color components and enlarged, shows a non-hybrid Rab7-vesicle (green, circled). The colocalization of Rab7-vesicles with LAMP1-vesicles (89±4%) and the reverse (89±6%) are similar to those obtained previously with the ECFP-Rab7/LAMP1-EYFP labeling scheme used in these experiments. Colocalization values were calculated for 25 vesicles per cell in 9 cells in 3 distinct experiments. Similar values were also obtained for HeLa cells (91±6% colocalization of Rab7-vesicles with LAMP1-vesicles and the reverse (91±4%), data not shown); 12-14 vesicles per cell, 5 cells, 2 distinct experiments.

representative fusion event between a Rab7-vesicle and a hybrid vesicle shows a change in signal only upon contact of vesicles (Figure 5.6B). Data was also recorded on a much faster timescale, 8.1 Hz, to ensure that no dynamics were overlooked (Figure 5.7). As with the 0.5 Hz results, no change in intensity was observed prior to contact between the vesicles.

5.3.5 Endo-lysosomal transport of fluid phase and endocytic cargo

Endo-lysosomal vesicles are not defined only by their protein composition, but also by their function; the transport of extracellular cargo. The lysosome has been conventionally defined as a terminal vesicle; the final stop on the endocytic pathway and

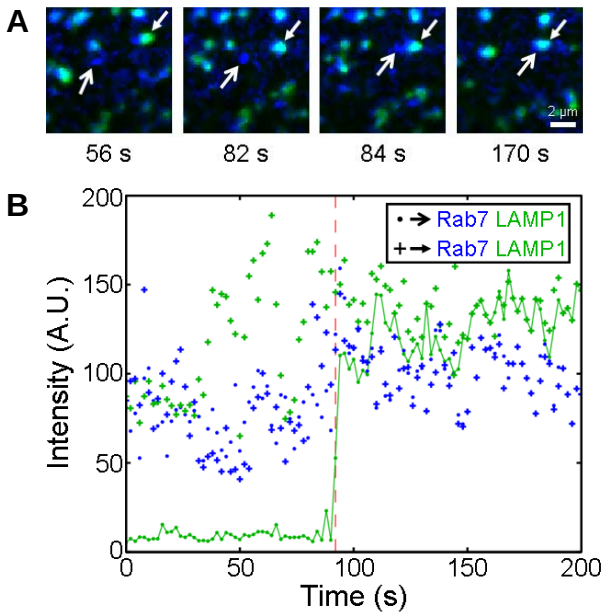

Figure 5.6 Endo-lysosomal vesicles undergo fusion. (A) Snapshots taken from a movie (0.5 Hz) showing the fusion of a Rab7-vesicle (blue, open arrow) with a hybrid vesicle (blue-green, solid arrow). The snapshots are 9 pixel median filtered. (B) An intensity trace of the same fusion event shows that the LAMP1 signal of the Rab7-vesicle (green, dots) is low prior to contact with the hybrid vesicle (pluses). The vertical red line shows the point at which the vesicles make contact. The snapshots and intensity trace are representative of 50 fusion events.

site of cargo degradation.[7] Previous work has established that degradation occurs upstream of the lysosome for many endocytic cargos including LDL,[14] BSA,[13] and ovalbumin.[17] We sought to characterize Rab7-, LAMP1-, and hybrid vesicles in terms of transport; essentially using cargo to determine if a true terminal vesicle exists, and if so, what is its protein composition.

Three classic extracellular cargos; LDL, BSA, and dextran were labeled with fluorophores and colocalization with hybrids, Rab7- and LAMP1-vesicles was measured using confocal fluorescence microscopy of fixed cells. As in previous experiments, Rab7 and LAMP1 were labeled with ECFP and EYFP, respectively, extracellular cargo was labeled with a red-emitting fluorophore. The conjugation of each red-emitting fluorophore is described in Experimental Procedure. For all cargo, colocalization was

scored manually for 9-12 cells, examining 9-15 of each type of vesicle per cell, in at least three distinct experiments. Specific values are noted in figure legends.

5.3.6 Dextran enters Rab7- and LAMP1-vesicles, but accumulates in LAMP1-vesicles

Dextran (10,000 MW) is a fluid-phase cargo, internalized by pinocytosis rather than receptor-mediated endocytosis.[28-31] Dextran was labeled with the red-emitting fluorophore, AlexaFluor647 (AF647, Invitrogen), and incubated with cells for 1 hr or 18 hr at a concentration of 0.25 mg/mL. After 1 hr, cells were rinsed twice in PBS, fixed

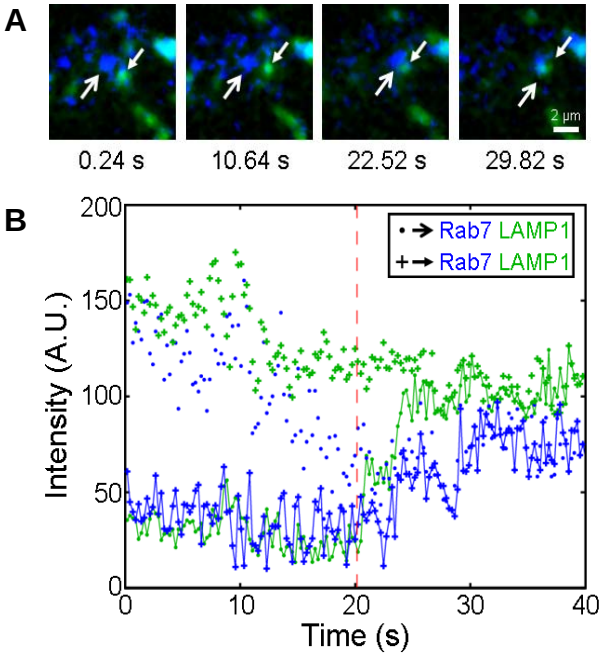

Figure 5.7 Imaging vesicle interactions with high time resolution shows fusion-dependent hybrid vesicle formation. (A) Snapshots taken from a movie (8.1 Hz) showing the fusion of a Rab7-vesicle (blue, open arrow) with a LAMP1-vesicle (green, solid arrow). The snapshots are 9 pixel median filtered. (B) An intensity trace of the same fusion event shows that the LAMP1 signal of the Rab7-vesicle (green, dots) and the Rab7 signal of the LAMP1-vesicle (blue, pluses) are non-existent prior to contact with the other vesicle. The vertical red line shows the point at which the vesicles make contact.

with 4% formaldehyde, and imaged (Figure 5.6A). Ten to fifteen of each type of vesicle, in 6-12 cells, were randomly identified and manually scored for colocalization with dextran as described in Materials and Methods. After a 30 min incubation with dextran, 42 ± 10% of Rab7-vesicles contained dextran. This level remained essentially the same (41 ± 11%) after a 1 hr incubation and then decreased to 14 ± 8% following a 4 hr chase. The decrease from 41% at 1 hr to 14% after a 4 hr chase is significant with a p-value less than 0.001. In comparison, 28 ± 9% of LAMP1-vesicles contained dextran after a 30 min incubation. This value increased to 57 ± 16% after a 1 hr incubation and remained high

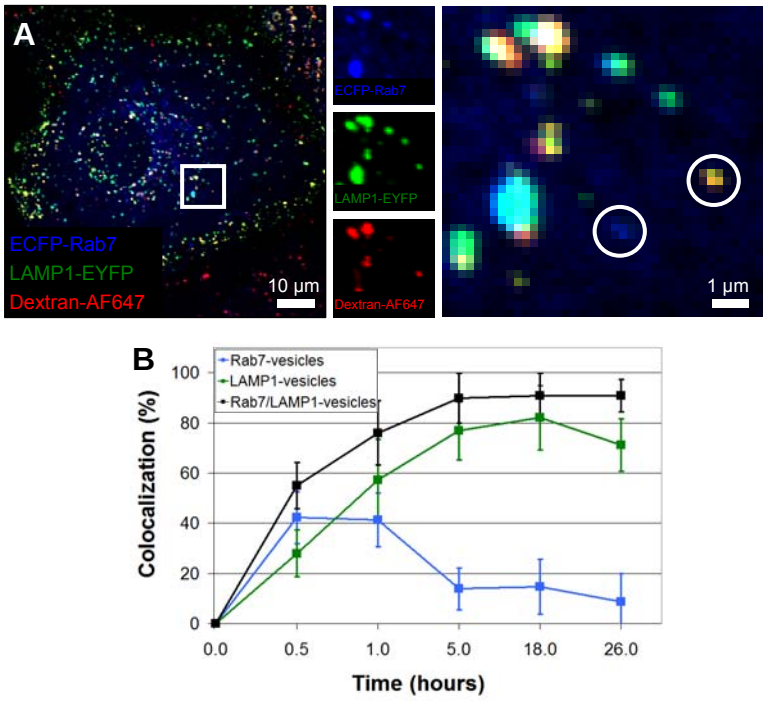

Figure 5.8 Dextran enters Rab7- and LAMP1-vesicles, but accumulates in LAMP1-vesicles. (A) Confocal microscopy image of dextran-AF647 (red), Rab7 (blue), and LAMP1 (green) after an 18 hr incubation with dextran. The inset, split into its three color components and enlarged, shows a Rab7-vesicle in the absence of dextran and a LAMP1-vesicle containing dextran, both circled. (B) At 1 hr, a large fraction of Rab7- and LAMP1-vesicles contain dextran, 67±11% and 67±15%, respectively. After 18 hr, the fraction of Rab7-vesicles containing dextran decreases significantly to 14±11%, $p<0.001$, while the fraction of LAMP1-vesicles containing dextran increases to 87±9%, $p<0.001$. Error bars represent standard deviation. At each time point, analysis was carried out for 10-15 vesicles per cell in 12 cells in 4 distinct experiments.

0(>70%) at later times. After a 30 min incubation with dextran, 55 ± 9% of Rab7/LAMP1-vesicles contained dextran. Like LAMP1-vesicles, this value increased after a 1 hr incubation (76 ± 13%) and remained high (>90%) at all later time points.

5.3.7 LDL and BSA are retained in Rab7-vesicles

While dextran is a fluid-phase cargo, LDL and BSA are both internalized by cells via receptor-mediated endocytosis.[8,9,41-43] To probe the pathway of receptor-mediated cargo, LDL was labeled with the red-emitting lipophilic fluorophore, DiD, and BSA was labeled with AF647. Both were incubated with cells for 1 hr and 18 hr, then fixed, imaged, and analyzed using the same procedure as described for dextran (Figure 5.9). After a 1 hr incubation, LDL (10 μg/mL) was found in 22% of Rab7-vesicles and 24% of LAMP1-vesicles. These values are nearly unchanged after 18 hr with 20% of Rab7-

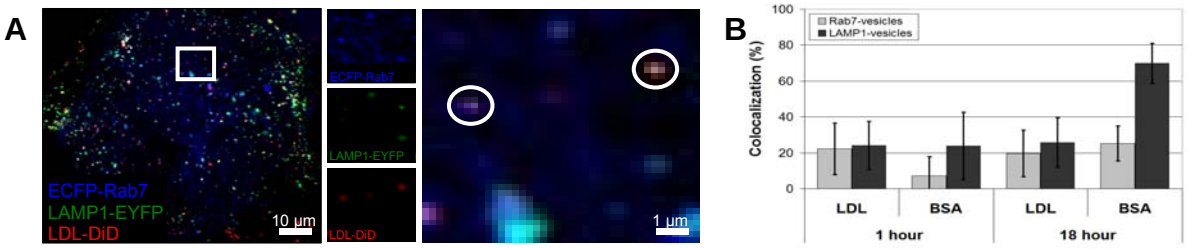

Figure 5.9 LDL and BSA are retained in Rab7-vesicles. (A) Confocal microscopy image of LDL-DiD (red), ECFP-Rab7 (blue), and EYFP-LAMP1 (green) after a 1 hr incubation with LDL. The inset, split into its three color components and enlarged, shows a Rab7-vesicle containing LDL and a LAMP1-vesicle containing LDL (circles). (B) An equal percentage of Rab7- and LAMP1-vesicles contain LDL at 1 hr, 22±14% and 24±13%, respectively, and 18 hr, 20±13% and 26±14%, respectively. At each time point, analysis was carried out for 10-15 vesicles per cell in 9-11 cells in 3 distinct experiments. Three-fold more LAMP1-vesicles than Rab7-vesicles contain BSA at 1 hr, 7±11% and 24±19%, respectively. This ratio is maintained at 18 hr; 25±10% Rab7-vesicles contain BSA compared to 70±11% LAMP1-vesicles. At each time point, analysis was carried out for 9-14 vesicles per cell in 9-11 cells in 3 distinct experiments. Error bars represent standard deviation.

vesicles containing LDL and 26% of LAMP1-vesicles containing LDL. In comparison, a similar receptor-dependent endocytic molecule, BSA, is rarely found in Rab7-vesicles at 1 hr (7%) with LAMP1-vesicles three-fold more likely to contain BSA (24%, p=0.04). After a 18 hr incubation with BSA, both Rab7-vesicles and LAMP1-vesicles show an increase in BSA colocalization, 25% and 70%, although the ratio remains the same with LAMP1-vesicles containing approximately three-fold more BSA.

5.3.8 Majority of cargo is localized in hybrids and enters in a concentration- and time-dependent manner

The majority of hybrid vesicles, 70% of the endo-lysosomal vesicle population, contain cargo. After a 1 hr incubation, 78% and 75% of hybrid vesicles contain dextran and LDL, respectively (Figure 5.10). Fewer hybrids contain BSA (36%). After 18 hr the values increase and are similarly high for dextran (94%), LDL (85%), and BSA (79%). In addition to an increase with time, hybrid vesicles also show increased levels of cargo as a function of cargo concentration. LDL was incubated with cells for one hour at three different concentrations; 0.2, 1, and 10 μg/mL. After one hour, cells were rinsed, fixed, and imaged. Ten to fifteen hybrid vesicles in a minimum of 9 different cells were randomly identified and manually scored for colocalization with LDL. At the lowest concentration, 0.2 μg/mL, 6% of Rab7- and 4% of LAMP1-vesicles had LDL localized within them. At 1 μg/mL colocalization increased to 17% and 20%, respectively. This value remained essentially the same at 10 μg/mL with 22% and 24% colocalization of LDL with Rab7- and LAMP1-vesicles, respectively.

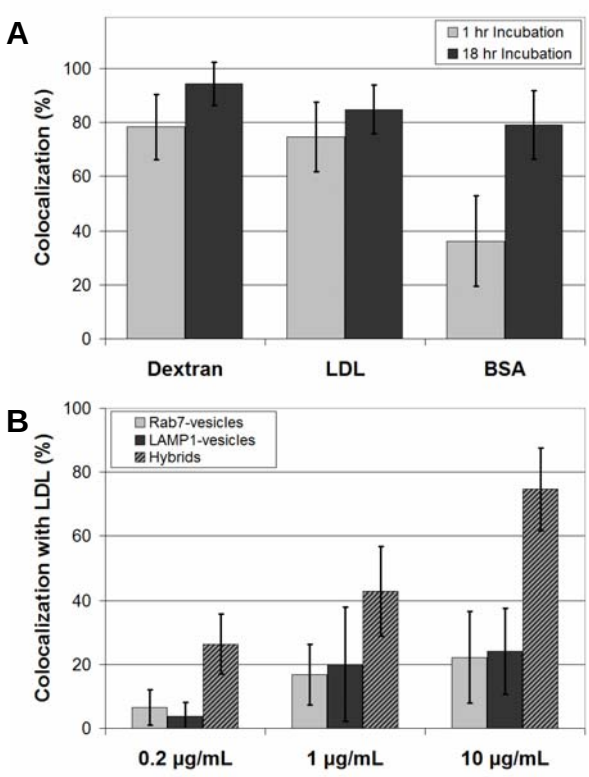

Figure 5.10 Majority of cargo is localized in hybrids and enters in a concentration- and time-dependent manner. (A) The fraction of hybrid vesicles containing cargo is high at 1 hr for dextran (78±12%) and LDL (75±13%), BSA is an exception (36±17%). At 18 hr, the fraction of hybrids containing cargos is uniformly high: dextran (94±8%), LDL (85±9%), and BSA (79±13%). Analysis is the same as for Rab7- and LAMP1-vesicles, described above. Error bars represent standard deviation. (B) Fraction of each vesicle population containing LDL after a 1 hr incubation. The standard LDL concentration used in the course of experiments was 10 µg/mL. The data and analysis are described above. 0.2 µg/mL of LDL was found in a small fraction of Rab7- (6±6%), LAMP1- (4±4%), and hybrid (26±9%) vesicles. Increasing the concentration to 1 µg/ml increased the percentage of each type of vesicle containing LDL: Rab7- (17±10%), LAMP1- (20±18%), and hybrid (43±14%) vesicles. Analysis was carried out for 10-15 vesicles per cell in 9 cells in 3 distinct experiments. Error bars represent standard deviation.

5.4 Discussion

Understanding the endo-lysosomal pathway is fundamental to cell biology and plays an increasingly important role in applications such as gene and nanoparticle delivery, which depend on endocytic targeting. To that end, characterizing the organelles that comprise the endo-lysosomal pathway is a necessary first step. Understanding how

cargo is transported through these endo-lysosomal vesicles is the essential second step. The experiments described above use fluorescence microscopy to image endo-lysosomal vesicles directly in fixed and live cells. Single particle tracking is further used to characterize the dynamics and cargo transport of these vesicles. This fluorescence imaging-based approach makes it possible to characterize the non-hybrid vesicles which exist as a minority of endo-lysosomal vesicles and would not be detected using standard biochemical or electron microscopy approaches. While a hybrid population of endosomes-lysosomes had been observed previously,[3,18-23,44] this work is the first to characterize the minority fraction of non-hybrid vesicles, to determine how they interact to form hybrid vesicles, and to determine how cargo is transported in the three populations of vesicles.

5.4.1 M6PR colocalization reveals sub-populations of endo-lysosomal vesicles

We sought to unify the characterization of the endo-lysosomal pathway by simultaneously imaging the proteins most closely associated with late endosomes and lysosomes; Rab7, LAMP1, and M6PR (Figure 5.1). A review of the literature generally describes Rab7 as a late endosomal protein[24,32-36] although it has also been associated with lysosomes.[37] LAMP1 has been described as both lysosomal, the source of the name, and late endosomal.[4] The lysosome is defined to be M6PR-negative.[18,19,25-27] Late endosomes, as well as early endosomes, can be M6PR-positive although not all endosomes will necessarily be M6PR-positive.[34,37-39]

The existence of hybrid vesicles immediately resolves the discrepancy of Rab7-lysosomes and LAMP1-late endosomes as the majority of endo-lysosomal vesicles are

positive for both (Figure 5.3). As 63% of hybrid vesicles were positive for M6PR, this suggests that two sub-populations of hybrids exist; one that is late endosomal, the other lysosomal. Previous work, has described the incomplete colocalization of M6PR with Rab7-positive vesicles.[34,37-39] The less than 100% colocalization of Rab7-vesicles, as well as hybrid vesicles, with M6PR can be attributed to either an experimental artifact, as immunostaining may be less than 100% efficient, or the existence of a true subset of organelles: Rab7-positive lysosomes. In a similar manner, the small fraction of LAMP1-vesicles positive for M6PR can be considered LAMP1-endosomes or false positives due to non-specific staining of the M6PR antibody. However, control experiments show that non-specific staining in the absence of the primary M6PR antibody is minimal, suggesting that there exists a small population of LAMP1-endosomes (Figure 2.4).

5.4.2 Rab7- and LAMP1-vesicles undergo fusion

The use of GFP-labeled proteins provides fluorescent probes that can be used to directly monitor the formation of hybrid vesicles as Rab7-vesicles and LAMP1-vesicles undergo transport in live cells. This approach was used to distinguish between two models of hybrid formation. The first is a maturation model in which one protein is recruited to a pre-existing vesicle positive for the other protein, as is observed in the maturation of early endosomes to late endosomes.[24,39] The second model is a direct fusion of two populations of vesicles to form hybrid vesicles. Single particle tracking analysis of two-color fluorescence microscopy images support a direct fusion model, in which no accumulation of protein is observed prior to the contact of vesicles. This observation is in good agreement with pulse-chase experiments which probed vesicle fusion by imaging

cargo exchange,[45] although these experiments were unable to distinguish between hybrid and non-hybrid vesicles. Rhodamine-labeled dextran was incubated with cells for a 4 hr pulse followed by a 20 hr chase in the absence of dextran. This pulse-chase resulted in dextran loaded into electron-dense, lgp120 (LAMP1)-positive vesicles. A shorter pulse was then used to load Oregon green 488-labeled dextran into M6PR-positive vesicles. This method revealed a direct fusion between the two populations of vesicles, however it fails to factor in the presence of hybrid vesicles which would be both LAMP1- and M6PR-positive. In comparison, our results suggest a long incubation with dextran would result in hybrid and LAMP1-vesicle loading, the short pulse would load Rab7-vesicles, LAMP1-vesicles and hybrid vesicles. It remains formally possible that hybrid vesicles can also be formed directly, independently of fusion or maturation, which will be probed in future experiments.

5.4.3 Disruption of microtubules increases the percentage of Rab7-vesicles

The non-hybrid vesicles are highly mobile with transport speeds indicative of active transport carried out by motor proteins moving on the cytoskeleton.[22] Treatment of cells with nocodazole disrupts the microtubules and allows us to test the effect of cytoskeleton-dependent dynamics on the distribution of vesicle populations. The number of hybrid vesicles in untreated and nocodazole-treated cells is difficult to compare since this value is highly dependent on cell size. A better comparison can be made between the percent of Rab7- and LAMP1-vesicles as a function of total vesicle population. The percent of Rab7-vesicles increases significantly upon nocodazole treatment, from 13% to 26% of the total vesicle population, $p<0.001$. The percent of LAMP1-vesicles is not

affected by nocodazole. While this clearly shows that the disruption of microtubules changes the distribution of endo-lysosomal vesicles, and that Rab7- and LAMP1-vesicles have different responses to the disruption of microtubules, the underlying reason is not clear. One possibility is that the disruption of microtubules alters the fusion dynamics leaving Rab7-vesicles unable to form hybrids. However, previous work has shown that nocodazole leads to the disruption of a reticulated Rab7 structure that is associated with microtubules.[38] To that end, our observation of a greater number of Rab7-vesicles may reflect the appearance of new Rab7-vesicles that were previously associated with the reticulated structure.

5.4.4 Characterization of the endo-lysosomal pathway

This characterization scheme defines hybrid organelles by the presence of both Rab7 and LAMP1. Both Rab7- and hybrid vesicles show significant colocalization with M6PR (Figure 5.1), a protein that is defined as endosomal. Hybrid vesicles undergo repeated splitting and fusion events with Rab7- and LAMP1-vesicles, which exist as a minority population of vesicles within the cell (Figures 5.2 and 5.4). It should be noted that an alternative approach would be to define hybrid vesicles as M6PR-positive and LAMP1-positive. This approach has been used previously in the cryo-electron microscopic characterization of M6PR and lpg120 (LAMP1).[19] This research found that M6PR-negative, lpg120-positive vesicles served as a terminal organelle, defined as lysosomes. This is in good agreement with our results, which extend the characterization to include Rab7 as a distinct protein marker. To fully characterize the endo-lysosomal pathway, it is necessary to couple this level of characterization, colocalization with

protein markers, with an understanding of the function of the endo-lysosomal pathway, transport of extracellular cargo. To address this aspect of endo-lysosomal function, we probe the transport of a fluid-phase cargo, dextran, and two receptor-mediated endocytic cargos, LDL and BSA, in relation to Rab7- and LAMP1-vesicles. We sought to address the direction of cargo transport and the existence of a true terminal vesicle.

5.4.5 Transport of fluid phase cargo defines LAMP1-positive vesicles as terminal vesicles

Dextran, a fluid phase cargo, provides a marker of transport in the absence of an endocytic receptor. At early times, dextran is found at equally high levels (67%) in both Rab7- and LAMP1-vesicles suggesting initial entry into each population of vesicle (Figure 5.6). At longer times, there is a significant decrease in the Rab7-vesicle level (14%) and an increase in LAMP1-vesicles (87%). Colocalization with hybrid vesicles is high at both time points; 78% at 1 hr and 94% at 18 hr (Figure 5.10). Colocalization values combined with fusion dynamics (Figure 5.2D) provides a picture of fluid-phase transport though the cell. As Rab7- and LAMP1-vesicles have similar populations (Figure 5.3) and separation times,[22] it is expected that a steady-state system will result in a ten-fold greater amount of cargo in LAMP1-vesicles than Rab7-vesicles. This ratio is approximated at 18 hr at which time LAMP1-vesicles contain 6-fold more dextran than Rab7-vesicles. The high, and equivalent, entry of dextran into Rab7- and LAMP1-vesicles at early times suggests initial entry into both populations of vesicles followed by transport to hybrid and LAMP1-vesicles. These results demonstrate that LAMP1-vesicles are both terminal vesicles, a final destination for extracellular cargo, and largely M6PR-negative, suggesting they are best defined as lysosomes.

5.4.6 Transport of endocytic cargo reveals receptor-dependent dynamics

The transport of dextran provides a picture of cargo transport in the absence of a cell surface receptor. In comparison to dextran, LDL and BSA are internalized via receptor-mediated endocytosis.[8,9,43] Deviations from dextran transport suggest a role for receptors and upstream targeting in the retention of endocytic cargo in Rab7-vesicles. LDL, like dextran, enters Rab7- and LAMP1-vesicles at equal, although much lower, ratios; 22% for Rab7-vesicles and 24% for LAMP1-vesicles. Unlike dextran, these levels remain unchanged at 18 hr. These results suggest that LDL also enters both populations of vesicle directly and that the level of entry is determined by the endocytic receptor. While it is possible that LDL is degraded during this period, LDL localized in the hybrid vesicles serves as a control for the level of degradation and shows a slight increase during the 18 hr incubation.

BSA enters Rab7- and LAMP1-vesicles at a 1:3 ratio, compared to the 1:1 ratio observed for LDL. This ratio is maintained after an 18 hr incubation, although the absolute values increase over this period. The maintenance of a constant ratio, similar to the behavior of LDL, is distinct from that of dextran which showed a decrease in Rab7-vesicles and increase in LAMP1-vesicles. We propose that the constant ratio of cargo in Rab7- and LAMP1-vesicles as a function of time is a signature of receptor-mediated endocytic uptake with the specific ratio determined by the endocytic receptor.

5.4.7 Endo-lysosomal transport and the characterization of the endo-lysosomal pathway

In summary, the endo-lysosomal pathway is composed of at least three distinct populations of vesicles: Rab7-, LAMP1-, and Rab7/LAMP1-vesicles. The majority of

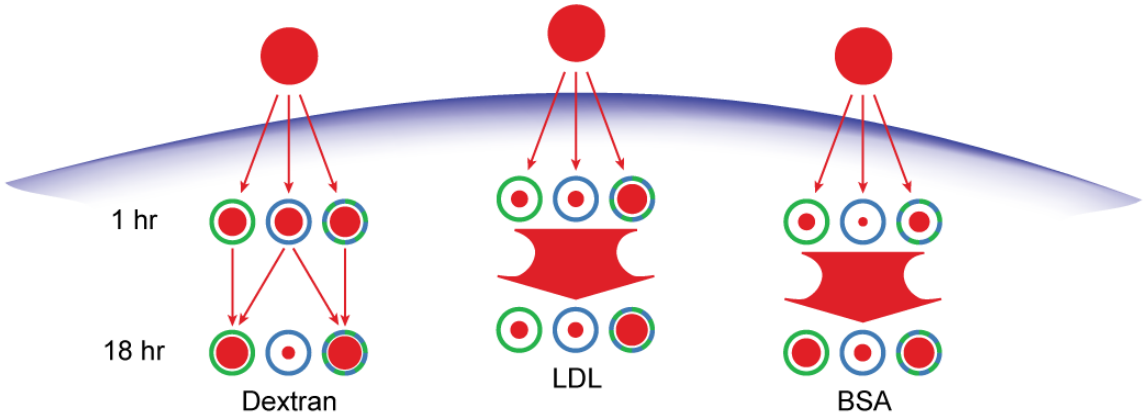

Figure 5.11 Schematic of cargo transport through the endo-lysosomal pathway. Cargo (red) enters into Rab7- (blue), LAMP1- (green), and hybrid (blue-green) vesicles and is redistributed as shown by the arrows. The area of each red circle represents the colocalization of each vesicle population with the cargo.

endo-lysosomal vesicles are positive for both Rab7 and LAMP1. Measuring the location of dextran, a fluid phase cargo, as it moves through the endo-lysosomal pathway allows us to examine the role of Rab7/LAMP1-vesicles in the endo-lysosomal pathway. Dextran is present in Rab7-, LAMP1-, and Rab7/LAMP1-vesicles at early times, but shifts to primarily LAMP1- and Rab7/LAMP1-vesicles at later times demonstrating that LAMP1- and Rab7/LAMP1-vesicles are terminal vesicles in the endo-lysosomal pathway.

Our research characterizes this vesicle, as well as two populations of non-hybrid vesicles defined by Rab7 and LAMP1 proteins. Tracking cargo as it moves through the endo-lysosomal pathway provides an additional dimension for analysis (Figure 5.11). The movement of dextran from Rab7-, LAMP1-, and hybrid vesicles at early times to primarily LAMP1- and hybrid vesicles at late times shows that LAMP1- and hybrid vesicles are terminal vesicles in the endo-lysosomal pathway. Coupled with the low colocalization with M6PR, LAMP1-vesicles can be defined as lysosomes. Unlike dextran, endocytic cargo such as LDL and BSA does not move from Rab7-vesicles to LAMP1- and hybrid vesicles, but instead maintains an equal distribution in Rab7- and

LAMP1-vesicles over 18 hr. In comparison to dextran, we suggest that the presence of endocytic cargo in Rab7-vesicles is due to upstream targeting and may reflect a more selective degradative environment.[46]

5.5 References

1 Pillay, C. S.; Elliott, E.; Dennison, C., Endolysosomal proteolysis and its regulation. *Biochemical Journal* **2002**, *363*, 417-429.

2 Saftig, P.; Klumperman, J., Lysosome biogenesis and lysosomal membrane proteins: trafficking meets function. *Nature Reviews Molecular Cell Biology* **2009**, *10*, 623-635.

3 Luzio, J. P.; Pryor, P. R.; Bright, N. A., Lysosomes: fusion and function. *Nature Reviews Molecular Cell Biology* **2007**, *8*, 622-632.

4 Clague, M. J., Molecular aspects of the endocytic pathway. *Biochemical Journal* **1998**, *336*, 271-282.

5 Cho, Y. W.; Kim, J. D.; Park, K., Pollycation gene delivery systems: escape from endosomes to cytosol. *Journal of Pharmacy and Pharmacology* **2003**, *55*, 721-734.

6 Duan, H. W.; Nie, S. M., Cell-penetrating quantum dots based on multivalent and endosome-disrupting surface coatings. *Journal of the American Chemical Society* **2007**, *129*, 3333-3338.

7 Alberts, B.; Bray, D.; Lewis, J.; Raff, M.; Roberts, K.; Watson, J. D. *Molecular Biology of the Cell*. 3 edn, (Garland Publishing, 1994).

8 Goldstein, J. L.; Brown, M. S.; Anderson, R. G. W.; Russell, D. W.; Schneider, W. J., Receptor-mediated endocytosis: concepts emerging from the LDL receptor system. *Annual Review of Cell Biology* **1985**, *1*, 1-39.

9 Davis, C. G.; Goldstein, J. L.; Sudhof, T. C.; Anderson, R. G. W.; Russell, D. W.; Brown, M. S., Acid-dependent ligand dissociation and recycling of LDL receptor mediated by growth-factor homology region. *Nature* **1987**, *326*, 760-765.

10 Trowbridge, I. S.; Collawn, J. F.; Hopkins, C. R., Signal-dependent membrane-protein trafficking in the endocytic pathway. *Annual Review of Cell Biology* **1993**, *9*, 129-161.

11 Mellman, I., Endocytosis and molecular sorting. *Annual Review of Cell and Developmental Biology* **1996**, *12*, 575-625.

12 Kjeken, R.; Brech, A.; Lovdal, T.; Roos, N.; Berg, T., Involvement of early and late lysosomes in the degradation of mannosylated ligands by rat-liver endothelial cells. *Experimental Cell Research* **1995**, *216*, 290-298.

13 Kundra, R.; Kornfeld, S., Asparagine-linked oligosaccharides protect Lamp-1 and Lamp-2 from intracellular proteolysis. *Journal of Biological Chemistry* **1999**, *274*, 31039-31046.

14 Humphries, W. H.; Fay, N. C.; Payne, C. K., Intracellular degradation of low-density lipoprotein probed with two-color fluorescence microscopy. *Integr. Biol.* **2010**, *2*, 536-544.

15 Bowser, R.; Murphy, R. F., Kinetics of hydrolysis of endocytosed substrates by mammalian cultured cells-Early introduction of lysosomal enzymes into the endocytic pathway. *Journal of Cellular Physiology* **1990**, *143*, 110-117.

16 Runquist, E. A.; Havel, R. J., Acid hydrolases in early and late endosome fractions from rat liver. *Journal of Biological Chemistry* **1991**, *266*, 22557-22563.

17 Tjelle, T. E.; Brech, A.; Juvet, L. K.; Griffiths, G.; Berg, T., Isolation and characterization of early endosomes, late endosomes and terminal lysosomes: Their role in protein degradation. *Journal of Cell Science* **1996**, *109*, 2905-2914.

18 Griffiths, G.; Hoflack, B.; Simons, K.; Mellman, I.; Kornfeld, S., The mannose 6-phosphate receptor and the biogenesis of lysosomes. *Cell* **1988**, *52*, 329-341.

19 Geuze, H. J.; Stoorvogel, W.; Strous, G. J.; Slot, J. W.; Bleekemolen, J. E.; Mellman, I., Sorting of mannose 6-phosphate receptors and lysosomal membrane-proteins in endocytic vesicles. *Journal of Cell Biology* **1988**, *107*, 2491-2501.

20 Bright, N. A.; Reaves, B. J.; Mullock, B. M.; Luzio, J. P., Dense core lysosomes can fuse with late endosomes and are re-formed from the resultant hybrid organelles. *Journal of Cell Science* **1997**, *110*, 2027-2040.

21 Ludwig, T.; Griffiths, G.; Hoflack, B., Distribution of newly synthesized lysosomal enzymes in the endocytic pathway of normal rat-kidney cells. *Journal of Cell Biology* **1991**, *115*, 1561-1572.

22 Szymanksi, C. J.; Humphries, W. H.; Payne, C. K., Single particle tracking as a method to resolve differences in highly colocalized proteins. *Analyst* **2011**, *136*, 3527-3533.

23 Mullock, B. M.; Bright, N. A.; Fearon, G. W.; Gray, S. R.; Luzio, J. P., Fusion of lysosomes with late endosomes produces a hybrid organelle of intermediate density and is NSF dependent. *Journal of Cell Biology* **1998**, *140*, 591-601.

24 Rink, J.; Ghigo, E.; Kalaidzidis, Y.; Zerial, M., Rab conversion as a mechanism of progression from early to late endosomes. *Cell* **2005**, *122*, 735-749.

25 Geuze, H. J.; Slot, J. W.; Strous, J. A. M.; Hasilik, A.; Vonfigura, K., Possible pathways for lysosomal-enzyme delivery. *Journal of Cell Biology* **1985**, *101*, 2253-2262.

26 Sahagian, G. G.; Neufeld, E. F., Biosynthesis and turnover of the mannose 6-phosphate receptor in cultured chinese-hamster ovary cells. *Journal of Biological Chemistry* **1983**, *258*, 7121-7128.

27 Brown, W. J.; Goodhouse, J.; Farquhar, M. G., Mannose-6-phosphate receptors for lysosomal-enzymes cycle between the golgi-complex and endosomes. *Journal of Cell Biology* **1986**, *103*, 1235-1247.

28 Hacker, U.; Albrecht, R.; Maniak, M., Fluid-phase uptake by macropinocytosis in Dictyostelium. *Journal of Cell Science* **1997**, *110*, 105-112.

29 Racoosin, E. L.; Swanson, J. A., Macropinosome maturation and fusion with tubular lysosomes in macrophages. *Journal of Cell Biology* **1993**, *121*, 1011-1020.

30 Sallusto, F.; Cella, M.; Danieli, C.; Lanzavecchia, A., Dendritic cells use macropinocytosis and the mannose receptor to concentrate macromolecules in the major histocompatibility complex class-II compartment - Down-regulation by cytokines and bacterial products. *Journal of Experimental Medicine* **1995**, *182*, 389-400.

31 Thilo, L.; Stroud, E.; Haylett, T., Maturation of early endosomes and vesicular traffic to lysosomes in relation to membrane recycling. *Journal of Cell Science* **1995**, *108*, 1791-1803.

32 Barbero, P.; Bittova, L.; Pfeffer, S. R., Visualization of Rab9-mediated vesicle transport from endosomes to the trans-Golgi in living cells. *Journal of Cell Biology* **2002**, *156*, 511-518.

33 Soldati, T.; Rancano, C.; Geissler, H.; Pfeffer, S. R., Rab7 and Rab9 are recruited onto late endosomes by biochemically distinguishable processes. *Journal of Biological Chemistry* **1995**, *270*, 25541-25548.

34 Vitelli, R.; Santillo, M.; Lattero, D.; Chiariello, M.; Bifulco, M.; Bruni, C. B.; Bucci, C., Role of the small GTPase RAB7 in the late endocytic pathway. *Journal of Biological Chemistry* **1997**, *272*, 4391-4397.

35 Chavrier, P.; Parton, R. G.; Hauri, H. P.; Simons, K.; Zerial, M., Localization of low-molecular-weight GTP-binding proteins to exocytic and endocytic compartments. *Cell* **1990**, *62*, 317-329.

36 Pfeffer, S. R., Rab GTPases: Specifying and deciphering organelle identity and function. *Trends in Cell Biology* **2001**, *11*, 487-491.

37 Bucci, C.; Thomsen, P.; Nicoziani, P.; McCarthy, J.; van Deurs, B., Rab7: A key to lysosome biogenesis. *Molecular Biology of the Cell* **2000**, *11*, 467-480.

38 Meresse, S.; Gorvel, J. P.; Chavrier, P., The Rab7 GTPase resides on a vesicular compartment connnected to lysosomes. *Journal of Cell Science* **1995**, *108*, 3349-3358.

39 Lakadamyali, M.; Rust, M. J.; Zhuang, X., Ligands for clathrin-mediated endocytosis are differentially sorted into distinct populations of early endosomes. *Cell* **2006**, *124*, 997-1009.

40 Payne, C. K.; Jones, S. A.; Chen, C.; Zhuang, X. W., Internalization and trafficking of cell surface proteoglycans and proteoglycan-binding ligands. *Traffic* **2007**, *8*, 389-401.

41 Tagawa, M.; Yumoto, R.; Oda, K.; Nagai, J.; Takano, M., Low-Affinity Transport of FITC-Albumin in Alveolar Type II Epithelial Cell Line RLE-6TN. *Drug Metabolism and Pharmacokinetics* **2008**, *23*, 318-327.

42 Yumoto, R.; Nishikawa, H.; Okamoto, M.; Katayama, H.; Nagai, J.; Takano, M., Clathrin-mediated endocytosis of FITC-albumin in alveolar type II epithelial cell line RLE-6TN. *American Journal of Physiology-Lung Cellular and Molecular Physiology* **2006**, *290*, L946-L955.

43 Schnitzer, J. E.; Oh, P., Albondin-mediated capillary-permeability to albumin-differential role of receptors in endothelial transcytosis and endocytosis of native and modified albumins. *Journal of Biological Chemistry* **1994**, *269*, 6072-6082.

44 Luzio, J. P.; Poupon, V.; Lindsay, M. R.; Mullock, B. M.; Piper, R. C.; Pryor, P. R., Membrane dynamics and the biogenesis of lysosomes (Review). *Molecular Membrane Biology* **2003**, *20*, 141-154.

45 Bright, N. A.; Gratian, M. J.; Luzio, J. P., Endocytic delivery to lysosomes mediated by concurrent fusion and kissing events in living cells. *Current Biology* **2005**, *15*, 360-365.

46 Authier, F.; Posner, B. I.; Bergeron, J. J. M., Endosomal proteolysis of internalized proteins. *FEBS Letters* **1996**, *389*, 55-60.

CHAPTER 6

THE INTRACELLULAR, VESICLE-MEDIATED OF INTRACELLULAR MEASUREMENT OF ENZYME-MEDIATED DEGRADATION: DEQUENCHING OF FLUOROPHORES AS A METHOD TO PROBE CHEMICAL REACTIONS IN LIVE CELLS

6.1 Summary

The ability to characterize the chemical activity of a cell is essential to understanding human health and disease. We describe a fluorescence assay that can be used to probe chemical reactions, including enzymatic activity, in live cells. By labeling molecules or particles of interest with multiple fluorophores, emission is quenched resulting in a weak fluorescent signal. Upon degradation of the molecule or particle, fluorescence emission increases indicating that a chemical reaction has occurred. This dequenching assay can be used across multiple scales - from subcellular measurements with fluorescence microscopy to the analysis of tens of thousands of cells with flow cytometry - without any modification to existing experimental platforms. We first use a protein, bovine serum albumin, and a lipid nanoparticle, low-density lipoprotein, to demonstrate fluorescent labeling schemes and *in vitro* measurements used to quantify dequenching. We show that dequenching is a function of the number of fluorophores bound to the protein or particle and that it occurs in response to enzymatic degradation. We then use this dequenching assay to characterize the intracellular degradation of bovine serum albumin. Using a combination of fluorescence microscopy and flow cytometry, we find that the dequenching of bovine serum albumin occurs in an endocytic vesicle that is positive for LAMP1 and that it is inhibited by pepstatin A, an acid protease inhibitor.

6.2 Introduction

The ability to characterize the chemical activity of a cell is essential to understanding human health and disease. Cells are highly heterogeneous with each organelle, or even different regions of a single organelle, providing a distinct microenvironment.[1] Cellular microenvironments are especially important for the intracellular reactions that degrade extracellular cargo for use by the cell. Extracellular cargo, such as nutrients, viruses, and toxins, bind to the plasma membrane of the cell, are internalized into membrane-bound endosomes, and trafficked through the cell.[1-6] The cargo is transported through a series of endocytic vesicles of decreasing pH and distinct enzyme environments. The specific type of cargo is sensitive to these changes in pH and enzyme activity resulting in the degradation of extracellular proteins for use by the cell or release of viruses into the cytosol leading to viral replication. Studies of the endocytic pathway require spatial information, to characterize the population of endocytic vesicles, and temporal information, as the endocytic cargo is in constant motion within the cell. Fluorescence microscopy, combined with single particle tracking, provides spatial and temporal information and has been well-utilized for the study of endocytosis.[6-15] However studies of the chemical reactions associated with the endocytic pathway require methods to probe chemical activity as well as place and time.

We describe a fluorescence assay that can be used to probe chemical reactions, including enzymatic activity, in live cells. In brief, we functionalize the molecule or particle of interest with multiple fluorophores resulting in a quenched fluorescent signal. Upon enzymatic degradation and the separation of the fluorophores, the fluorescent signal increases, referred to as dequenching, indicating that a reaction has occurred. This

approach has the advantage of an increase in signal as an indicator of a cellular event, as compared to decreases in signal which are difficult to decouple from photobleaching. This dequenching assay can be used across multiple scales - from subcellular measurements with fluorescence microscopy to the analysis of tens of thousands of cells with flow cytometry. Dequenching measurements can be made, without any modification, using multiple experimental platforms including fluorimeters, fluorescence microscopes, and flow cytometers. Conceptually, dequenching is similar to Förster resonance energy transfer, but requires only a single color fluorophore making it compatible with multicolor imaging and simple optical setups. Dequenching has been used previously to observe the effect of pH change on viral fusion,[8,16] the application described below is unique in probing chemical reactions.

We first use two common endocytic cargos to illustrate the use of dequenching in fluorescence measurements. The first cargo is a single protein molecule, bovine serum albumin (BSA), covalently labeled with an amine-reactive fluorophore. The second cargo is a single particle, low density lipoprotein (LDL), labeled with a lipophilic fluorophore. We first describe the labeling scheme used for BSA and LDL and the *in vitro* measurements used to quantify dequenching. The results described below demonstrate that dequenching is a function of the number of fluorophores and that it occurs in response to the separation of fluorophores due to the enzymatic degradation of proteins. We then use this dequenching assay to characterize the intracellular degradation of BSA, probed with subcellular, cellular, and high throughput measurements.

6.3 Results and discussion

6.3.1 Fluorescent labeling of BSA and LDL

We illustrate two labeling schemes; covalent attachment of fluorophores to an individual protein molecule, BSA, and the use of a lipophilic fluorophore to label a naturally occurring lipoprotein nanoparticle, LDL. Specifically, BSA was labeled with

AlexaFluor647 (AF647) according to the manufacturer's instructions as described in Chapter 2. LDL was labeled with a lipophilic fluorophore, DiD, that inserts into the lipid component of LDL. The ratio of fluorophores to BSA or LDL was calculated based on their absorption measured with UV-Vis spectrophotometry as described in Chapter 2.

6.3.2 Dequenching increases with the number of fluorophores

The number of fluorophores covalently bound to BSA or inserted into the lipids of LDL were controlled by the concentration of fluorophores added to BSA or LDL during labeling. Dequenching, defined as an increase in fluorescence in response to a decreased local concentration of fluorophores, was measured for increasing numbers of fluorophores bound to BSA or LDL. The measurements were carried out in solution using an enzyme to degrade BSA or LDL and thereby reduce the local concentration of fluorophores (Figure 6.1). BSA-AF647 was incubated with 0.1 mg/mL pepsin, an acid protease known to degrade BSA,[17,18] for 1 hr at 37ºC in a TCA solution at pH 1.2. As a control, BSA-AF647 was incubated in the same TCA solution at pH 1.2 to ensure the low pH did not lead to a change in emission. LDL-DiD was incubated with trypsin, a protease shown previously to degrade LDL,[13] in PBS for 2 hr at 37ºC. As a control, LDL-DiD was incubated in PBS at 37ºC in the absence of trypsin. Data were analyzed identically for

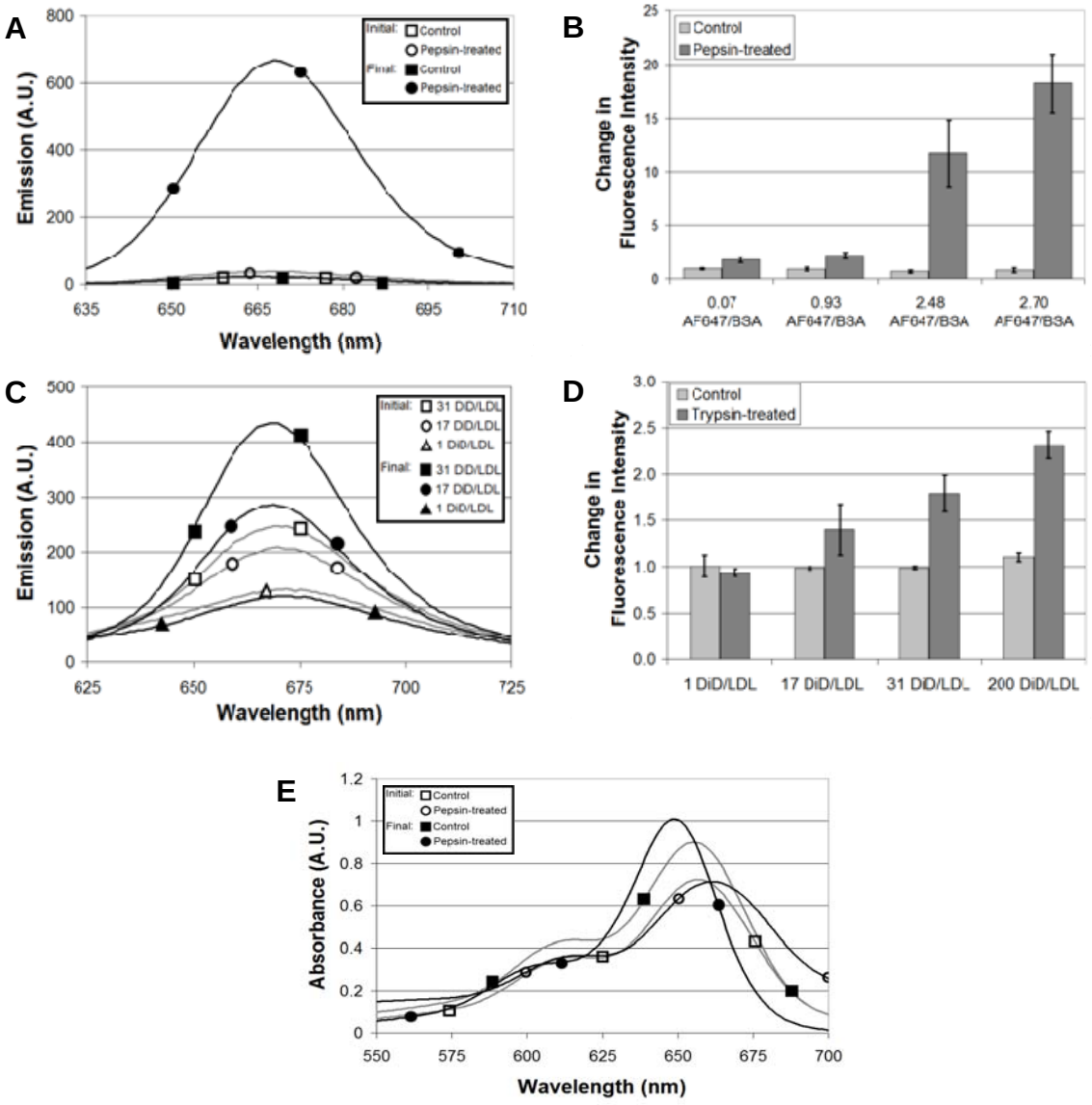

F**igure 6.1.** Dequenching as function of fluorophore number. A.) Emission spectra (625 nm excitation) of BSA-AF647 labeled with an average of 2.70 AF647 molecules per BSA molecule in solution (TCA, pH 1.2). Final spectra were measured after a 1 hr incubation at 37ºC. Absorption spectra showed little change after the 1 hr incubation (Figure 1E). B.) Fluorescence emission increased with increasing numbers of AF647 conjugated to BSA. A value of 1 indicates no change in emission. C.) Emission spectra (600 nm excitation) of LDL-DiD in a PBS solution. Final spectra were measured after a 2 hr incubation at 37ºC in the presence of trypsin. Absorption spectra showed little change after the 1 hr incubation. D.) Fluorescence emission increased with increasing numbers of DiD inserted into the lipid component of LDL. A value of 1 indicates no change in emission. Error bars represent the standard deviation of 3 experiments. E.) Absorption spectra of BSA-AF647 labeled with 2.70 AF647 molecules for each BSA molecule. Final spectra were measured after a 1 hr incubation at 37°C. The control is a 1 hr incubation at 37°C in TCA, but in the absence of pepsin. The absorption spectra of LDL also show little change after the 1 hr incubation.[1]

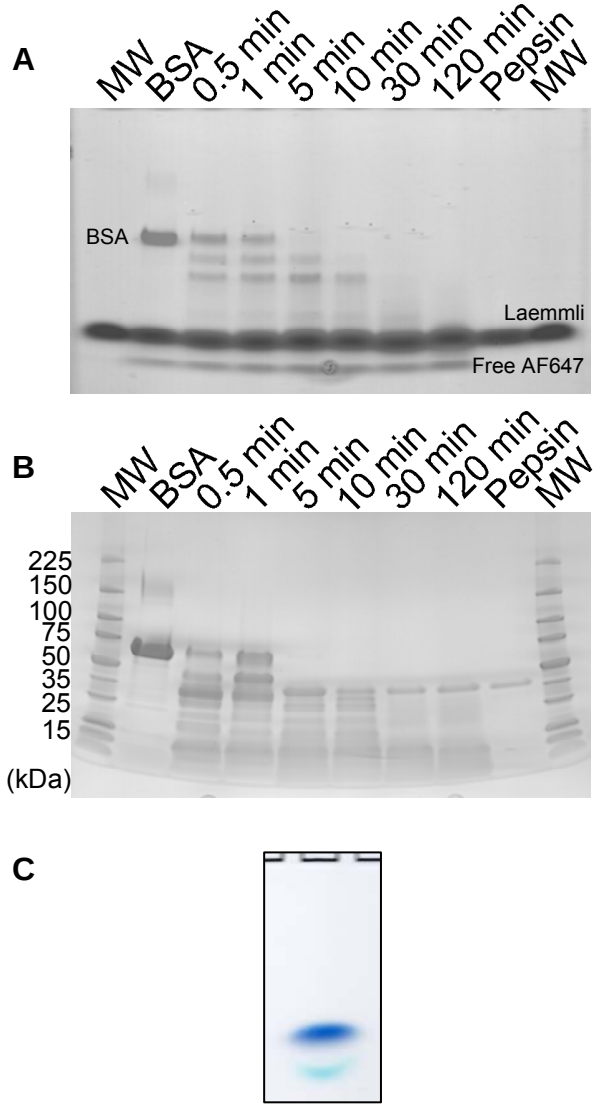

Figure 6.2. Degradation of BSA and LDL leads to an increase in fluorescence emission. A). The degradation of BSA-AF647 was confirmed with gel electrophoresis. The signal from AF647 in an unstained gel shows that AF647 remains bound to BSA fragments. B.) BSA, in the absence of AF647, was incubated with pepsin. The gel, stained with SimplyBlue SafeStain, shows a similar pattern of BSA fragments as well as a pepsin band at 35 kDa. C.) Gel electrophoresis of free AF647 in Laemmli SDS sample buffer. The top band (dark blue) is dye from the sample buffer and the lower (light blue) band is free AF647. Running conditions were identical throughout.

BSA and LDL. The emission of either BSA-AF647 or LDL-DiD was measured with a fluorimeter (RF-5301PC, Shimadzu, Japan) before and after incubation with the enzyme (Figure 6.1A and 6.1C). Emission measurements were normalized by the absorption of BSA-AF647 or LDL-DiD before and after incubation although there was little change in absorption (Figure 6.1E). Dequenching was measured as the change in fluorescence emission following enzymatic treatment. No change in emission would be indicated by a dequenching value of 1. For low numbers of fluorophores, little change was observed after incubation with pepsin or trypsin. For example, BSA labeled with an average of 0.93 AF647 molecules per BSA increased emission by a factor of 1.75 after incubation with pepsin. An identically labeled sample that was not exposed to pepsin had a change in fluorescence intensity of 0.97, essentially no change in emission. LDL labeled with 1 DiD molecule per LDL particle showed no change in emission (0.94) after incubation with trypsin. An identically labeled sample that was not exposed to trypsin also showed no change in emission (1.01). In comparison, increasing the number of fluorophores resulted in a greater change in fluorescence intensity (Figure 6.1B and 6.1D). BSA labeled with an average of 2.70 AF647 molecules increased emission by a factor of 18.25 and LDL labeled with an average of 200 DiD molecules increased emission by a factor of 2.32. BSA labeled with 2.48 AF647 molecules had a dequenching value of 11.73. Unless noted, this labeling ratio was used for the experiments described below.

6.3.3 Degradation of BSA and LDL leads to an increase in fluorescence

The increase in emission following treatment with proteolytic enzymes suggests that degradation of BSA and the protein component of LDL leads to a spatial separation

of the fluorophores and concomitant decrease in the local concentration of fluorophores. It is also possible that the fluorophores are cleaved from the BSA or LDL resulting in a spatial separation without protein degradation. To test this possibility, protein degradation following enzyme treatment was probed with gel electrophoresis. BSA-AF647, incubated with pepsin under the same conditions described above, was loaded on a 4-20% gradient polyacrylamide gel, and run at 130 V for 1 hr (Figure 6.2A). Rather than using a protein stain, the AF647 signal was recorded. BSA, prior to incubation with pepsin, shows a single band mid-way down the gel. Based on a comparison with BSA run under similar conditions, but stained for proteins, we can assign this band to BSA-AF647. The lower molecular weight bands include the Laemmli loading buffer and free AF647 (Figure 6.2C). After incubation with pepsin, lower molecular weight fragments are present in good agreement with previous pepsin fragmentation studies.[18] After 5 min intact BSA is no longer visible and the number of smaller fragments increases. This gel can be compared to a protein-stained gel run under the same conditions (Figure 6.2B). Similarly, BSA is present initially and rapidly degrades to increasingly smaller fragments. Pepsin (35 kDa) is also visible on the gel.

Electron microscopy images have demonstrated that proteolysis of LDL leads to an increase in the diameter of LDL particles.[19] We used DLS to investigate a possible change in size of LDL particles following trypsin-mediated degradation. DLS measurements of LDL in PBS showed a single population of particles with a diameter of 27 ± 3 nm, in good agreement with the established diameter of LDL.[20] We found that the incubation of LDL with trypsin resulted in two populations of particles. The majority (83%) of LDL particles had a diameter of 35 ± 2 nm. The remainder had a diameter of

410 ± 68 nm. The increase in diameter, suggested to result from the creation of fusion-competent LDL particles following proteolysis, likely leads to the spatial separation of DiD molecules.[19]

6.3.4 Dequenching is specific to enzyme activity

Control experiments described above demonstrate that dequenching does not occur in response to pH or temperature, but instead requires the presence of a proteolytic enzyme. To confirm that enzymatic activity was specific, dequenching was measured in the presence of an enzyme inhibitor. The enzymatic activity of pepsin, and other acid proteases, is inhibited by pepstatin.[21,22] AF647-BSA, with a 2.48 labeling ratio, was incubated with both pepsin and pepstatin for 1 hr. While treatment with pepsin results in a dequenching value of 11.7, the addition of pepstatin decreases dequenching to 0.5 (Figure 6.3A). Gel electrophoresis confirms that the degradation of BSA by pepsin is inhibited by pepstatin (Figure 6.3B).

6.3.5 Dequenching as a cellular assay of enzyme activity

Dequenching provides a method to probe protein or particle degradation in solution, as described above, and also in live cells. Cellular experiments can be carried out on the subcellular level, probing the degradation of cargo in individual endocytic vesicles, or on the cellular level using either fluorescence microscopy to image individual cells or flow cytometry to measure dequenching in tens of thousands of cells.

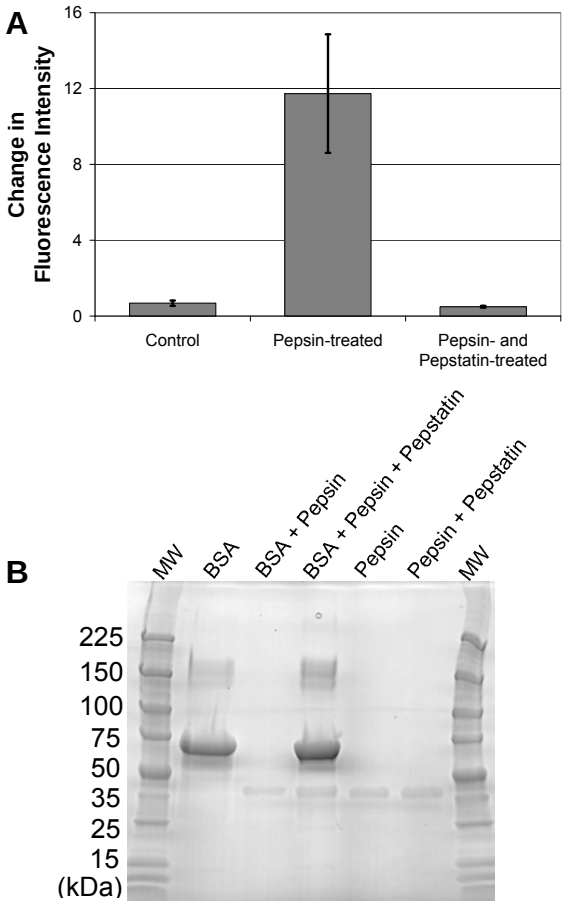

Figure 6.3. Dequenching of BSA is specific to protease activity. A.) Dequenching was not observed when BSA-AF647 was incubated with a combination of pepsin and pepstatin, a pepsin inhibitor. B.) Gel electrophoresis (4-20% gradient, polyarcrylamide, SimplyBlue SafeStain) shows that the degradation of BSA (67 kDa) by pepsin is inhibited by pepstatin. Pepsin (35 kDa) is visible on the gel while pepstatin (0.7 kDa) is too small to observe.

6.3.6 Subcellular imaging: BSA is degraded in LAMP1-positive vesicles

LAMP1, a late endosomal and lysosomal protein,[6,23-28] was labeled with EYFP and used to generate BS-C-1 monkey kidney cells that stably express LAMP1-EYFP.[13,29] BSA-AF647 was incubated with cells at a concentration of 80 μg/mL for 30 min in full growth medium. These conditions allow BSA-AF647 to be internalized into endocytic vesicles.[30,31] Two-color live cell imaging, using a custom built microscope with laser excitation, was used to image LAMP1-EYFP and BSA-AF647 simultaneously in real

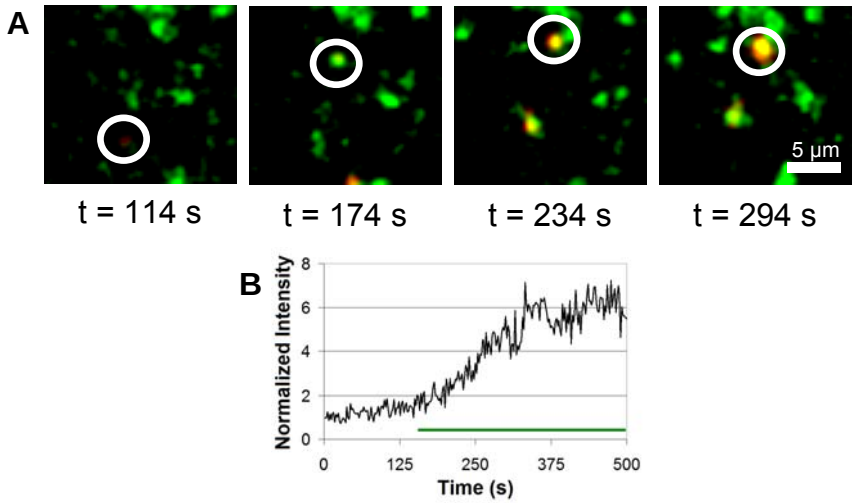

Figure 6.4. Two-color single particle tracking of BSA-AF647 and LAMP1-EYFP. A.) Snapshots illustrate the dequenching of BSA-AF647 (red) in a LAMP1-positive endo-lysosomal vesicle (green). Images were recorded at a rate of 0.5 Hz. B.) Intensity of the BSA-AF647 as a function of time. The horizontal bar under the intensity trace indicates the period of time during which BSA-AF647 was colocalized with a LAMP1-vesicle.

time in live cells. Data were collected as a series of images (0.5 Hz) and analyzed to detect increases in the BSA-AF647 signal (Figure 6.4). BSA-AF647 was considered to dequench if the emission intensity increased by at least a factor or 2 within 100 s. BSA-AF647 molecules that underwent dequenching were then scored for the presence of LAMP1-EYFP. BSA-AF647 and LAMP1-EYFP were considered colocalized if they overlapped and moved through the cell together for at least 10 seconds. Of 10 BSA-AF647 dequenching events, all were localized in a LAMP1-positive vesicle. Two-color imaging with LAMP1-EYFP provides the first confirmation that BSA is degraded in a LAMP1-positive vesicle.

6.3.7 Cellular imaging: Degradation of BSA is inhibited by pepstatin.

Subcellular imaging of BSA-AF467 allows us to determine the intracellular site of degradation directly. The second step is to determine which late endosomal or

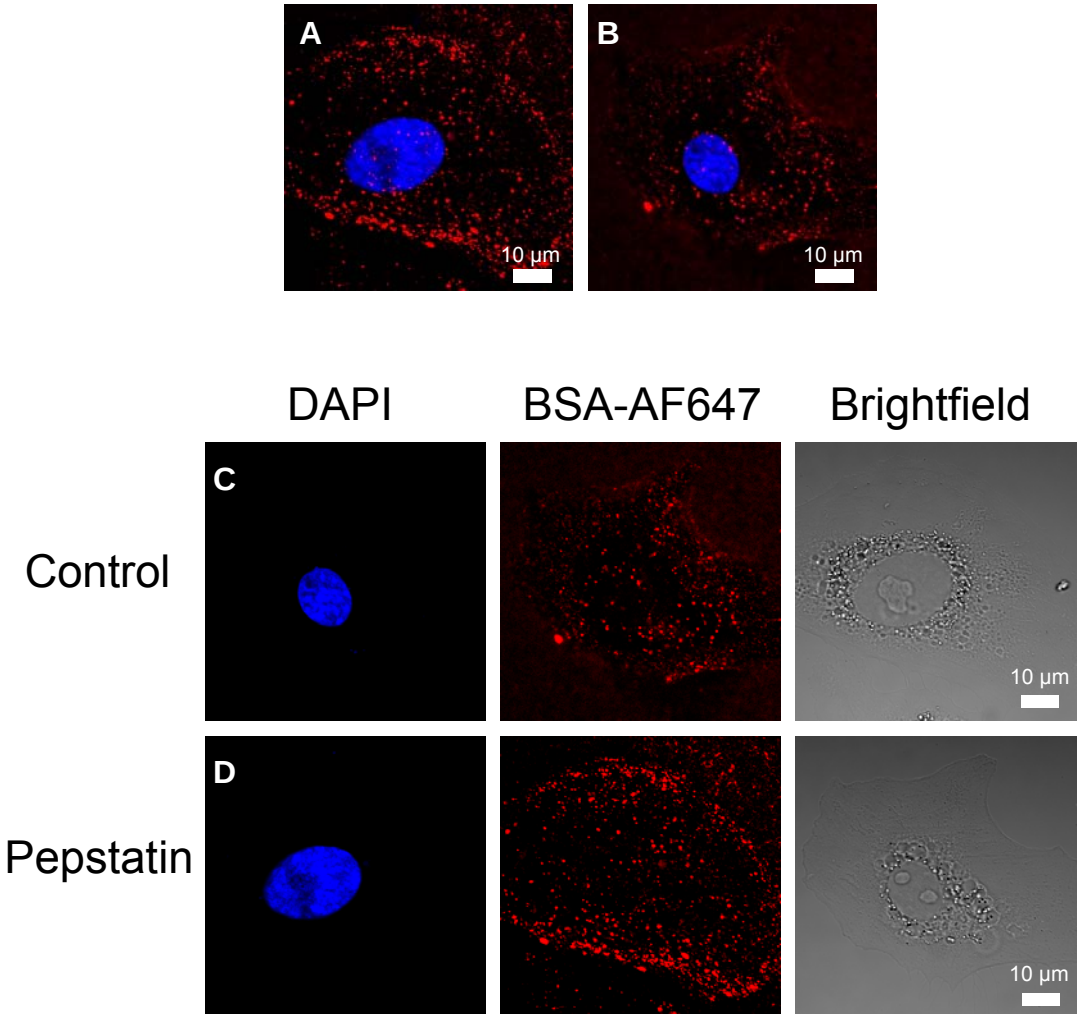

Figure 6.5. Cellular imaging of BSA dequenching. A.) A representative confocal fluorescence microscopy image of a cell following a 1 hr incubation with BSA-AF647. B.) The same incubation and imaging parameters were used to image cells treated with pepstatin, an inhibitor of acid proteases. Nuclei were stained with DAPI (blue). Unmerged and brightfield images are included as C.) Control and D.) Pepstatin-treated

lysosomal enzyme is responsible for degradation. Based on previous experiments that characterized albumin as a substrate for cathepsin D,[32,33] we tested the importance of acid proteases in the degradation of BSA. Confocal fluorescence microscopy was used to image cells incubated with 80 µg/mL BSA-AF647 for 1 hr at 37ºC. Fluorescence microscopy images show a punctate BSA-AF647 signal indicative of BSA-AF647 within endocytic vesicles (Figure 6.5A). In comparison, cells incubated with pepstatin, which

inhibits pepsin, as described above, as well as endo-lysosomal acid proteases such as cathepsin D, show the same punctate staining, but weaker fluorescence (Figure 6.5B).

The intensity of BSA-AF647-containing endosomes, referred to as particles, was determined using ImageJ with the MOSAIC plugin.[34] The MOSAIC Particle Tracker 2D/3D feature was used to detect the center of each particle in the image. Coordinates and images were imported into MATLAB and a custom written function which determined the average intensity within a 2 pixel radius of each particle was applied. The average background was determined in ImageJ for an area within the cell that did not contain particles (typical area 30-60 μm^2). The background was then subtracted from the particle intensities and any remaining values that were below zero were eliminated from further analysis as false-positive detections. The particle intensities (3039 particles in the control cells, 3259 in pepstatin-treated cells values) were then compared using a Wilcoxon signed-rank test for a p-value of 0.005. Images for publication were background subtracted and intensities were adjusted equally within each data set.

This analysis showed that, on average, the intensity of the BSA-AF647-containing endosomes was 1.5-fold greater in control cells than in pepstatin-treated cells. The intensity analysis was carried out for >3000 endosomes for 7 cells of each condition, $p = 0.005$. The reduced degradation of BSA-AF647 in pepstatin-treated cells was confirmed with gel electrophoresis (Figure 6.6).

6.3.8 High throughput analysis: Degradation of BSA is inhibited by pepstatin

Cellular and subcellular imaging have the advantage of providing spatial information, but are relatively low throughput as individual cells or organelles must be

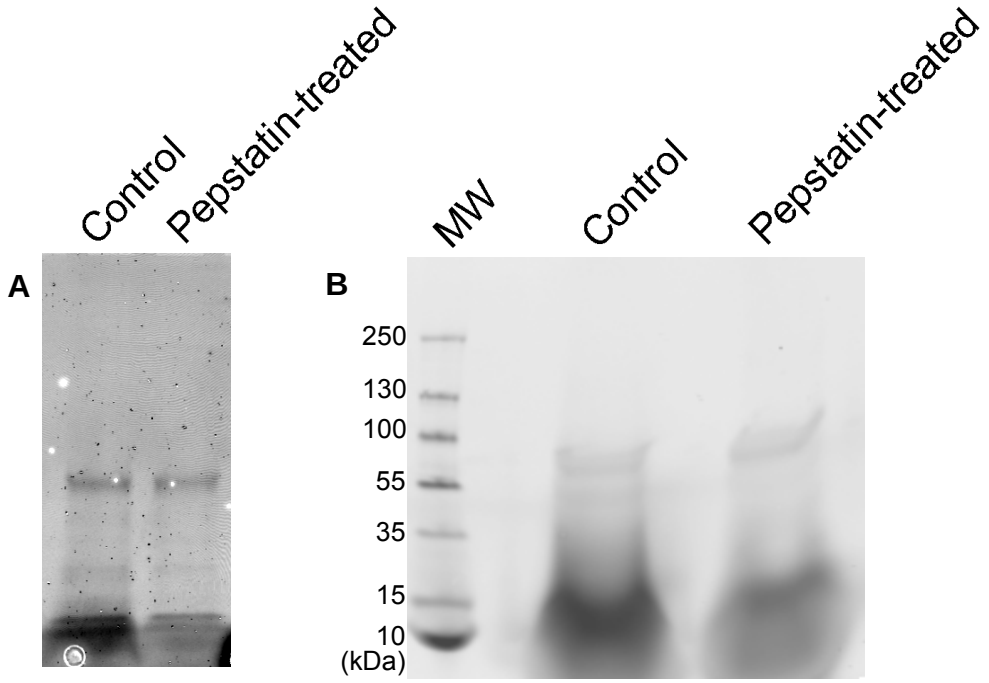

Figure 6.6. Imaging of BSA degradation in cellular lysate**.** To confirm that pepstatin inhibited the degradation of BSA-AF647, cells were incubated with BSA-AF647 using the same parameters as described for Figure 5. After treatment with BSA-AF647, control and pepstatin-treated cells were lysed in a 1% TritonX-100, 50 mM Tris, 150 mM NaCl (pH = 8) solution supplemented with a protease inhibitor cocktail (Halt, 78441, Pierce) for 30 minutes at 4ºC. Insoluble components were removed by centrifugation at 14,000 rpm at 4 ˚C for 20 minutes. The protein concentration of the resulting lysate was determined using a bicinchoninic acid assay (BCA, 23250, Pierce). Lysate was prepared for gel electrophoresis using a dye-free sample buffer and run as described in the Experimental Section. The AF647 signal was used for detection (Typhoo Imager). A.) BSA-AF647 signal from lysate (50 μg) isolated following a 1 hr incubation with cells. Pepstatin-treated cells show a significantly lower concentration of protein fragments. B.) BSA-AF647 signal from lysate (75 μg) isolated following a 2.5 hr incubation with cells.

imaged and analyzed. In comparison, flow cytometry measures the fluorescence intensity of individual cells at relatively high speeds (~60,000 cells/min). While spatial information is lost, there are clear advantages to acquiring large amounts of data rapidly.

Flow cytometry (BD LSR-II) was used to measure the emission of cells following a 1 hr incubation with 80 μg/mL BSA-AF647 in either untreated or pepstatin-treated cells (Figure 6.7). Cells were cooled to 4ºC for 15 minutes before incubation with BSA-AF647

for 15 minutes. Unbound BSA-AF647 was removed by washing 2 times with 2 mL of full growth medium. After a 1 hr incubation at 37ºC, cells were trypsinized, pelleted (9000 rcf for 5 min), and washed with Leibovitz's L-15 medium (21083, Invitrogen). Flow cytometry was carried out on a BD LSR-II flow cytometer (Becton Dickinson, Franklin Lakes, NJ). For each experiment, 30,000 cells were sampled. Analysis of flow cytometry data shows that untreated, control cells show greater fluorescence intensity, normalized to 90%, as compared to pepstatin-treated cells, 44%.

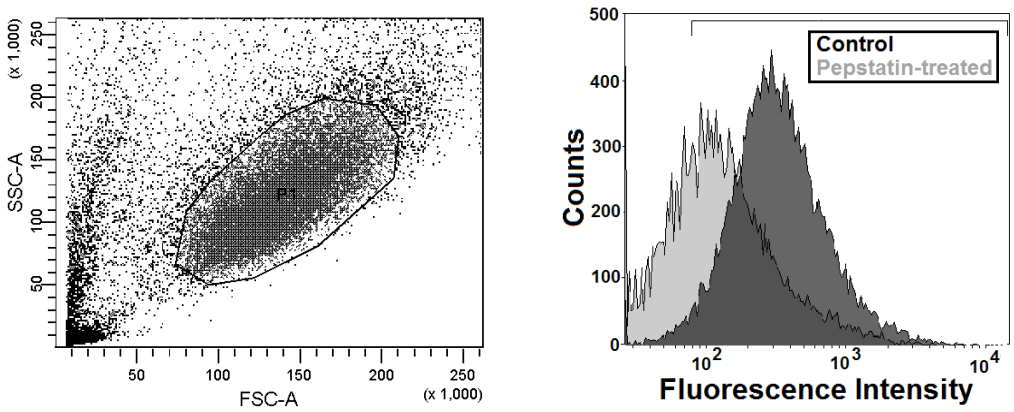

Figure 6.7. Analysis of BSA degradation with flow cytometry. A.) A representative scatter plot . B.) Flow cytometry was used to measure the emission of cells incubated with BSA-AF647. Treatment of cells with pepstatin decreased the BSA-AF674 signal.

6.4 Conclusions

We describe a method that can be used to probe enzymatic activity in live cells, as well as in solution. By labeling molecules or particles of interest with multiple fluorophores, emission is quenched resulting in a weak fluorescent signal. Upon degradation of the molecule or particle, fluorescence increases indicating that a chemical reaction has occurred. This dequenching assay can be incorporated into existing

fluorescence microcopy and flow cytometry platforms without any modifications. We have used this method to probe the degradation of BSA in live cells. BSA, or the human analog, is essential for human health.[35,36] It is also increasingly important in nanobiotechnology for nanoparticle and drug delivery.[37-39] Determining the intracellular site and mechanism of BSA degradation is essential for the design of BSA-mediated delivery systems. While the use of standard fluorophores makes it possible to probe cellular location as a function of time, the change in intensity of quenched cargo is an indicator for the site at which cargo undergoes a chemical reaction. Using a combination of single particle tracking, confocal fluorescence microscopy, and flow cytometry, we find that the degradation of BSA occurs in an endocytic vesicle that is positive for LAMP1 and that degradation is inhibited by pepstatin, an acid protease inhibitor.

6.5 References

1 Alberts, B.; Bray, D.; Lewis, J.; Raff, M.; Roberts, K.; Watson, J. D. *Molecular Biology of the Cell*. 3 edn, (Garland Publishing, 1994).

2 Conner, S. D.; Schmid, S. L., Regulated portals of entry into the cell. *Nature* **2003**, *422*, 37-44.

3 Gruenberg, J., The endocytic pathway: a mosaic of domains. *Nat. Rev. Mol. Cell Bio.* **2001**, *2*, 721-730.

4 Mellman, I., Endocytosis and molecular sorting. *Annual Review of Cell and Developmental Biology* **1996**, *12*, 575-625.

5 Marsh, M.; Helenius, A., Virus entry: Open sesame. *Cell* **2006**, *124*, 729-740.

6 Szymanksi, C. J.; Humphries, W. H.; Payne, C. K., Single particle tracking as a method to resolve differences in highly colocalized proteins. *Analyst* **2011**, *136*, 3527-3533.

7 Brandenburg, B.; Zhuang, X. W., Virus trafficking - learning from single-virus tracking. *Nature Reviews Microbiology* **2007**, *5*, 197-208.

8 Lakadamyali, M.; Rust, M. J.; Babcock, H. P.; Zhuang, X. W., Visualizing infection of individual influenza viruses. *Proceedings of the National Academy of Sciences of the United States of America* **2003**, *100*, 9280-9285.

9 Lakadamyali, M.; Rust, M. J.; Zhuang, X., Ligands for clathrin-mediated endocytosis are differentially sorted into distinct populations of early endosomes. *Cell* **2006**, *124*, 997-1009.

10 Payne, C. K.; Jones, S. A.; Chen, C.; Zhuang, X. W., Internalization and trafficking of cell surface proteoglycans and proteoglycan-binding ligands. *Traffic* **2007**, *8*, 389-401.

11 Rink, J.; Ghigo, E.; Kalaidzidis, Y.; Zerial, M., Rab conversion as a mechanism of progression from early to late endosomes. *Cell* **2005**, *122*, 735-749.

12 Hess, G. T.; Humphries, W. H.; Fay, N. C.; Payne, C. K., Cellular binding, motion, and internalization of synthetic gene delivery polymers. *Biochimica Et Biophysica Acta-Molecular Cell Research* **2007**, *1773*, 1583-1588.

13 Humphries, W. H.; Fay, N. C.; Payne, C. K., Intracellular degradation of low-density lipoprotein probed with two-color fluorescence microscopy. *Integr. Biol.* **2010**, *2*, 536-544.

14 Payne, C. K., Imaging gene delivery with fluorescence microscopy. *Nanomedicine* **2007**, *2*, 847-860.

15 Ewers, H.; Smith, A. E.; Sbalzarini, I. F.; Lilie, H.; Koumoutsakos, P.; Helenius, A., Single-particle tracking of murine polyoma virus-like particles on live cells and artificial membranes. *Proc Natl Acad Sci USA* **2005**, *102*, 15110-15115.

16 van der Schaar, H. M.; Rust, M. J.; Chen, C.; van der Ende-Metselaar, H.; Wilschut, J.; Zhuang, X. W.; Smit, J. M., Dissecting the Cell Entry Pathway of Dengue Virus by Single-Particle Tracking in Living Cells. *Plos Pathogens* **2008**, *4*.

17 Weber, G.; Young, L. B., Fragmentation of boine serum albumin by pepsin. 1. Origin of acid expansion of albumin molecule. *J. Biol. Chem.* **1964**, *239*, 1415-&.

18 Weber, G.; Young, L. B., Fragmentation of bovine serum albumin by pepsin. 2. Isolation, amino acid composition, and physical properties of fragments. *J. Biol. Chem.* **1964**, *239*, 1424-&.

19 Linke, M.; Gordon, R. E.; Brillard, M.; Lecaille, F.; Lalmanach, G.; Bromme, D., Degradation of apolipoprotein B-100 by lysosomal cysteine cathepsins. *Biological Chemistry* **2006**, *387*, 1295-1303.

20 Voet, D.; Voet, J. G. *Biochemistry*. 3 edn, (John Wiley & Sons, 2004).

21 Kageyama, T., Pepsinogens, progastricsins, and prochymosins: structure, function, evolution, and development. *Cell. Mol. Life Sci.* **2002**, *59*, 288-306.

22 Rich, D. H.; Sun, E. T. O., Mechanism of inhibition of pepsin by pepstatin-effect of inhibitor structure on dissociation constant and and time-dependent inhibition. *Biochem. Pharmacol.* **1980**, *29*, 2205-2212.

23 Chen, J. W.; Murphy, T. L.; Willingham, M. C.; Pastan, I.; August, J. T., Identification of two lysosomal membrane glycoproteins. *J. Cell Biol.* **1985**, *101*, 85-95.

24 Lewis, V.; Green, S. A.; Marsh, M.; Vihko, P.; Helenius, A.; Mellman, I., Glycoproteins of the lysosomal membrane. *J. Cell Biol.* **1985**, *100*, 1839-1847.

25 Lippincott-Schwartz, J.; Fambrough, D. M., Lysosomal membrane dynamics: Structure and interoganellar movement of a major lysosomal membrane glycoprotein. *J. Cell Biol.* **1986**, *102*, 1593-1605.

26 Clague, M. J., Molecular aspects of the endocytic pathway. *Biochemical Journal* **1998**, *336*, 271-282.

27 Griffiths, G.; Hoflack, B.; Simons, K.; Mellman, I.; Kornfeld, S., The mannose 6-phosphate receptor and the biogenesis of lysosomes. *Cell* **1988**, *52*, 329-341.

28 Geuze, H. J.; Stoorvogel, W.; Strous, G. J.; Slot, J. W.; Bleekemolen, J. E.; Mellman, I., Sorting of mannose 6-phosphate receptors and lysosomal membrane-proteins in endocytic vesicles. *Journal of Cell Biology* **1988**, *107*, 2491-2501.

29 Sherer, N. M.; Lehmann, M. J.; Jimenez-Soto, L. F.; Ingmundson, A.; Horner, S. M.; Cicchetti, G.; Allen, P. G.; Pypaert, M.; Cunningham, J. M.; Mothes, W., Visualization of retroviral replication in living cells reveals budding into multivesicular bodies. *Traffic* **2003**, *4*, 785-801.

30 Tagawa, M.; Yumoto, R.; Oda, K.; Nagai, J.; Takano, M., Low-Affinity Transport of FITC-Albumin in Alveolar Type II Epithelial Cell Line RLE-6TN. *Drug Metabolism and Pharmacokinetics* **2008**, *23*, 318-327.

31 Yumoto, R.; Nishikawa, H.; Okamoto, M.; Katayama, H.; Nagai, J.; Takano, M., Clathrin-mediated endocytosis of FITC-albumin in alveolar type II epithelial cell line RLE-6TN. *American Journal of Physiology-Lung Cellular and Molecular Physiology* **2006**, *290*, L946-L955.

32 Mego, J. L., Role of thiols, pH and cathepsin D in the lysosomal catabolism of serum albumin. *Biochem. J.* **1984**, *218*, 775-783.

33 Baricos, W. H.; Zhou, Y. W.; Fuerst, R. S.; Barrett, A. J.; Shah, S. V., The role of aspartic and cysteine proteinases in albumin degradation by rat kidney cortical lysosomes. *Arch. Biochem. Biophys.* **1987**, *256*, 687-691.

34 Sbalzarini, I. F.; Koumoutsakos, P., Feature Point Tracking and Trajectory Analysis for Video Imaging in Cell Biology. *J. Struct. Biol.* **2005**, *151*, 182-195.

35 Anderson, N. L.; Anderson, A. G., The human plasma proteome. *Molecular & Cellular Proteomics* **2002**, *1*, 845-867.

36 Osicka, T. M.; Houlihan, C. A.; Chan, J. G.; Jerums, G.; Comper, W. D., Albuminuria in patients with type 1 diabetes is directly linked to changes in the lysosome-mediated degradation of albumin during renal passage. *Diabetes* **2000**, *49*, 1579-1584.

37 Hanaki, K.; Momo, A.; Oku, T.; Komoto, A.; Maenosono, S.; Yamaguchi, Y.; Yamamoto, K., Semiconductor quantum dot/albumin complex is a long-life and highly photostable endosome marker. *Biochem. Biophys. Res. Commun.* **2003**, *302*, 496-501.

38 Kratz, F., Albumin as a drug carrier: Design of prodrugs, drug conjugates and nanoparticles. *J. Control. Release* **2008**, *132*, 171-183.

39 Doorley, G. W.; Payne, C. K., Cellular binding of nanoparticles in the presence of serum proteins. *Chemical Communications* **2011**, *47*, 466-468.

CHAPTER 7

CONCLUSIONS

7.1 Summary

In this thesis, multi-color single particle tracking fluorescence microscopy is used to investigate the vesicle-mediated enzymatic degradation of extracellular cargo. Specifically, the degradation of low-density lipoprotein and bovine serum albumin are characterized using a dequenching labeling scheme which allows for sensing a chemical reaction in solution as well as inside of live, intact cells. These studies are the first to directly observe the degradation of extracellular cargo within a cell and describe in new detail the endo-lysosomal pathway.

7.2 General conclusions

In the conventional description of the degradation of extracellular cargo, the lysosome is where the enzymes available for degradation are active and cause productive chemical reactions. Lysosomes were considered the organelle of the cell responsible for degradation because lysosomes contain 80% of the enzymes available to the endocytic pathway.[1-6] Other groups have found degraded proteins in the late endosome, but no group had been able to directly show that degradation occurs in the late endosome rather than the lysosome.[4,5,7]

The data presented in this thesis directly demonstrates that degradation of extracellular cargo occurs in the late endosome. Using two-color degradation coupled with dequenching labeling schemes on extracellular cargo, we directly observe the degradation of extracellular cargo in Rab7-positive vesicles.[8] Because Rab7 is a classic late endocytic protein, it can be concluded that degradation occurs in the late endosome.

This supports the previously suggested hypothesis that degradation occurs in the late endosome, which changes the previously assigned functions of these organelles.[4,5,7] In the context of the experiments described in this thesis, lysosomes are considered enzyme storage vesicles and endosomes are the chemically-active vesicle of the cell.

Colocalization experiments reveal that Rab7 and LAMP1, the Lysosome Associate Membrane Protein, typically localize on the same vesicle.[9] Even though it is well known that LAMP proteins localize on late endosomes and lysosomes, the extremely high level of colocalization calls into question whether Rab7 proteins are late endosomal. Using single particle tracking fluorescence microscopy, Rab7-vesicles were shown to have a faster velocity than LAMP1-vesicles. These vesicle populations also have different efficiencies in finding a fusion partner to become a hybrid, Rab7- LAMP1-vesicle.

While vesicle mobility differences are important for suggesting that multiple vesicle populations exist, the functional differences are paramount to cellular biology. The functional differences between Rab7-, LAMP1-, and hybrid vesicles are characterized by colocalization experiments with the extracellular cargo dextran, a fluid phase marker.[10-13] Colocalization with Rab7-, LAMP1- and hybrid vesicles point to an upstream Rab7-pathway that is targeted by receptor-mediated extracellular cargo but void of fluid phase markers such as dextran.

These results and conclusions taken together support the hypothesis that lysosomes are enzyme storage vesicles.[4,5,7] In this hypothesis, LAMP1-vesicles define reactive, enzyme rich vesicles that transport and deliver enzymes to the hybrid Rab7-LAMP1 vesicles where degradation occurs. Further work is necessary to confirm the role

of lysosomes, including identifying the molecular character of the vesicle. This is discussed in detail in Section 7.3.

Furthermore, the terminology late endosome and lysosome may not fit how the end of the endocytic pathway truly works. Using the Rab7, LAMP1 and M6PR membrane proteins provides a realistic description of the endocytic vesicle, but do not completely fit into the previously used terminology. The addition of the hybrid vesicle, a Rab7- and LAMP1-vesicle capable of degradation but still with proteins considered late endosomal, completes the picture of the endocytic pathway. It is important to mention that this work is not the first to identify the hybrid vesicle,[5,14] but this is the first work to assign a functional responsibility to this vesicle.

7.3 Future work

7.3.1 Three-color microscopy

Three-color microscopy, imaging the interactions of Rab7-vesicles, LAMP1-vesicles and extracellular cargo simultaneously, should be used to reproduce the conclusions in this work. Using the dequenching labeling schemes described in this thesis along with multi-color fluorescence microscopy, all the dynamics discussed in this thesis can be confirmed in a single cell. Also, the dependence of motion on cargo can be further studied by incorporating the added dimension of being able to identify vesicles that contain active enzymes.

7.3.2 Molecular description of lysosomes

One of the major questions left is, "What molecular features distinguish is the lysosome and endosome?" Lysosomes were previously defined as mannose 6-phosphate receptor negative vesicles.[15-19] However, colocalization measurements (Figure 5.1) suggest that this is not a sufficient molecular description of the lysosome. Furthermore, measurements suggest that LAMP1, Rab7 and M6PR proteins in combination with one another may not be sufficient to describe the lysosome.

First, to confirm this hypothesis, cells expressing M6PR labeled with a variant of GFP and extracellular cargo with a dequenching labeling scheme can be imaged using the two-color microscopy discussed in Chapter 2.5.1. If lysosomes are M6PR negative, once the cargo is no longer colocalized with a M6PR-vesicle, dequenching, or degradation of the extracellular cargo can occur. Furthermore, three-color microscopy could be used to show that the extracellular cargo is in a LAMP1-vesicle during degradation. If M6PR is not related to the enzymatic capacity of the vesicle, dequenching will be seen while the cargo is still in a M6PR-vesicle. This would then require an additional set of experiments to attempt to distinguish a protein or set of proteins that labels lysosomes and only lysosomes.

7.3.3 Isolation of enzymatic vesicles for cell-free studies

Of fundamental importance in cell biology is the isolation of organelles. In this case, isolation of the vesicles responsible for degradation could be used for a variety of cell-free assays. Many groups have isolates late endosomes and lysosomes using a variety of methods including FACS[20] and flow-field fractionation.[21] In these publications,

isolated vesicles are characterized based on their Rab7 or LAMP1 character. As demonstrated throughout this thesis, but specifically in Chapter 4 and 5, the characterization must include Rab7, LAMP1 and M6PR. This expansion will help with the questions posed in the previous section regarding the molecular character of endosomal-lysosomal vesicles. The isolation of vesicles in fractions and their characterization by identification of these three proteins could open many new doors to describing the vesicles of the endocytic pathway.

Furthermore, the isolated vesicles can be examined to find which ones are chemically active and what aspects of the environment are important for the enzymes in the vesicles to become chemically active. It is well known that pH is important for enzyme activity,[22] but are there other environmental factors, such as viscosity, that assist or inhibit enzymatic degradation in endocytic vesicles? These studies could lead to a method for recreating the environment of the endosome without cells.

7.4 References

1 Saftig, P.; Klumperman, J., Lysosome biogenesis and lysosomal membrane proteins: trafficking meets function. *Nat Rev Mol Cell Biol* **2009**, *10*, 623-635.

2 Kornfeld, S.; Mellman, I., The biogenesis of lysosomes. *Annu. Rev. Cell Biol.* **1989**, *5*, 483-525.

3 Mullins, C.; Bonifacino, J. S., The molecular machinery for lysosome biogenesis. *Bioessays* **2001**, *23*, 333-343.

4 Pillay, C. S.; Elliott, E.; Dennison, C., Endolysosomal proteolysis and its regulation. *Biochem. J* **2002**, *363*, 417-429.

5 Luzio, J. P.; Pryor, P. R.; Bright, N. A., Lysosomes: fusion and function. *Nat Rev Mol Cell Biol* **2007**, *8*, 622-632.

6 Clague, M. J., Molecular aspects of the endocytic pathway. *Biochem. J* **1998**, *336*, 271-282.

7 Tjelle, T. E.; Brech, A.; Juvet, L. K.; Griffiths, G.; Berg, T., Isolation and characterization of early endosomes, late endosomes and terminal lysosomes: Their role in protein degradation. *J. Cell Sci.* **1996**, *109*, 2905-2914.

8 Humphries, W. H.; Fay, N. C.; Payne, C. K., Intracellular degradation of low-density lipoprotein probed with two-color fluorescence microscopy. *Integr. Biol.* **2010**, *2*, 536-544.

9 Szymanksi, C. J.; Humphries, W. H.; Payne, C. K., Single particle tracking as a method to resolve differences in highly colocalized proteins. *Analyst* **2011**, *136*, 3527-3533.

10 Hacker, U.; Albrecht, R.; Maniak, M., Fluid-phase uptake by macropinocytosis in Dictyostelium. *J. Cell Sci.* **1997**, *110*, 105-112.

11 Racoosin, E. L.; Swanson, J. A., Macropinosome maturation and fusion with tubular lysosomes in macrophages. *J. Cell Biol.* **1993**, *121*, 1011-1020.

12 Sallusto, F.; Cella, M.; Danieli, C.; Lanzavecchia, A., Dendritic cells use macropinocytosis and the mannose receptor to concentrate macromolecules in the major histocompatibility complex class-II compartment - Down-regulation by cytokines and bacterial products. *J. Exp. Med.* **1995**, *182*, 389-400.

13 Thilo, L.; Stroud, E.; Haylett, T., Maturation of early endosomes and vesicular traffic to lysosomes in relation to membrane recycling. *J. Cell Sci.* **1995**, *108*, 1791-1803.

14 Mullock, B. M.; Bright, N. A.; Fearon, G. W.; Gray, S. R.; Luzio, J. P., Fusion of lysosomes with late endosomes produces a hybrid organelle of intermediate density and is NSF dependent. *J. Cell Biol.* **1998**, *140*, 591-601.

15 Geuze, H. J.; Slot, J. W.; Strous, J. A. M.; Hasilik, A.; Vonfigura, K., Possible pathways for lysosomal-enzyme delivery. *J. Cell Biol.* **1985**, *101*, 2253-2262.

16 Geuze, H. J.; Stoorvogel, W.; Strous, G. J.; Slot, J. W.; Bleekemolen, J. E.; Mellman, I., Sorting of mannose 6-phosphate receptors and lysosomal membrane-proteins in endocytic vesicles. *J. Cell Biol.* **1988**, *107*, 2491-2501.

17 Griffiths, G.; Hoflack, B.; Simons, K.; Mellman, I.; Kornfeld, S., The mannose 6-phosphate receptor and the biogenesis of lysosomes. *Cell* **1988**, *52*, 329-341.

18 Sahagian, G. G.; Neufeld, E. F., Biosynthesis and turnover of the mannose 6-phosphate receptor in cultured chinese-hamster ovary cells. *J. Biol. Chem.* **1983**, *258*, 7121-7128.

19 Brown, W. J.; Goodhouse, J.; Farquhar, M. G., Mannose-6-phosphate receptors for lysosomal-enzymes cycle between the golgi-complex and endosomes. *J. Cell Biol.* **1986**, *103*, 1235-1247.

20 Murphy, R. F., Analysis and isolation of endocytic vesicles by flow cytometry and sorting: demonstration of three kinetically distinct compartments involved in fluid-phase endocytosis. *Proc. Natl. Acad. Sci. U. S. A.* **1985**, *82*, 8523-8526.

21 Marsh, M.; Schmid, S.; Kern, H.; Harms, E.; Male, P.; Mellman, I.; Helenius, A., Rapid analytical and preparative isolation of functional endosomes by free flow electrophoresis. *J. Cell Biol.* **1987**, *104*, 875-886.

22 Alberts, B.; Bray, D.; Lewis, J.; Raff, M.; Roberts, K.; Watson, J. D. *Molecular Biology of the Cell*. 3 edn, (Garland Publishing, 1994).

VITA

WILLIAM HENRY HUMPHRIES IV

HUMPHRIES was born in Pittsburgh, Pennsylvania. He attended Avonworth High School in Pittsburgh, PA and received a B.S. in Biochemistry and B.M. in Music Performance with High Distinction from Ohio Northern University, Ada, Ohio in 2005. He came to Georgia Institute of Technology in 2006 to pursue a doctorate in Chemistry. Outside of his scientific endeavors, Mr. Humphries enjoys spending time with his wife, Jessica, and dogs, Kelvin and Stella and takes pleasure in sports of all types.